Earthquake Planning and Protection Organization

European Centre on Prevention and Forecasting of Earthquakes

Seismic Risk Assessment of the Historical Center of Lefkas

Athens, 2019

Seismic risk assessment of the historical center of Lefkas

Research team

Coordinator

Ioannis Psycharis, Ph.D.
Professor of Earthquake Engineering, NTUA
email: ipsych@central.ntua.gr

Members of the research team

Ioannis Taflampas, Ph.D.
Research and Teaching Associate, NTUA
email: taflan@central.ntua.gr

Ioannis Dourakopoulos, Ph.D.
Civil Engineer
Email: jdour@mail.ntua.gr

Konstantina Mastrodimou
Graduate student, NTUA

Table of Contents

1. Introduction

1.1. Scope of work

The island of Lefkas (or Lefkada), located in the Ionian Sea on the west side of Greece, is one of the most earthquake prone areas of the Mediterranean Sea. Due to the high seismic risk, the traditional houses built at the historical center of the city are constructed with a "special" timber-framed masonry system, which is not encountered in other places. In previous strong earthquakes (1953, 1973, 2003), this structural system behaved quite satisfactorily, although there were several cases of severe damage, or even collapse.

In this report, the seismic risk assessment of this structural system is performed, based on the seismic performance of three typical buildings. First, a seismic hazard analysis is performed following two approaches: a probabilistic one, in which the ground acceleration is estimated versus the annual frequency of occurrence (inverse of the return period); and a deterministic one, based on the characteristic of a large fault that exists at the west side of the island. Then, the capacity curves of the selected buildings are derived through pushover analyses. Finally, the results are combined to assess the seismic risk.

1.2. Timber-framed masonry system

Unreinforced masonry buildings, in general, cannot resist strong earthquakes. In fact, the low tensile, and hence the shear strength, and the low ductility of the structure's components result, in most cases, in poor seismic performance with local out-of-plane mechanisms before the in-plane capacity of the masonry is reached. However, the performance of vulnerable unreinforced masonry can be enhanced if a wood frame is combined with the masonry, which can provide the necessary seismic capacity. Timber-framed masonry is a traditional structural system that in seismic areas has proved to effectively resist earthquakes (Kouris and Kappos 2009), Vieux-Champagne et al. 2014).

An important evolution of the timber-framed masonry structural system is the inclusion of diagonal timber members in the wooden frame. This diagonally braced timber-framed masonry has been used as an anti-seismic construction since the 18th century in seismic-prone areas, as well as in regions without considerable seismic risk to resist wind actions or, when the buildings were founded on soft soils, differential settlements (Vieux-Champagne et al. 2014). A similar, but more advanced from the structural engineering point of view, timber-framed masonry construction appears in Lefkas Island (Figure 1).

The structures in the historical part of the city of Lefkas can be distinguished in two broad categories: (i) the pure timber-framed masonry system, in which the building is a single-storey house; and (ii) the dual system, in which a multi-storey building is constructed according to the traditional structural system of Lefkas: the multi-storey buildings consist of an unreinforced masonry ground storey and one or two (maximum) timber-framed brick masonry storeys. The intermediate floors and the roof, which is covered with tiles, are made of timber. The openings, usually symmetrically arranged along the facades of the buildings, have a rectangular shape of approximately 1.0 m width (Vintzileou and Touliatos 2005).

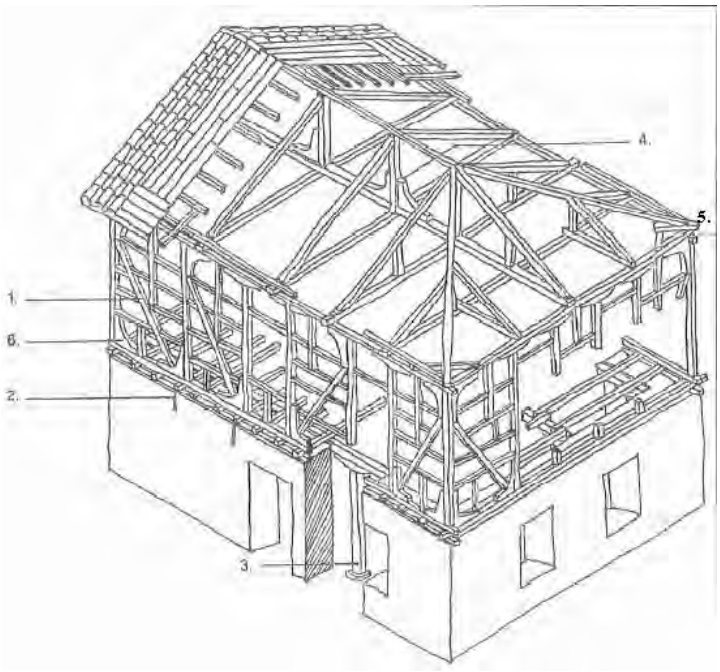

1. Inclined timber stiffness elements
2. Anchoring of the timber frames In masonry
3. Secondary system supporting upper stories
4. Stiffness elements of the bearing system of the wooden roof
5. Strengthened connections
6. Angular timber elements for adding stiffness at the connections

Figure 1. Typical two-storey building of traditional architecture in Lefkas Island (Vintzileou and Touliatos 2005).

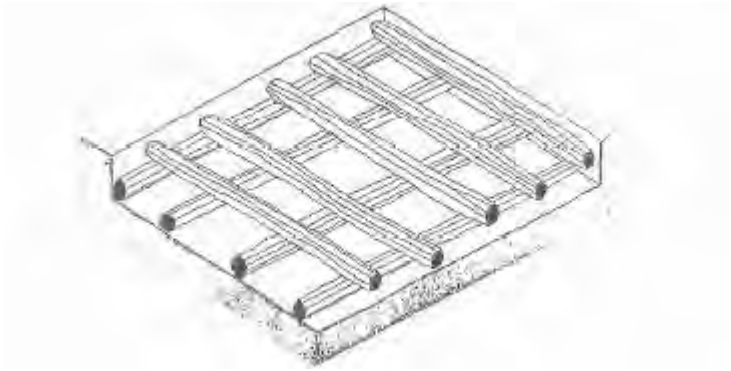

Figure 2. Foundation grid of trunks of the traditional buildings in Lefkas.

The foundation of the traditional building is implemented on low strength alluvia, leading to the construction of a grid of trunks at a depth of 0.6 to 1.0 m under the ground, in order to increase stability Figure 2. The space between the trunks is filled with sand, rubble stones and hydraulic mortar.

The stone masonry walls in the ground floor have a maximum height of 3.0 m and consist of two leaves-facades and an infill material. The external façade is made with semi-cut stones, while ashlars are used at the corners of the building and along the perimeter of openings. Rubble stones in irregular courses are used in the internal leaf of the ground floor walls. The space between the two leaves is filled with small size stones mixed with pieces of bricks and mortar. The binding mortar between the stones comprises of lime together with straw whereas, in poorer structures, clay mortar was used. It should be noted that this mortar

replaced the natural pozzolan, which was used in the buildings constructed up to the end of the 19th century (Vintzileou and Touliatos 2005).

The total thickness of the stone masonry walls varies among the traditional buildings of Lefkas, from 0.5 m to 1.0 m. Given their limited height, stone masonry walls in the ground floor can be considered as thick enough, well interconnected in the corners of the buildings, and pierced by a limited number of openings. Thus, they are conceived to provide the stiffness that is necessary for the building to be able to bear rather small deformations during seismic events. This favorable behavior is enhanced by the floor, consisting of closely spaced timber beams and timber roofing, carefully connected to each other, as well as with the stone masonry.

The perimeter walls of the upper floors are made of timber-framed masonry (typically, 10 to 20 cm thick) and they are connected to the ground masonry through timber beams arranged along the perimeter of the stone masonry walls. The timber frame has spans that vary from 1 up to 2.2 m. Diagonal members join opposite corners, but sometimes one of them may be missing or be halved (Figure 3).

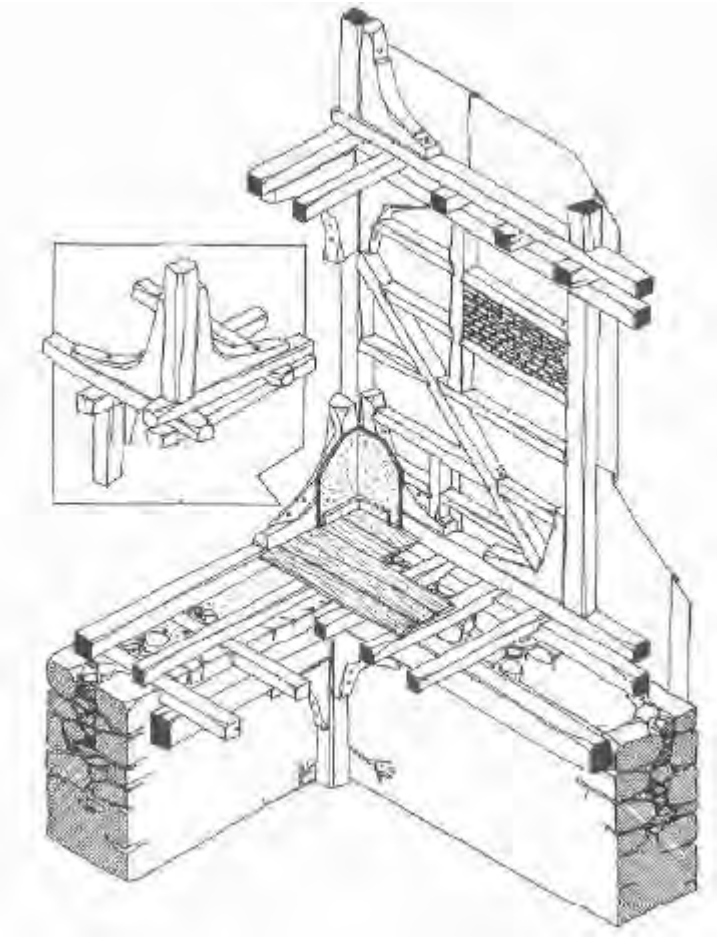

Figure 3. Timber-framed wall of traditional buildings in Lefkas.

Metal ties are used to connect the timber elements of the floor with the stone masonry and/or with the timber frame of the upper floors. Due to the small thickness of the upper floor perimetric walls, a significant reduction to the total weight of the building is achieved.

On the other hand, the stiffness of timber-framed walls is ensured thanks to the closely spaced horizontal, vertical and diagonal timber elements and their connections. Furthermore, the limited dimensions of brick masonry panels, well confined by the timber elements, ensure their satisfactory in-plane and out-of-plane behavior and reduce the possibility of failure of several brick masonry panels. In order to stiffen the connection of the timber columns (posts) with the beams, curved timber elements, of L-shape for single-sided connections or T-shaped for double-sided connections, are used.

To protect timber-framed masonry from humidity, the upper storeys are covered along their perimeter by timber planks. The high cost for the replacement of this cover (decayed with time) led to their replacement by plane or corrugated metal sheets.

In addition to masonry walls, a secondary timber bearing system is constructed also at the ground floor (Figure 4). It comprises of timber columns arranged close to the masonry walls, with rectangular or square cross section of 0.10 m to maximum 0.20 m side length. The typical distance between consecutive timber columns is 2.0 m to 3.0 m. Normaly, a single timber post corresponds to each pier, placed a few centimeters away from the wall. These timber posts are connected with the floor beams and, at the same time, are embedded into the unreinforced masonry walls of the ground storey. Moreover, the timber-framed masonry walls of the upper storey are also connected with the floor beams. Hence, the beams and the timber-framed masonry walls are supported by both the primary (masonry of the ground floor) and the secondary (timber frame) system.

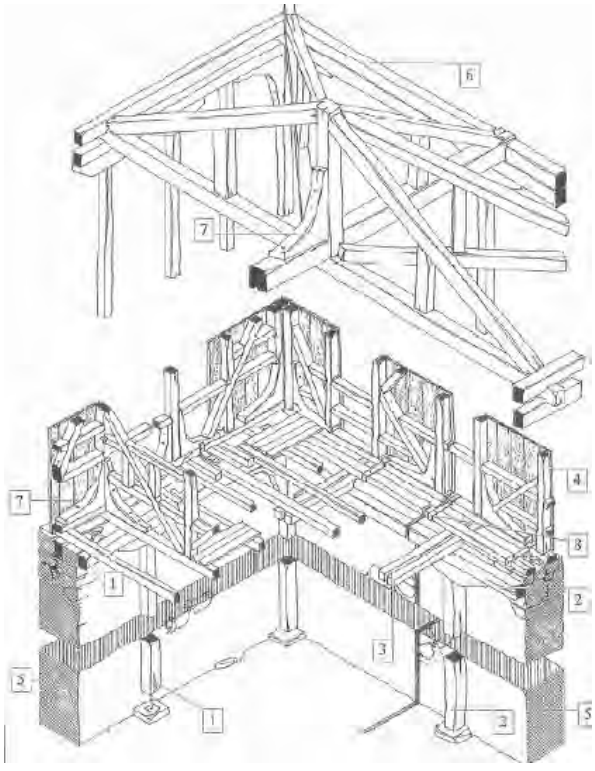

1) Secondary bearing system of timber elements next to the masonry of the ground floor supporting upper floor beams.
2) Secondary bearing system of timber elements next to the masonry of the ground floor which is parallel to the upper floor beams.
3) After the appearance of cracks in masonry, the secondary supporting timber columns start carrying the vertical loads of the upper floors
4) Timber-framed walls of the upper floors.
5) Bearing masonry walls of the ground floor supporting the timber-framed walls which are also supported by the secondary timber system consisting of timber columns and beams parallel to the masonry walls
6) Bearing system of roof base on timber-framed walls.
7) The right-angled wooden element that connects the horizontal with the vertical wooden elements ensuring the connection and the necessary stiffness.
8) Anchoring of the wooden beam of the timber-framed wall which is parallel to the floor beams. This wooden beam which supports the timber-framed walls is not directly connected to the floor beams as is the case with the wall which are perpendicular to the floor beams.

Figure 4. Structural system of a typical traditional house in Lefkas, comprising of the main and secondary bearing system.

Due to its flexibility, compared to the masonry walls, the secondary system cannot contribute immediately and significantly to the seismic response of the building. Nevertheless, its presence and its sophisticated construction in the totality of the buildings of the historical center of Lefkas indicate that it plays an important structural role in the earthquake behaviour of the building.

More specifically, during a seismic event, the interstorey drift of the ground floor is large and, therefore, the brittle stone masonry may be cracked or even partially collapsed, which can be classified as severe damage (Figure 5). In such a case however, the secondary system will be activated and it will carry the vertical loads (mainly, the self-weight of the building) until the stone masonry of the ground floor will be reconstructed or repaired. Thus, the building will be able to sustain the next earthquake. The importance of the secondary system was fully confirmed by the observed pathology of the buildings after the earthquake of 2003.

It should be noted that, due to the much higher deformability of the timber columns compared to the unreinforced masonry walls, this secondary system has displacement reserves, able to accommodate the increased displacement demand of the earthquakes, at the expense, of course, of significant damage. Consequently, the building will be able to avoid collapse, but damage will be high or possibly irreparable due to permanent displacements after the earthquake; however, adequate life safety is ensured.

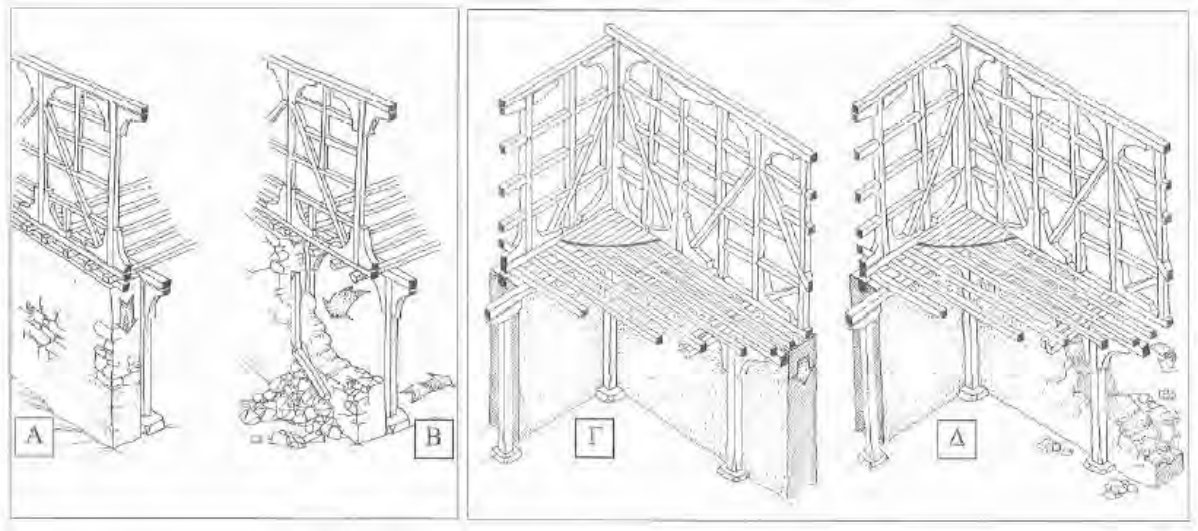

A The ground masonry supporting the floor beams
B After the appearance of cracks on masonry or of partial collapses due to the occurrence of earthquakes, the vertical timber columns support the upper floors
Γ The walls that are parallel to the floor beams together with the ground timber columns bear the upper floors loads
Δ After any partial collapse of the ground masonry due to earthquake, the beams of the upper floor are supported by the timber columns through the wooden beams.

Figure 5. Survival of the upper level timber-framed walls while the masonry walls of the ground floor collapse (Vintzileou 2003).

2. Seismic Hazard analysis

2.1. Seismicity of Lefkas

The Ionian islands present an exceptionally intense seismicity, since they are located at the transition zone between the Hellenic subduction and the continental collision between northwestern Greece and the Apulian platform in the west. Lefkas is located close to this westernmost termination of the Hellenic subduction bounded to the north by the Apulian continental collision zone. The high seismicity of the area is due to the intense crustal deformation, the highest in the whole Aegean area. Seismological evidence suggests strike slip motion in the area. The use of accurate aftershock location and fault plane solutions for the March 1973 event in the area permitted the identification of the so called Cephalonia Transform Fault, CTF, and suggested that the strike slip motion continues further north in the area of the Lefkas Island. This northern portion has been indicated as the Lefkas segment of CTF. This segment starts from the northern part of Cephalonia, strikes in the NNE-SSW direction and has a length of 40 km. This fault length is compatible with a largest 6.8 earthquake magnitude, equivalent to the largest event that struck Lefkas during the last four centuries. This Lefkas segment is characterized by dextral strike slip motion and the typical focal mechanism for an earthquake has strike 14°, dip 65° and rake 167°. This fault, along with its Cephalonia segment and other smaller faults, connect the thrust belt along the Hellenic arc in the south and the Apulian thrust belt along northwestern Greece and western Albania in the north. GPS results show that the sites at the Apulian thrust belt north of Lefkas and the Amvrakikos gulf present very small motion, whereas the Ionian islands show a homogeneous rapid southwest oriented movement, reaching 3.5 cm/year relative to southeast Italy.

The earthquakes of Lefkas are attributed to:

- the Lefkas segment of CTF such as the events of 1914, 1948, 2003 and 2015
- the thrust structure offshore northwestern Lefkas associated with the Apulian plate as the 1973 event, and
- the non-well identified faults between Lefkas and Ithaca Islands.

The earthquake documentation exists since the 16th century. Table 1 and Table 2 present the historical seismicity up to 1869 and events recorded by instruments from 1911 up to 2003.

Table 1. Events up to 1869 with different surface magnitude estimations. (Fokaefs and Papadopoulos, 2004)

Date	φN(P)	λE(P)	I_m (P)	I_{m1}-I_{m2}(FP)	M_s(P)	M_{s1}- M_{s2}	M_s(FP)
1577			8.0	?	6.20	?	?
1612 05 26	38.8	20.8	8.0	9.0-10.0	6.50	6.10-6.40	6.25
1613 10 02	38.8	20.8	8.0	9.0-10.0	6.40	6.10-6.40	6.25
1625 06 18	38.8	20.7	9.0	10.0	6.60		6.40
1630 07 02	38.8	20.8	9.0	10.0	6.70		6.40
1704 11 22	38.8	20.7	9.0	10.0	6.30		6.40
1722 06 05	38.7	20.6	8.0	8.0-9.0	6.40	5.90-6.10	6.00
1723 02 22	38.6	20.65	8.0	9.0	6.70		6.10
1769 10 12	38.8	20.6	9.0	10.0	6.70		6.40
1783 03 23	38.71	20.61	10.0	10.0-11.0	6.70	6.40-6.60	6.50
1815	38.8	20.7	8.0	9.0	6.30		6.10
1820 02 21	38.8	20.6	9.0	8.0-9.0	6.40	5.90-6.10	6.00
1825 01 19	38.7	20.6	10.0	9.0-10.0	6.50	6.10-6.40	6.25
1869 12 28	38.85	20.80	10.0	10.0	6.40		6.40

Table 2. Instrumentally recorded events up to 2003. (Fokaefs and Papadopoulos 2004)

a/a	Date (YYYY. MM. DD)	φ°_N	λ°_E	M_s	I_m
1	1911.05.24	38.70	20.70	5.30	7.00
2	1914.11.23	38.80	20.60	4.90	4.25*
3	1914.11.23	38.80	20.60	5.30	6.00*
4	1914.11.27	38.80	20.60	6.30	9.00
5	1915.02.20	38.80	20.70	5.00	4.00
6	1915.08.08	38.50	20.70	5.00	3.00
7	1915.08.10	38.50	20.70	5.30	5.00
8	1921.05.10	38.70	20.70	5.40	7.00
9	1921.10.25	39.00	20.50	5.30	5.00
10	1923.10.09	38.80	21.00	5.00	5.00
11	1938.03.11	38.80	20.60	5.60	7.00
12	1938.03.13	38.80	20.60	5.80	8.00
13	1948.04.22	38.70	20.50	6.50	9.00*
14	1948.06.30	38.80	20.60	6.40	10.00*
15	1951.01.09	38.80	20.60	5.00	4.00
16	1953.09.15	38.50	20.80	5.00	4.00
17	1957 10 08	38.90	20.60	5.20	6.00
18	1960.02.23	39.00	20.60	5.00	5.25
19	1961.12.18	38.80	20.60	5.00	5.25
20	1963.06.04	38.90	20.50	5.00	6.25
21	1971.04.19	38.70	20.50	5.30	7.00*
22	1973.11.04	38.78	20.55	5.90	7.25
23	1976.01.18	38.70	20.40	5.70	7.25
24	1978.09.14	38.90	20.60	5.10	5.25
25	1980.04.12	38.60	20.30	5.60	5.00
26	1988.04.24	38.84	20.33	5.00	6.00
27	1994.11.29	38.66	20.46	5.40	6.00
28	1994.12.01	38.69	20.55	5.30	5.00
29	2003.08.14	38.79	20.56	6.40	8.00

Local chroniclers and other sources describe the earthquake effects for the referred events:

- 1577 – The event caused serious damage at Lefkas' castle walls.
- 1612 – Two strong shakings struck the island causing the collapse of many houses as well as ground failure at different sites
- 1613 – According to local witnesses many buildings collapsed, arcades among them. A better behaviour was shown by buildings with timber framing where only roof tiles

fell while adjacent stone buildings were heavily damaged. A lot of aristocratic residences collapsed.

- 1625 – Arcades at the center of the city as well as many stone and brick masonry buildings collapsed. Widespread damage occurred at the city and its suburbs. There was report of extensive damage at the coasts of Amvrakikos gulf.
- 1630 – Arcades and many buildings collapsed at the city and its castle. Many people were killed. Ground rupturing was reported. Damage and casualties were reported from the islands of Cephalonia and Ithaca.
- 1704 – Masonry buildings were mainly damaged. Timber-framed structures resisted the shaking. 34 people were killed and many wounded. The event was felt at Corfu, Zakynthos, Preveza and Arta.
- 1722 – Two shakings struck the island and many houses collapsed.
- 1723 – A violent shaking caused the collapse of many houses. A lot of damage, especially in churches, is reported at the city of Lefkas.
- 1769 – From a total of 826 houses at the city 497 collapsed. All the churches and the eastern walls of the fortification presented extensive damage. Only seven people were killed.
- 1783 – Many villages were destroyed. There were extensive landslides. In total 855 houses and 7 churches collapsed although the number of casualties was small.
- 1815 – A lot of buildings collapsed and there were many casualties.
- 1820 – All masonry buildings, including churches, collapsed.
- 1825 - The earthquake destroyed many villages and the whole city with the exception of one house. Since then buildings started being constructed with a timber framing more resistant to ground shaking.
- 1869 – Only 20-25 buildings remained safe. Masonry buildings collapsed but those with timber framing suffered slight damage. 15 casualties were reported.
- 1914 – Mainly the western part of the island was damaged. There were 16 casualties. Timber-framed structures behaved very well with only tiles falling and minimum cracking. In many parts of the island ground failure was reported. A tsunami was also observed.
- 1948 – The southwestern part of the island was mainly affected. 244 buildings collapsed, 998 presented serious damage 2 people were killed and 45 wounded. Ground failing was observed.

Since then the large events of 1973, 2003 and 2015 present mainly extensive ground failing, although there is no extensive building damage because of adequate construction regulations. A good description of the earthquake mechanism exists for the November 15, 2015 event. The NNE-SSW alignments of aftershocks suggest rupture of the CTF which accommodates thrust motion at its two ends by a right lateral slip motion at a rate of 2-3 cm/yr. The majority of the destructive Lefkas earthquakes occurred towards the northeastern part of the fault, while the southwestern part experienced fewer. The main slip area for the 2003 event has been associated with the northern end of the fault. This event left a seismic gap in the southern part of the Lefkas part of CTF, which was filled by the 2015 event. For this event, focal mechanism solutions suggest major right lateral slip, with minor dip slip on the steep SE dipping fault offshore, the imposing cliffs of western Lefkas. There appear to exist two major slip patches at shallow depth and unilateral rupture

propagation SSW of the Lefkas part of the fault. It appears that the 2015 earthquake ruptured the shallow part of the fault, although the main slip patch goes down to 25 km depth. A slip model for the 2003 event suggests two slip patches on a deeper part of the fault, suggesting a thicker brittle crust for this region. The SW end from the uniform slip model of the 2003 event is adjacent to the northern slip patch of the 2015 earthquake.

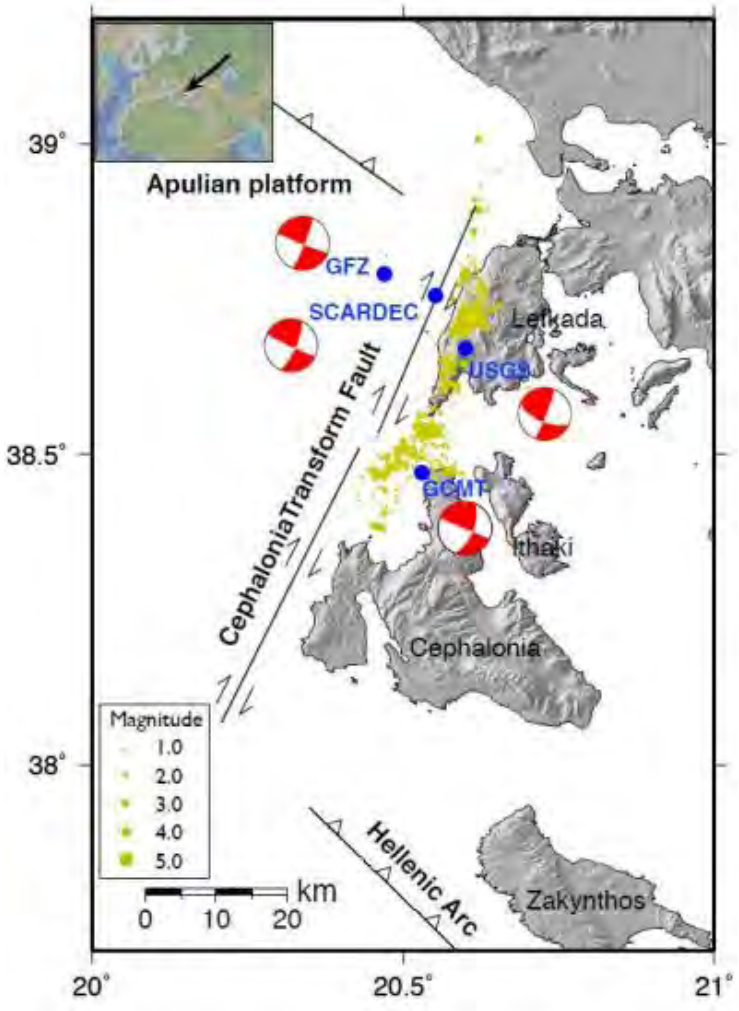

Figure 6. Seismotectonic setting of the Ionian sea region. From south to north are depicted the western end of the Hellenic arc, the Cephalonia Transform fault with its Cephalonia and Lefkas segments and the Apulian collision zone that gave the 1973 event (Bie et al. 2017).

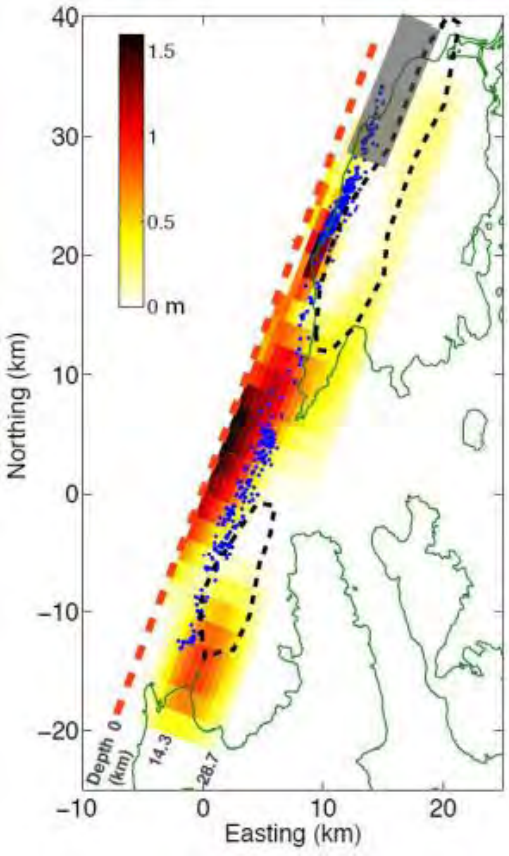

Figure 7. The focal mechanisms of the 2003 and 2015 events. The grey northern area is associated with the 2003 event slip. Black dashed lines suggest the coseismic rupture of the 2015 event. Blue dots depict the recorded aftershocks. The major slip areas of the 2015 event are shown. The thick red dashed line indicates the surface fault rupture just offshore western Lefkas (Bie et al 2017).

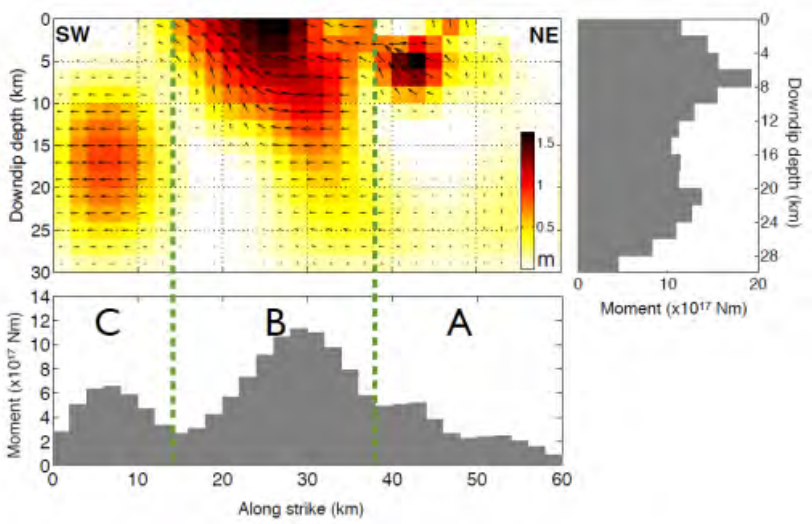

Figure 8. Slip distribution along the southern segment of the Lefkas fault for the 2015 event. Histograms present moment releases along the striking and the dipping direction of the fault (Bie et al 2017).

2.2. Probabilistic evaluation of the seismic hazard

The probabilistic approach is based on the European Facilities for Earthquake Hazard and Risk (EFEHR). EFEHR is a non-profit network of organizations and community resources aimed at advancing earthquake hazard and risk assessment in the European-Mediterranean area. Among its key objectives is to enable national and local hazard assessment by providing access to contemporary software and expertise as well as to provide access to state of the art data, models and information on earthquake hazard harmonized across Europe.

The hazard evaluation is based on the 2013 Euro-Mediterranean Seismic Hazard Model (ESHM13), which is the result of a probabilistic hazard assessment for the region carried out within the SHARE Project (Giardini et al 2014). The Model is based on the European Database of Seismogenic Faults (EDSF), a compilation of fault sources capable of generating moment magnitude earthquakes equal or larger than 5.5. The events equal or larger than 6.5 are considered to occur on the geometry of the faults, while for smaller events a background seismicity is taken into account, meaning a region containing a system of faults.

The referred model was used for the corresponding town of Lefkas with geographical coordinates of 38.83 degrees latitude and 20.70 degrees longitude. The site was considered on rock and the hazard arithmetic mean was evaluated for the peak ground acceleration and the 0.2 and 1.0 sec spectral values. It must be noted that, according to EFEHR, the main event source for Lefkas is considered the CTF fault. The hazard curves are given in Figure 9 to Figure 11 for the peak ground acceleration, the spectral acceleration at 0.2 sec period, characteristic of the constant spectral acceleration region, and the spectral acceleration at 1.0 sec period, characteristic of the constant spectral velocity region. The hazard curves are given for a rock site. Following the IBC seismic loading regulations the values are transformed in Figure 12 to spectral values for a $V_{s,30}$ = 250 m/sec ground class.

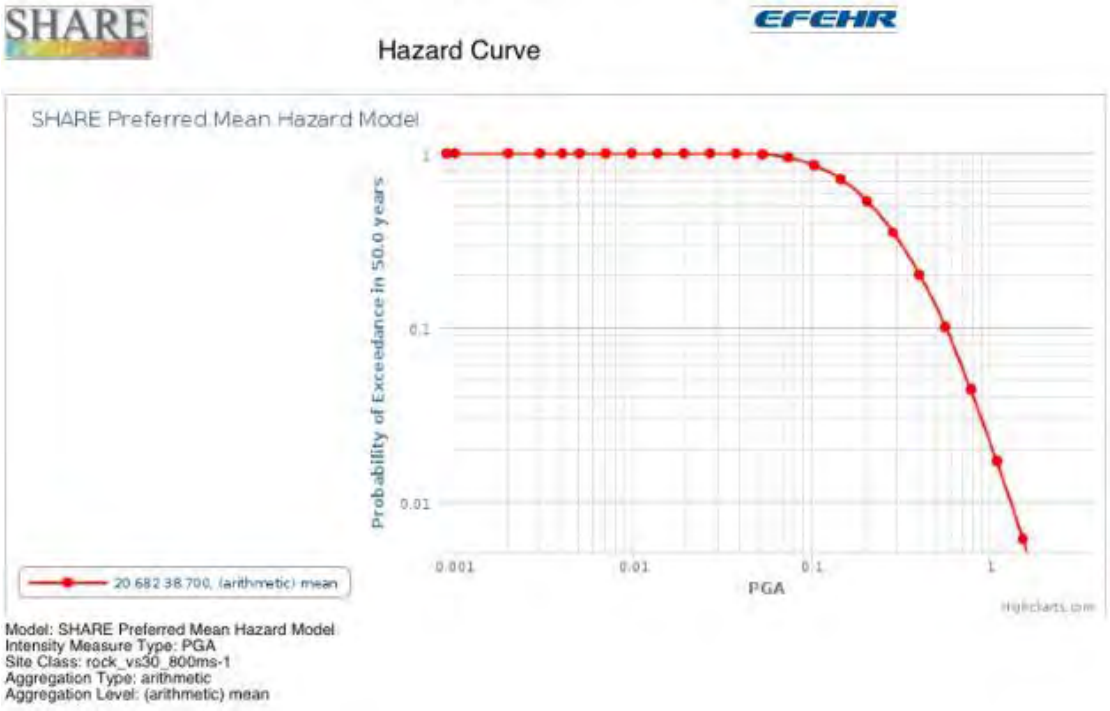

Figure 9. Peak ground acceleration hazard curve for rock site.

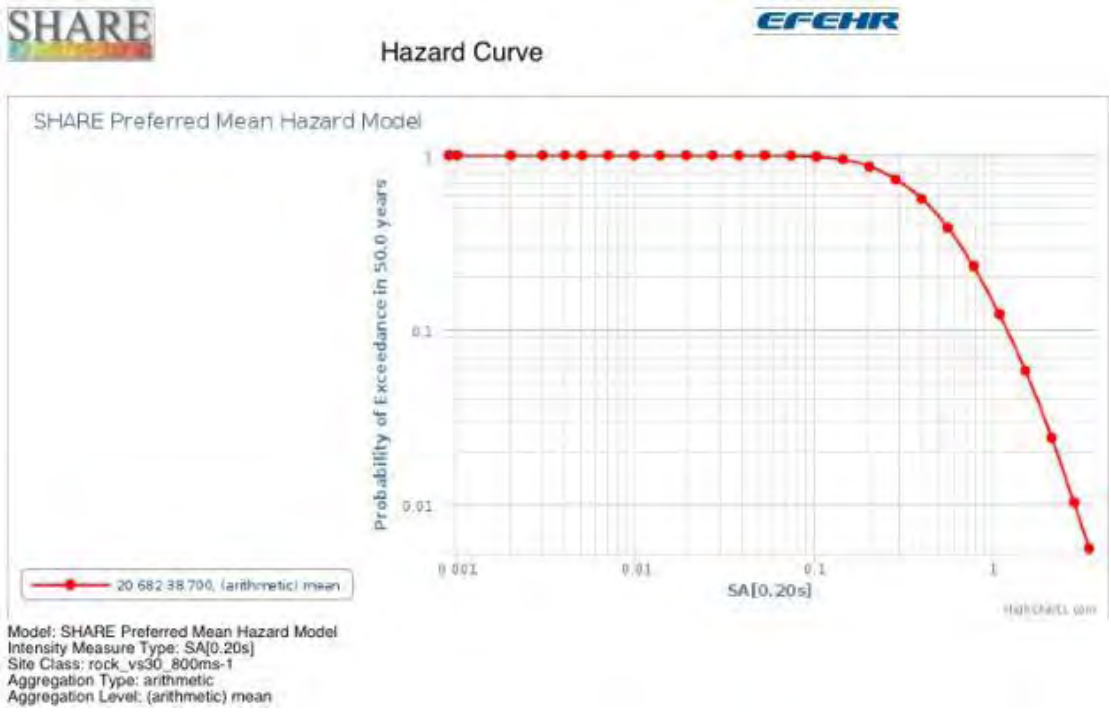

Figure 10. Spectral acceleration at T = 0.2 s, SA(0.2), hazard curve for rock site.

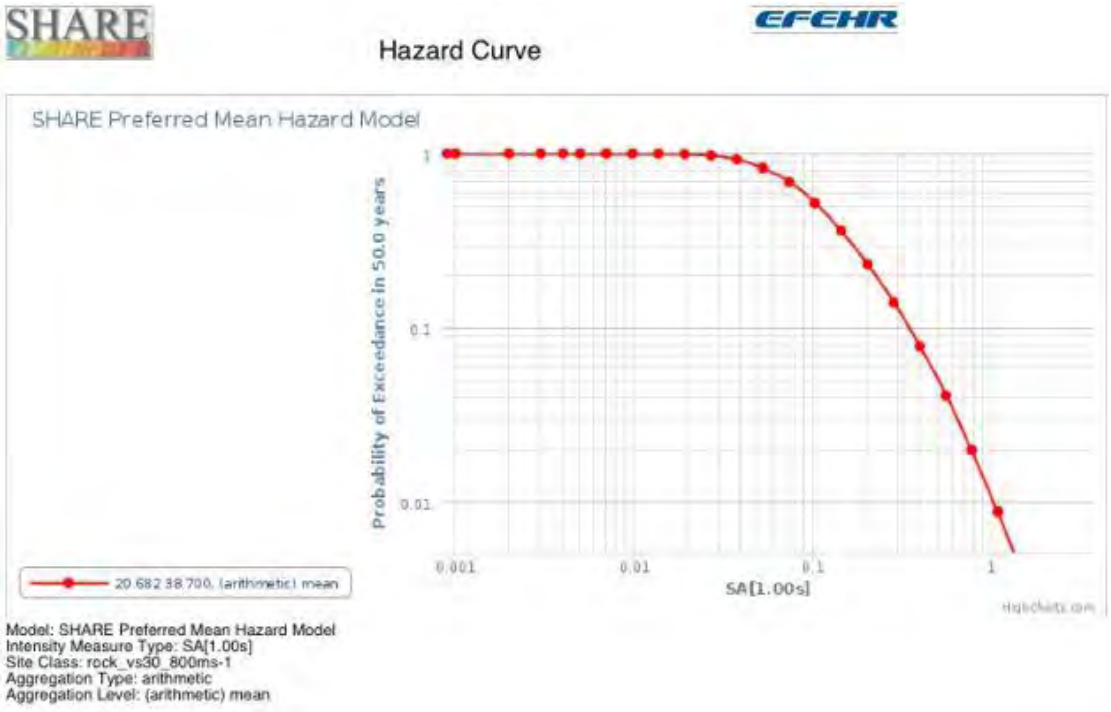

Figure 11. Spectral acceleration at T = 1.0 s, SA(1.0), hazard curve for rock site.

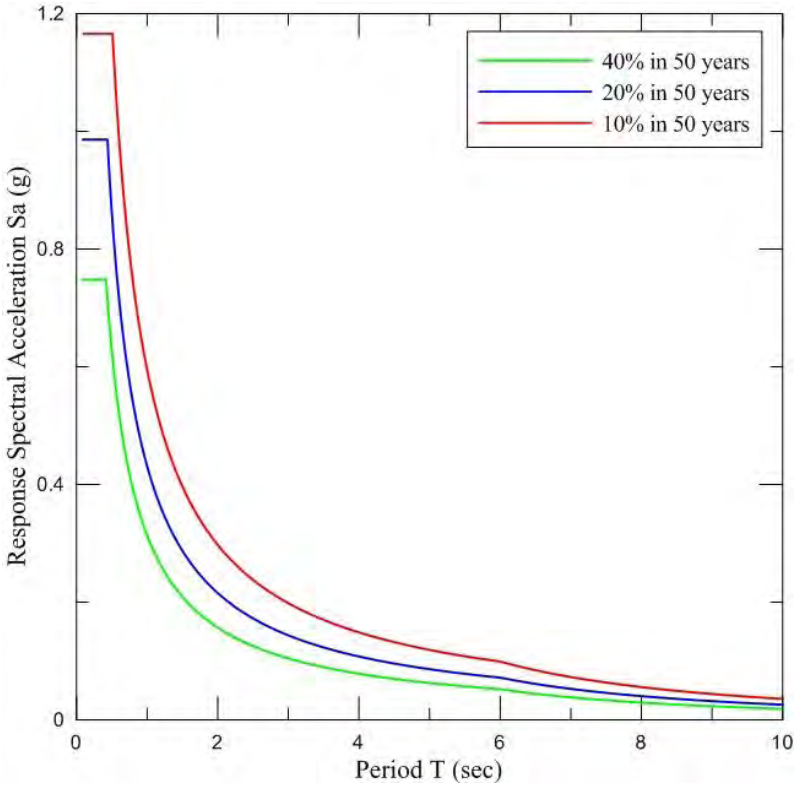

Figure 12. Uniform hazard spectra for the city of Lefkas. The spectra are given for a $V_{s,30}$ = 250 m/sec site class. The spectra exceedance probabilities are 10, 20 and 40% in a 50 year time corresponding to return periods of 475, 225 and 100 years. Spectral values are adjusted from rock site values according to IBC.

From the hazard curves, the values shown in Table 3 were evaluated for the peak ground acceleration, *PGA*, and the spectral accelerations $S_a(T$=0.2 s) and $S_a(T$=1.0 s).

Table 3. *PGA* and S_a values for T = 0.2 s and T = 1.0 s for rock sites ($V_{S,30}$ = 760 m/s) according to EFEHR hazard curves and for soft soil sites ($V_{s,30}$ = 250 m/s) according to IBC.

Probability of exceedance in 50 years	*PGA*		*Sa*(T=0.2 s)		*Sa*(T=1.0 s)	
	Rock	Soft soil	Rock	Soft soil	Rock	Soft soil
40%	0.26 g	0.30g	0.55 g	0.75 g	0.14 g	0.31 g
20%	0.40 g	0.40g	0.85 g	0.99 g	0.22 g	0.43 g
10%	0.57 g	0.47g	1.10 g	1.17 g	0.35 g	0.60 g

2.3. Fault specific seismic hazard analysis

For geologically active faults, the seismic hazard assessment can be evaluated by a fault specific approach and geological data, in order to overcome the scarcity of historical records.

The 'New Generation Attenuation Relationships' (NGA project) were used in this seismic risk analysis. The NGA project is a multidisciplinary and multi-year research program presented in 2008 for the first time while the last improved version was given in 2014 (Power et al., 2008, Bozorgnia et al., 2014). The results of the original project presentation contain an extended worldwide database with earthquakes records and metadata, a set of five ground motion attenuation models and several supporting research projects. Attenuation models are constituted by ground motion prediction equations for shallow crustal earthquakes in active tectonic regions. The use of the NGA project is expanded for a wide range of applications, from research to seismic design codes, site-specific earthquake design and evaluation and financial loss estimation. A more detailed presentation of the NGA relationships and relevant parameters is presented in Appendix A.

In the present analysis, the Lefkas segment of the CTF fault is taken into account. Its characteristics are presented in Table 4. Based on these parameters, the peak ground acceleration, *PGA*, and the spectral values $S_a(T=0.2\text{ s})$ and $S_a(T=1.0\text{ s})$ are calculated for the different methodologies of NGA (see Appendix A) and three scenarios, specifically:

- Scenario 1: extreme event of magnitude M_w=7.2 (Table 5)
- Scenario 2: Moderate to extreme event of magnitude M_w=6.8 (0)
- Scenario 3: Moderate event of magnitude M_w=6.3 (0).

The corresponding response spectra are presented in Figure 13 to Figure 24.

Table 4. Parameters considered for the fault and the attenuation relationships.

Parameter	Lefkada fault	Parameter	Lefkada fault
M	7.2/6.8/6.3	Z_{TOR} (km)	3
V_{S30} (m/s)	250	$Z_{1.0}$ (m)	-
U	0	$Z_{2.5}$ (km)	-
SS	1	ΔZ_{TOR} (km)	-
NS	0	$\Delta Z_{1.0}$ (m)	-
RS	0	Z_{HYPO} (km)	20
F_{RV}	0	DPP	-
F_{NM}	0	ΔDPP	0
F	0	F_{AS}	0
W (km)	25	Event Type	0
Dip/δ (°)	65	F_{HW}	1
λ (°)	167	HW Taper	1
R_{JB} (km)	0	Region	3
R_{RUP} (km)	7.44	F_{CL}	1
R_X (km)	8.21	F_{CN}	0
CR_{JB} (km)	0	F_{JP}	0
R_{Y0} (km)	-	F_{TW}	0
R_{EPI} (km)	-	S_J	0
R_{HYPO} (km)	-	F_{INF}	1
		F_{MEAS}	0

Table 5. *PGA*, $S_a(T=0.2)$ and $S_a(T=1.0)$ (median values) for Scenario 1 (M_w=7.2)

Method	*PGA* (g)	*Sa*(*T*=0.2) (g)	*Sa*(*T*=1.0) (g)
ABS13	0.463	0.945	0.440
ITA10	0.642	1.613	0.927
ASK14	0.394	0.847	0.388
BSSA14	0.527	1.056	0.616
CB14	0.518	0.975	1.057
CY14	0.514	1.012	0.810
IM14	1.088	2.556	0.733
AS08	0.512	0.889	0.631
BA08	0.399	0.981	0.488
CB08	0.369	0.782	0.639
CY08	0.447	0.856	0.552
I08	0.404	0.966	0.434

Table 6. *PGA*, $S_a(T=0.2)$ and $S_a(T=1.0)$ (median values) for Scenario 2 (M_w=6.8)

Method	*PGA* (g)	*Sa*(*T*=0.2) (g)	*Sa*(*T*=1.0) (g)
ABS13	0.455	0.937	0.384
ITA10	0.448	1.310	0.921
ASK14	0.368	0.802	0.317
BSSA14	0.508	1.049	0.540
CB14	0.500	0.967	0.915
CY14	0.462	0.934	0.677
IM14	0.828	1.944	0.510
AS08	0.450	0.812	0.487
BA08	0.395	0.974	0.460
CB08	0.361	0.779	0.532
CY08	0.404	0.786	0.462
I08	0.325	0.734	0.275

Table 7. *PGA*, $S_a(T=0.2)$ and $S_a(T=1.0)$ (median values) for Scenario 3 (M_w=6.3)

Method	*PGA* (g)	*Sa*(*T*=0.2) (g)	*Sa*(*T*=1.0) (g)
ABS13	0.363	0.761	0.244
ITA10	0.351	0.939	0.437
ASK14	0.303	0.695	0.205
BSSA14	0.485	1.041	0.457
CB14	0.480	0.845	0.570
CY14	0.387	0.815	0.505
IM14	0.604	1.392	0.322
AS08	0.331	0.641	0.288
BA08	0.352	0.776	0.319
CB08	0.303	0.678	0.349
CY08	0.348	0.692	0.349
I08	0.248	0.521	0.155

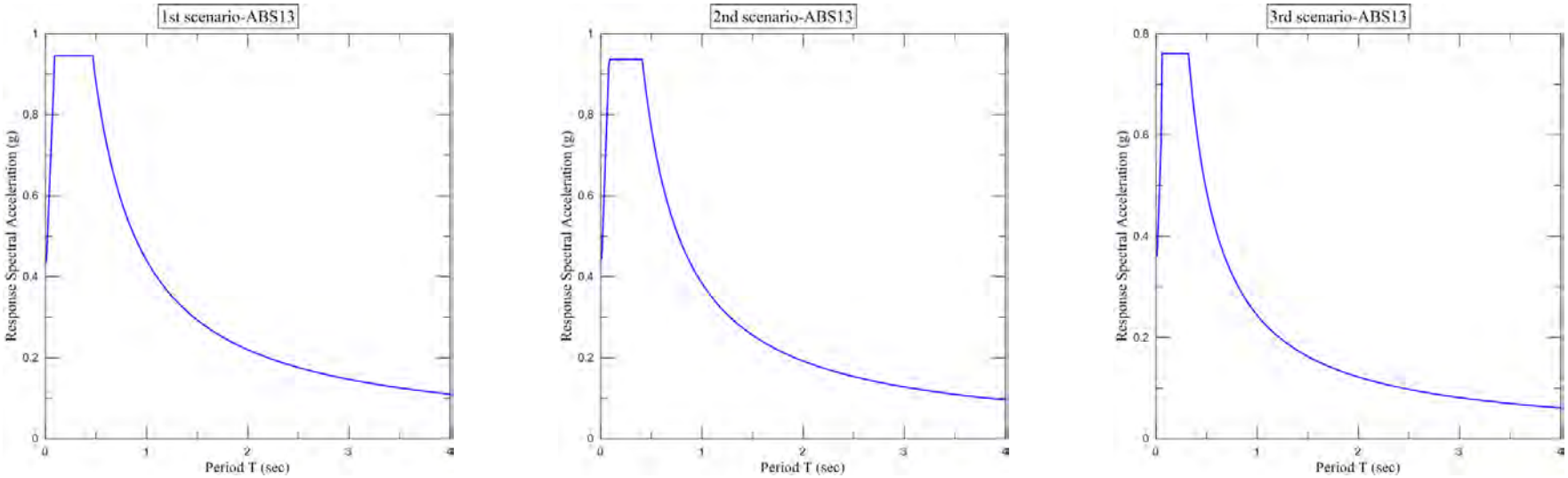

Figure 13. Response spectra for the three scenarios according to the ABS13 attenuation relationship.

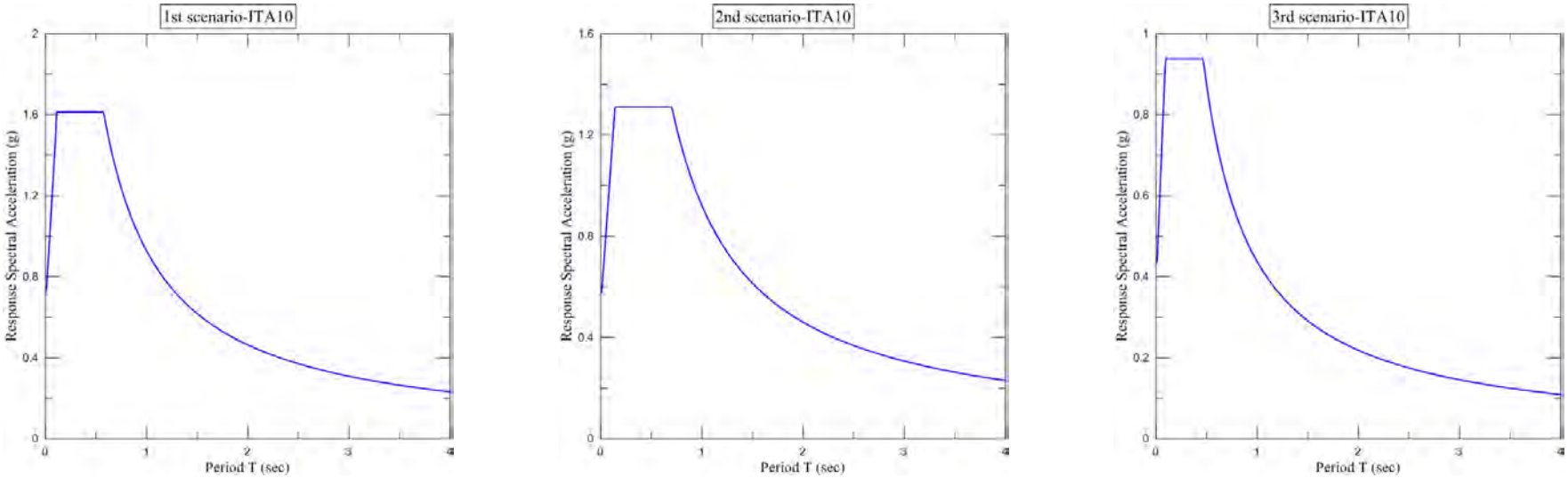

Figure 14. Response spectra for the three scenarios according to the ITA10 attenuation relationship.

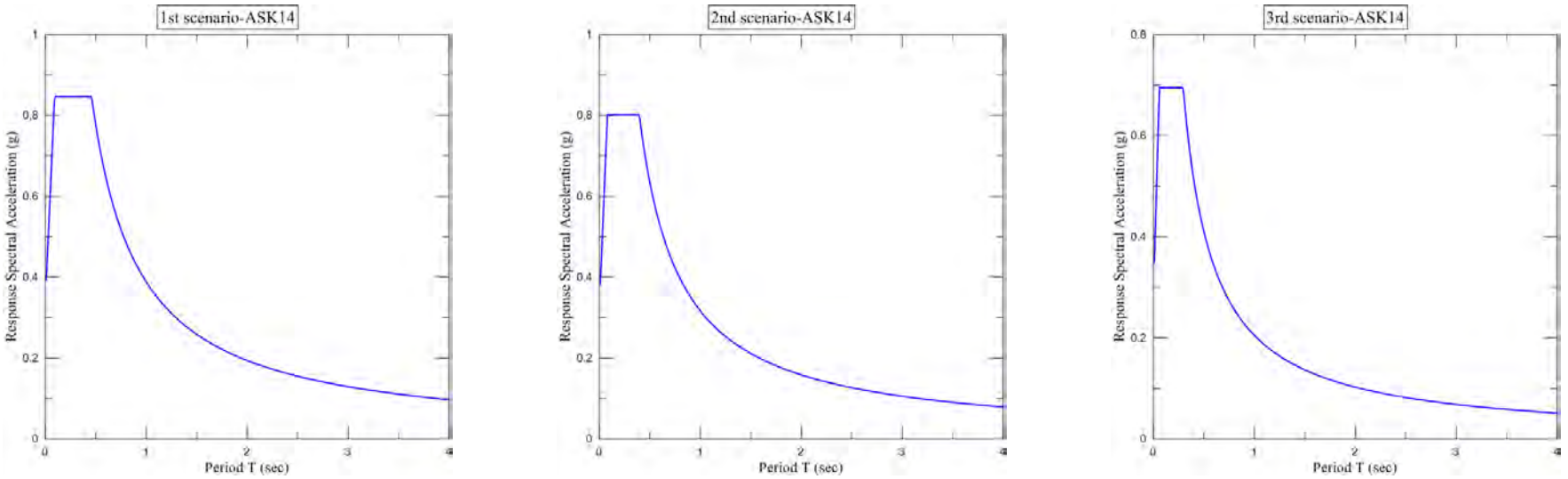

Figure 15. Response spectra for the three scenarios according to the ASK14 attenuation relationship.

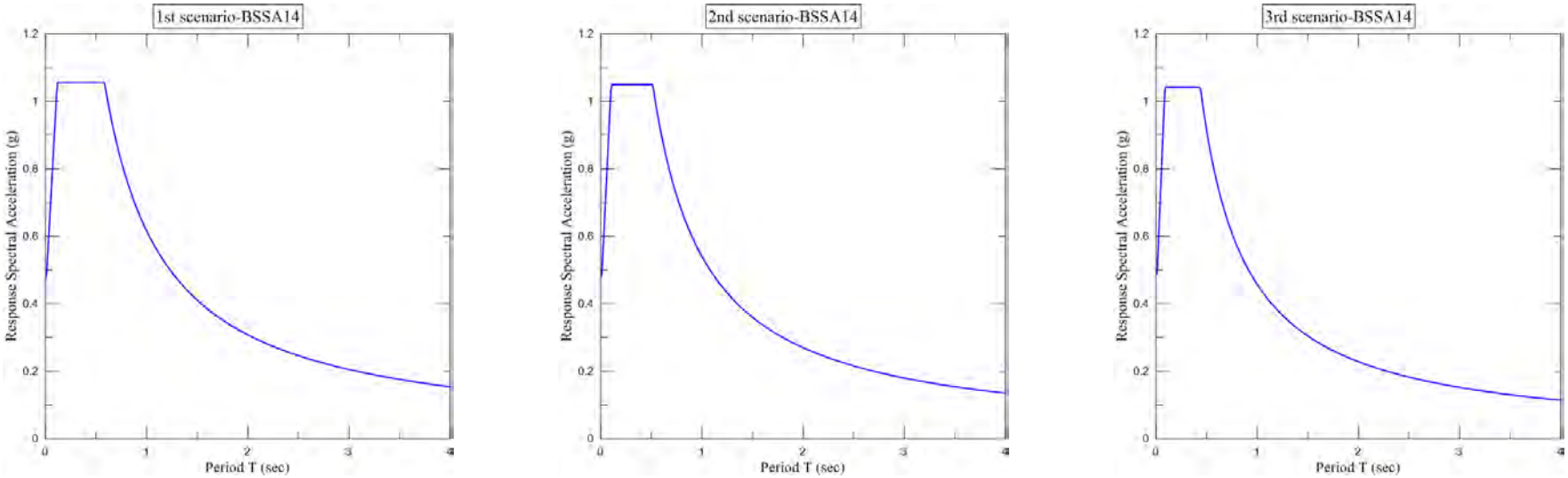

Figure 16. Response spectra for the three scenarios according to the BSSA14 attenuation relationship.

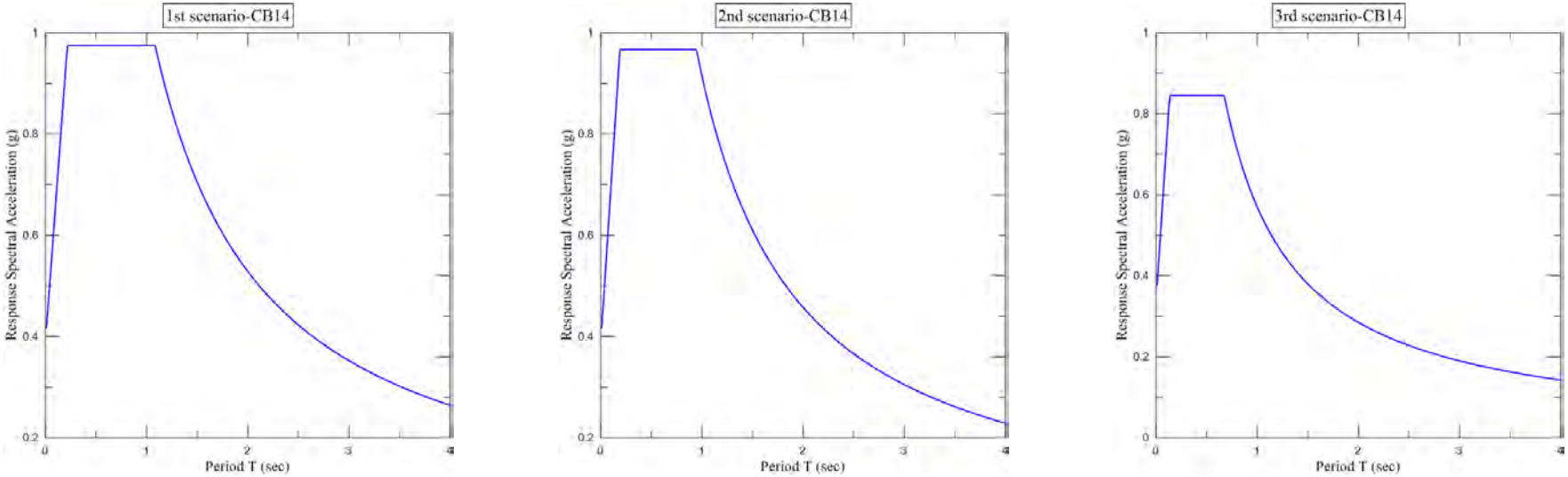

Figure 17. Response spectra for the three scenarios according to the CB14 attenuation relationship.

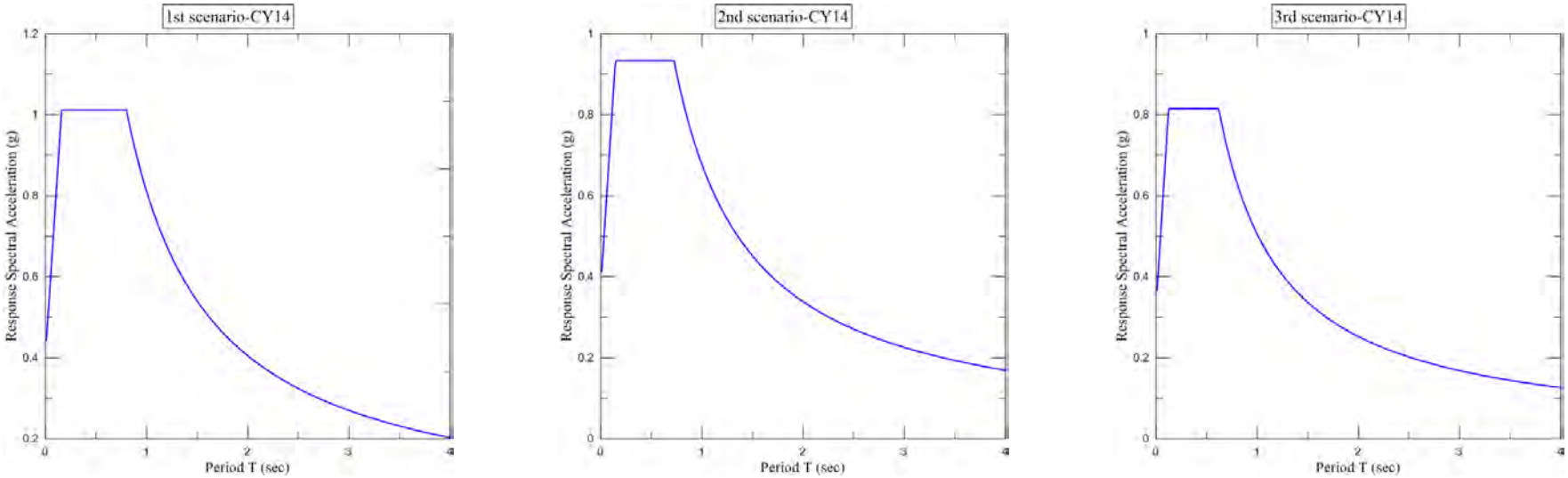

Figure 18. Response spectra for the three scenarios according to the CY14 attenuation relationship.

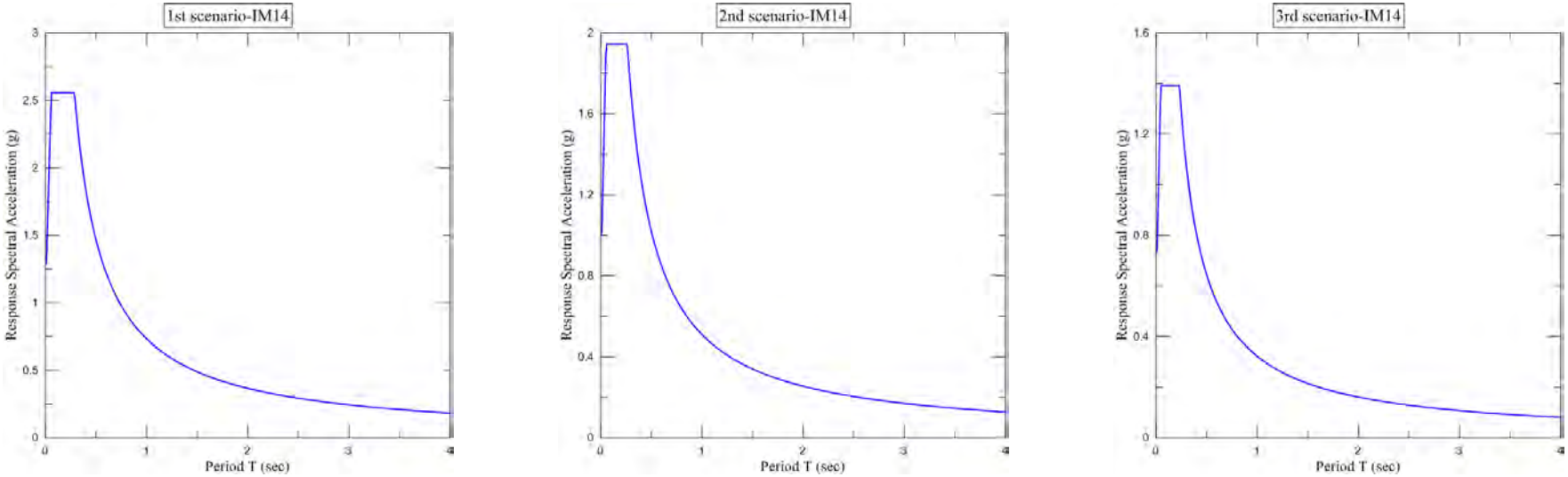

Figure 19. Response spectra for the three scenarios according to the IM14 attenuation relationship.

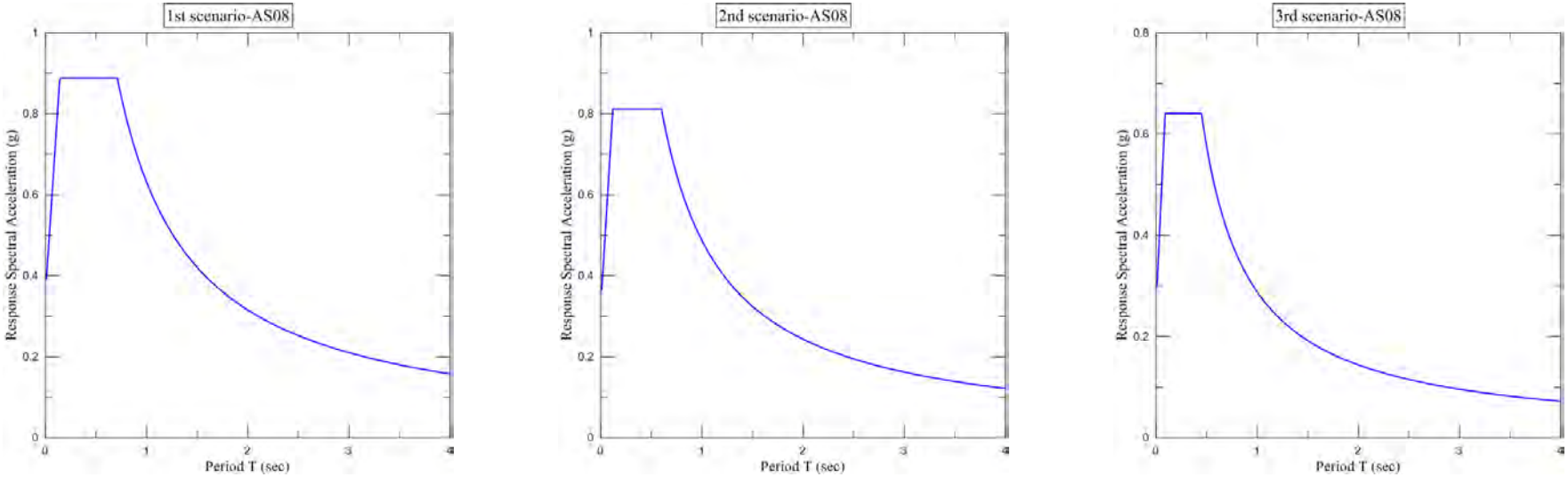

Figure 20. Response spectra for the three scenarios according to the AS08 attenuation relationship.

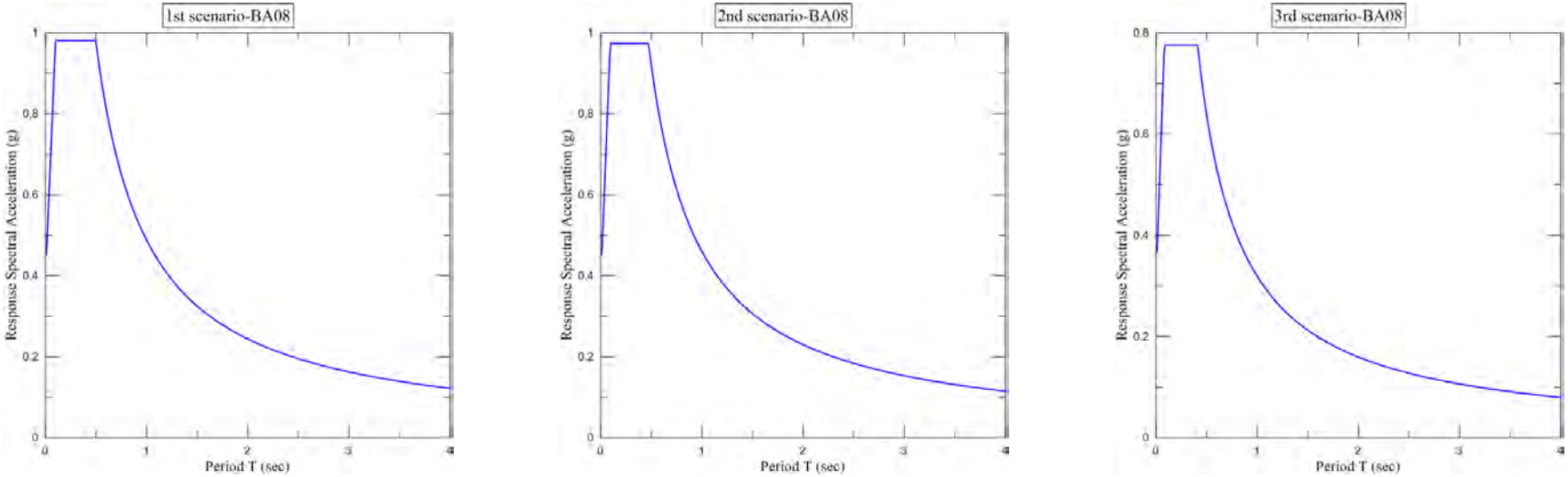

Figure 21. Response spectra for the three scenarios according to the BA08 attenuation relationship.

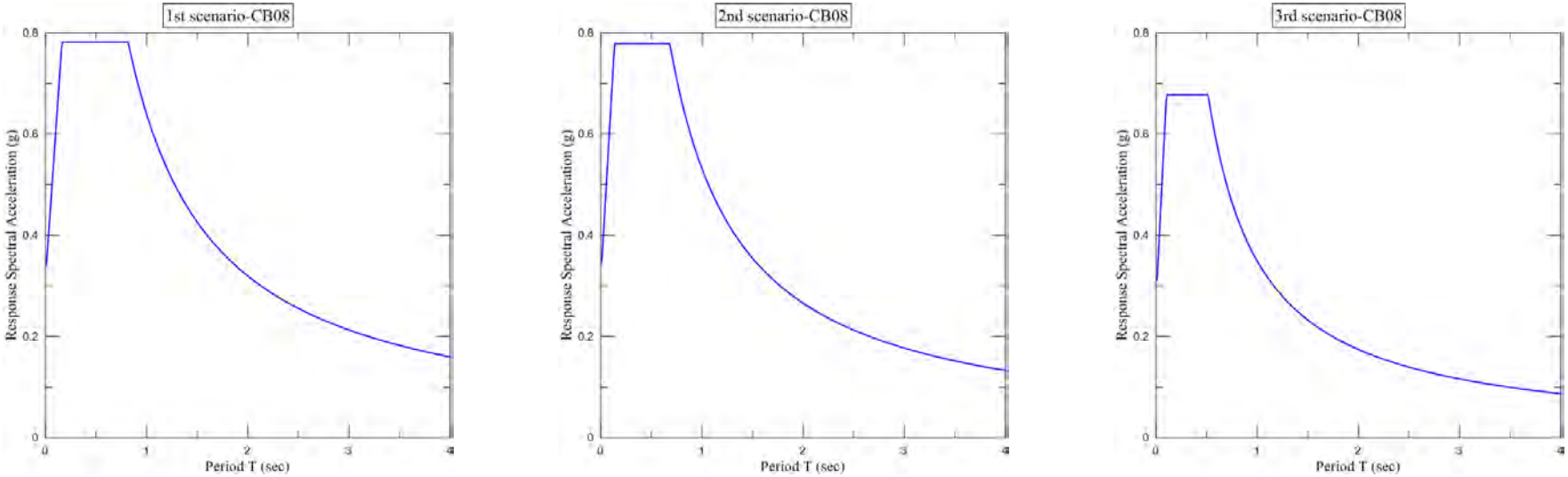

Figure 22. Response spectra for the three scenarios according to the CB08 attenuation relationship.

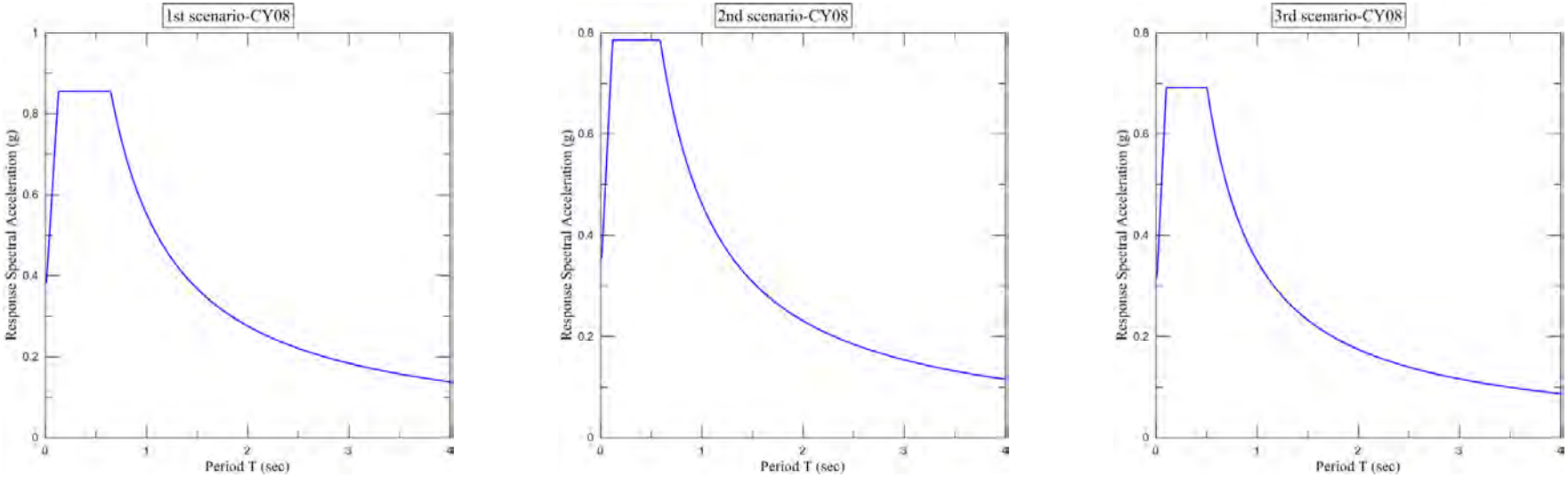

Figure 23. Response spectra for the three scenarios according to the CY08 attenuation relationship.

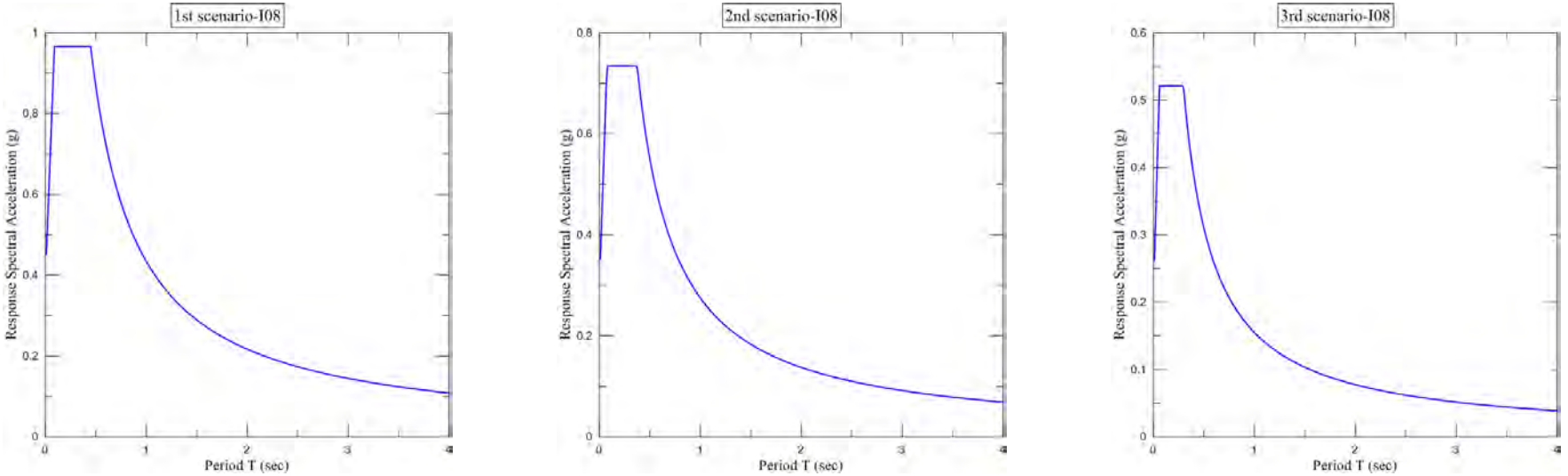

Figure 24. Response spectra for the three scenarios according to the I08 attenuation relationship.

3. Capacity analyses of the considered buildings

3.1. Introduction

In the following sections, timber-framed masonry buildings, with the previously described dual system, are examined for the determination of their capacity curves. The selected buildings have geometrical and mechanical characteristics that are typical of the timber-framed masonry structures found in the old town of Lefkas and can be used for the understanding of how the secondary bearing system is activated after the partial failure of the primary one. In order to examine at least one typical case of all the traditional buildings, two and three-storey buildings were analyzed. It should be noted that small alterations to the geometrical or material characteristics have also been examined, so as to cover a variety of structures in Lefkas. Moreover, one-storey buildings do not have two bearing systems but only one, that of the timber-framed masonry.

3.2. Description of the considered buildings

3.2.1. Three storey building

The first structure examined is a three storey building comprising of a ground floor with masonry walls and two upper stories with timber-framed walls. A typical example of a three-storey structure is the "Verikiou" building (Figure 25) which was constructed during the 1860 decade in the central square of the Lefkas city. Its size and its careful construction testify that it has been an important building, a mansion. During the rapid post-damage survey after the Lefkas 2003 earthquake, only low damage faults were observed in the building.

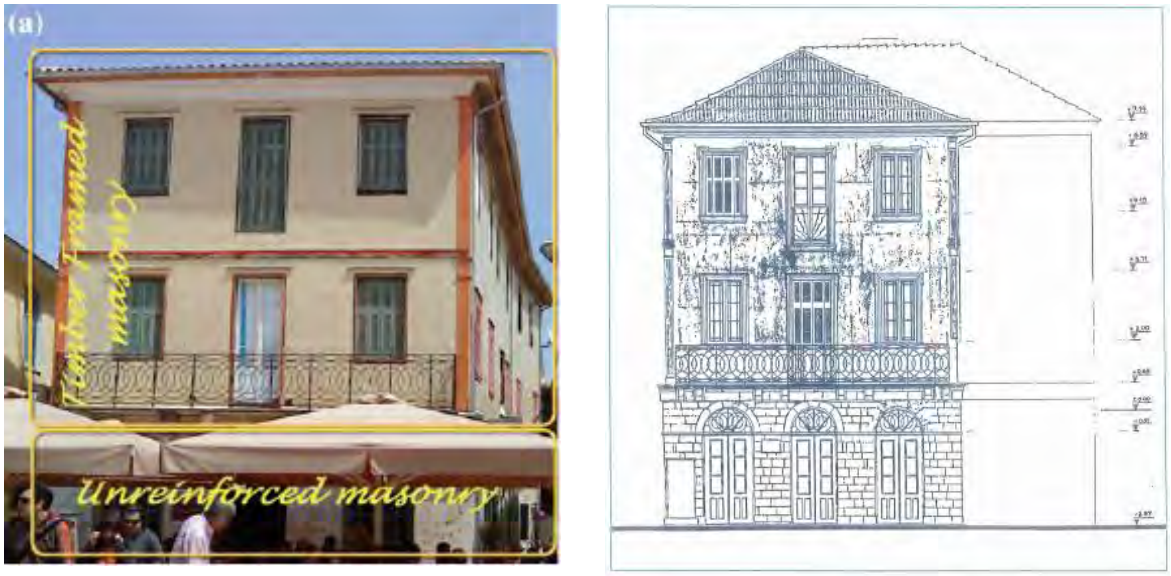

Figure 25. The Verikiou building at the central square of the Lefkas city. Left: the façade, right: architectural survey (Touliatos and Gante 1995).

The masonry of the ground floor is made of limestone, while the first upper storey is a timber-framed masonry which is assumed to have a configuration consisting of two diagonals. For the protection of the timber against weathering and dry rot, considering the vicinity to the sea, the upper storey walls are covered with thin galvanized iron sheathing.

For the analysis purposes, the cross section of the timber elements and the infill material of the timber-framed masonry were assumed 10 cm × 10 cm and 10 cm thick, respectively (Kouris, 2015) and their mechanical properties were considered to correspond to those of timber class C24. Additionally, timber columns (posts) of the secondary system were considered with a square cross section of 15 cm × 15 cm, while the distance between them was assumed about 2.5 m. The L and T-shaped angles between the beams and the posts, together with the carpentry joints and the masonry infills, result in a moment resisting connection of the timber frame. Thus, the connections of beams and posts were considered stiff, in contrast with the connections of the diagonals of the timber-framed masonry which were set free to rotate.

For the ground masonry, two different cases of material characteristics were examined. According to the first one, the ground masonry was assumed of low elasticity modulus E=2 GPa (Vintzileou et al. 2007, Kouris 2012) and a small width (0.40 m) while the second one describes a more stiff masonry having 0.9 m width and greater elasticity modulus E=4 GPa (Vintzileou 2003). The mechanical properties of the masonry and the timber elements are presented in Table 8.

For the simulation of the structure's seismic response, a beam model was utilized (Figure 26) which considers the possible crack mechanisms of a pier submitted to bending with vertical load. Masonry was considered isotropic in this beam-modelling approach as the strength differences in the two axes are not substantial, however timber was treated as orthotropic.

Table 8. Material characteristics of masonry and timber elements of the three storey building.

	Masonry (1st case)	Masonry (2nd case)	Wood
Compressive strength $f_{c,x}$ (MPa)	3.50	3.50	18.9
Compressive strength $f_{c,y}$ (MPa)	3.50	3.50	4.77
Tensile strength $f_{t,x}$ (MPa)	0	0	18.9
Tensile strength $f_{t,y}$ (MPa)	0	0	4.77
Modulus of elasticity E_x (MPa)	2000	4000	11000
Modulus of elasticity E_y (MPa)	2000	4000	370
Shear modulus G (MPa)	833	1665	690
Weight (kN/m^3)	20	20	3.5
Poisson ratio v	0.2	0.2	0.3

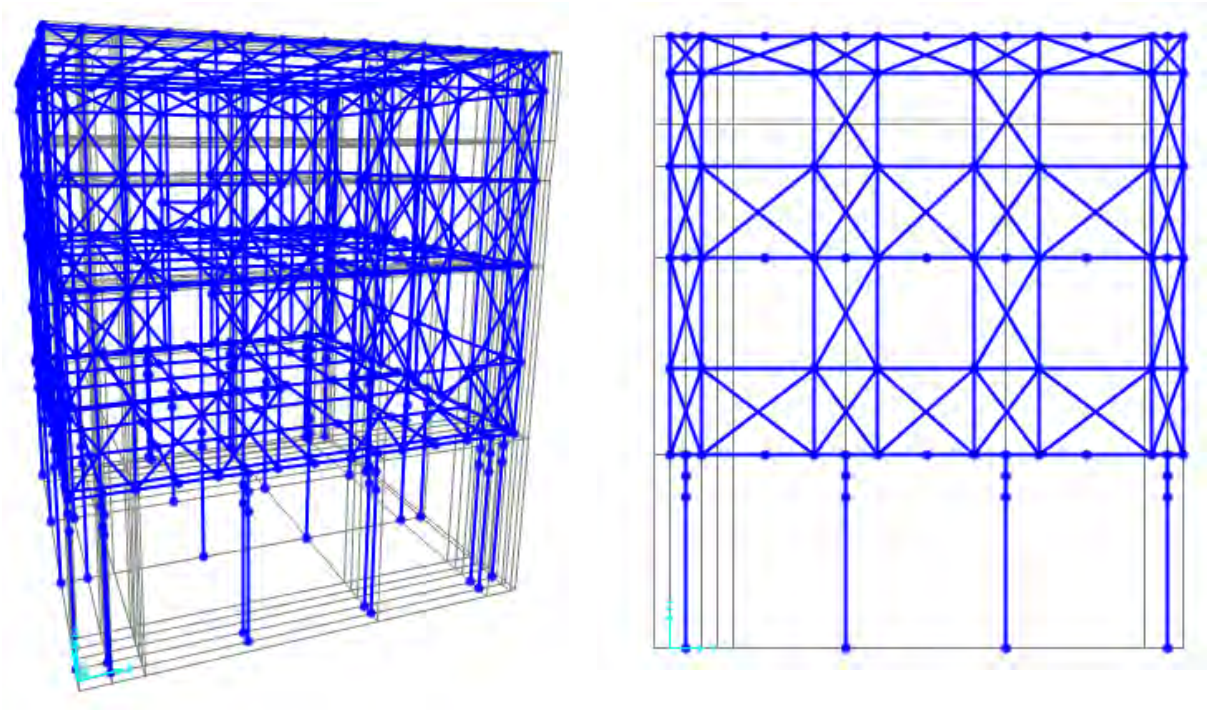

Figure 26. The numerical model of the three storey building and its façade.

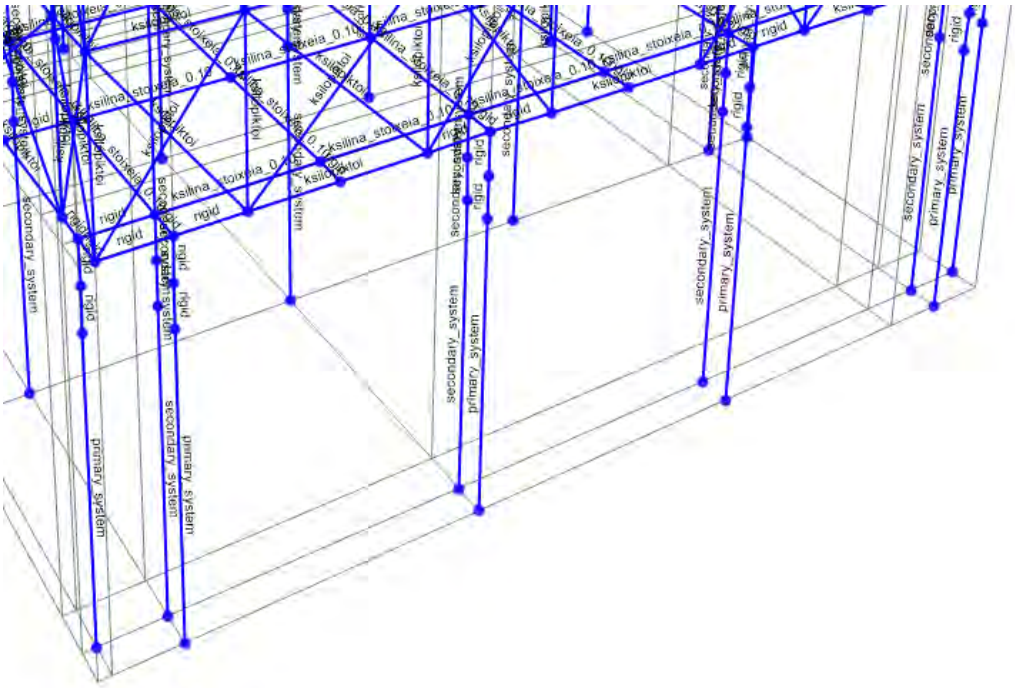

Figure 27. Piers and timber columns of the primary and secondary systems respectively. The timber columns are 10cm behind the ground masonry wall.

As it is easily noticed from the façade (Figure 27), the upper storeys were based on the masonry piers of the ground plan (cross section in Figure 27, named primary system) while the floor stands on the secondary system (cross section in Figure 27, named secondary system).

3.2.2. Two storey building

The second examined structure belongs to Lefkas two storey buildings and was based on the geometry of "The Zambelion" house (Figure 28) located in the heart of the traditional Lefkas town. Today it is owned by the Municipality of the Island and it has been declared preserved. Opposite the Zambelion House is the temple of St. Nicholas, one of the central temples of the old town with particularly Architectural features. The house has so far been rescued by all major earthquakes of the last 200 years, especially the 1825 earthquake which was particularly devastating. The earthquake of August 14, 2003, just like the previous catastrophic earthquakes, had little impact on the wonderfully structured building.

Figure 28. The Zambelion house. Top: the façade; bottom: plan view of the ground floor (Papadatou-Giannopoulou 2014).

The ground floor has an area of 294.64 m^2 and the upper floor is 259.74 m^2. However, for the analysis purposes, the two floors were considered to have the same area. The ground walls are made of 0.60 m width stone masonry and the outer/inner walls of the upper floor are timber-framed masonry of 20 cm thickness. Apart from the ground masonry walls, the upper floor was also based on a system of timber columns with 3.0 m distance between them. The mechanical properties of the masonry and the timber elements are presented in Table 9. Similar to the three storey building, for the simulation of the structure's seismic response, a beam model was utilized (Figure 29).

Apart from the "Zambelion house", another two-storey building having the same geometrical and material characteristics of ground and upper floor with the three-storey presented in the previous section, was analyzed for comparison reasons (Figure 30).

Table 9. Material characteristics of masonry and timber elements of the two storey building.

	Masonry	Wood
Compressive strength $f_{c,x}$ (MPa)	3.50	18.9
Compressive strength $f_{c,y}$ (MPa)	3.50	4.77
Tensile strength $f_{t,x}$ (MPa)	0	18.9
Tensile strength $f_{t,y}$ (MPa)	0	4.77
Modulus of elasticity E_x (MPa)	4000	11000
Modulus of elasticity E_y (MPa)	4000	370
Shear modulus G (MPa)	1665	690
Weight (kN/m^3)	20	3.5
Poisson ratio v	0.2	0.3

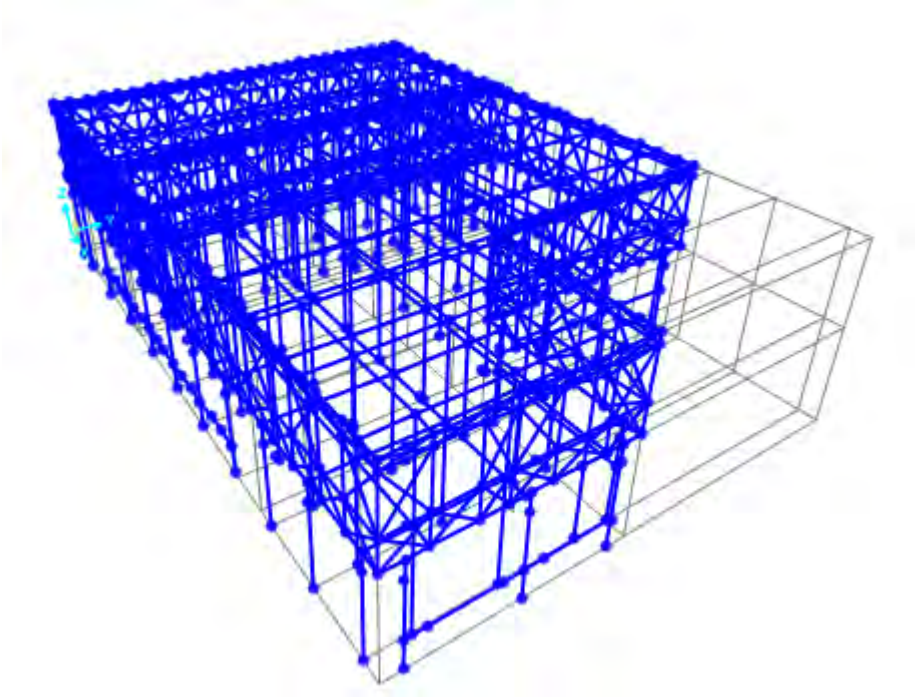

Figure 29. The numerical model of the two storey building (geometry based on the Zambelion House)

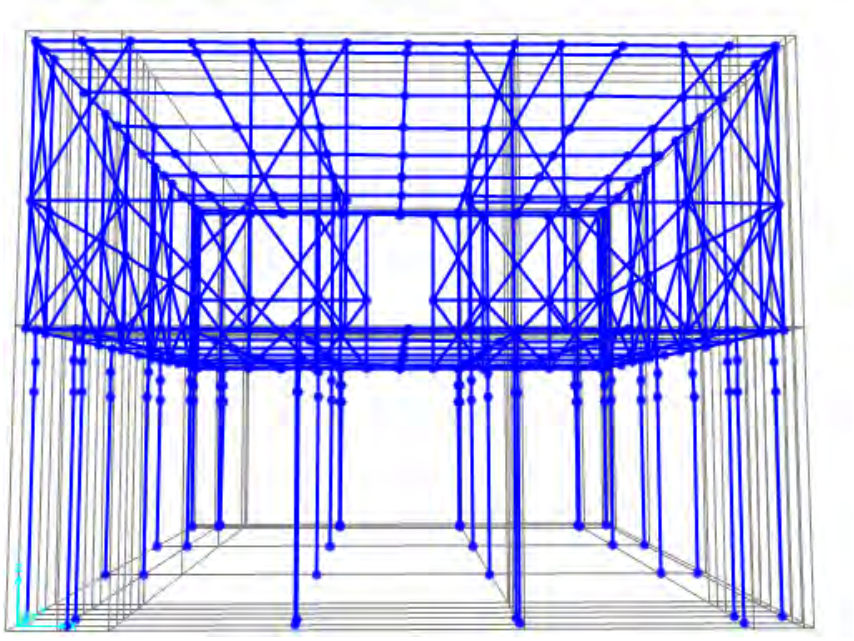

Figure 30. The numerical model of the two storey building (geometry based on the three storey presented in the previous paragraph after removing one floor).

3.3. Capacity curves

A numerical model with yielding beam elements, simulating the seismic response of the entire structure, was developed in order to determine the capacity curves of the examined structures. The model comprises of strut elements and non-linear hinges on the diagonals of the timber-framed masonry to accommodate all plastic deformation of the timber-framed walls. A set of empirical formulas were used to determine the nonlinear law of the axial hinges (Kouris 2012) in the diagonal struts in terms of axial load versus displacement, and then they were inserted in the diagonals as point plastic hinges. In fact, these formulas have been derived from the nonlinear analysis based on Hill-type plasticity of a detailed model of timber-framed masonry panels subjected to horizontal loading and computing the corresponding displacements. The nonlinear law of the plastic hinges in terms of axial load versus deformation was formed using the yield and ultimate shear and displacement from the following expression

$$N_{diag} = V\frac{\sqrt{H^2+L^2}}{L},\ \mu_d = \frac{\delta_u}{\delta_y} = \frac{u_{diag,u}}{u_{diag,y}}$$

$$u_u = 1.2\cdot u_{diag,\max}\ \textit{and}\ N_{res} = 0.2\cdot N_{diag,\max}$$

where u_u is the maximum axial deformation, $u_{diag,\max}$ the axial deformation at maximum axial force, N_{res} is the residual axial force after the drop in strength, $N_{diag,\max}$ is the maximum axial load and μ_d is the displacement ductility, as well as the ductility in terms of axial deformation.

Moreover, the axial stiffness of the diagonals was modified in order to take into account their sliding according to the following equation [Kouris et al 2014]

$$k_s = \frac{\left(H^2+L^2\right)^{3/2}+H^3}{EA}\cdot\frac{1}{L^2}\cdot\frac{V_y}{\delta_y}$$

where H, L are the height and the span of each timber frame, E is the elasticity modulus, A is the cross section area, u_y and V_y is the horizontal displacement and shear yield, respectively

The nonlinear law (Figure 31) set to the struts depends mainly on the geometrical characteristics of each timber frame, the strength of the timber elements and the vertical loads. Therefore, a discretization of the building into individual timber-framed panels and separate examination of them was performed before setting the nonlinear law.

The unreinforced masonry piers of the ground storey were modelled using moment-rotation lumped plasticity hinges (Figure 32) according to Kappos et al (2002) and Penelis (2006). This model and more specifically the determination of the strength of the masonry with respect to bending requires the estimation of the axial load of the piers from a preliminary linear elastic analysis. As a result, the constitutive M-ϑ law of the critical sections (top and bottom) of each pier is defined. It is important here to note that the failure of the piers depends significantly on the vertical load from the upper storeys. In fact, due to the low vertical load of the upper storeys, masonry is likely to fail due to out or in plane bending.

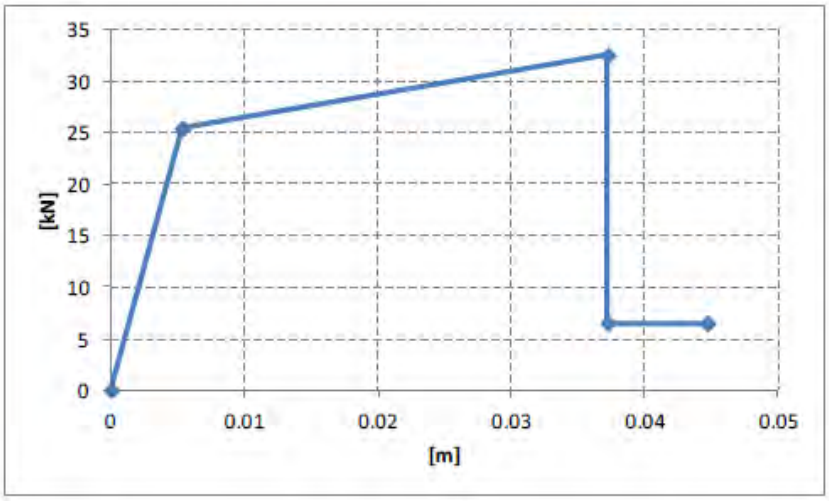

Figure 31. Nonlinear law of the plastic hinge set to the diagonals of three-storey building.

Figure 32. Presentation of nonlinear hinges set on masonry piers and diagonal elements of timber-framed masonry.

Concerning the boundary conditions of the piers and the timber columns (posts), masonry piers and timber columns are assumed to be fixed and hinged, respectively. The timber posts, which are next to the masonry walls in a distance of 5 to 10 centimeters, stand on a curved masonry base which has a nail in its center to achieve the connection with the timber column. Therefore, the choice of hinged support is justified.

Timber columns are not subjected to gravity loads under service conditions of the building and support to the upper floors gravity loads is provided solely by the primary system (i.e. the unreinforced masonry ground storey). Moreover, during the first phase of the seismic response (primary system) the contribution of the timber posts to the lateral capacity is negligible compared to that of the ground masonry. In fact, their contribution to the seismic response of the structure mainly starts after the partial collapse of the walls. However, both systems are considered in the same numerical model, simulating therefore the actual condition of the structure. As it is presented in the following sections, where the capacity curves are derived for each structure, the partial collapse of the masonry becomes noticeable during the pushover analysis due to the sudden reduction of the total base shear and the structure's stiffness.

3.3.1. Three-storey building

The total geometry of the structure was modeled using beam elements. Elastic dynamic analysis of the structure, assuming fixed supports for the masonry elements and hinges for the timber ones, was performed and the first eigenperiod was computed equal to T_1=0.27 sec for elasticity modulus E=2 GPa and masonry width 0.40 m and equal to T_1=0.23 sec for elasticity modulus E=4 GPa and masonry width 0.90 m. The first eigenmode corresponds to translation along the small side of the structure, namely direction x (Figure 33). It is noted that similar results were obtained from Kouris (2015) who developed two numerical models of the façade of the structure (2-d analysis); one for the primary system (masonry walls of the ground floor with thickness 0.80 m) and the other for the secondary system (ground timber columns).

It is noted here that both the primary and secondary systems were included in the same structure in order to reduce the assumptions of the numerical model and obtain results closer to the actual behaviour of the structure. Therefore, the eigenperiods calculated correspond to a structure where the two systems coexist. The simulation of both the primary and secondary system increase the accuracy of the analysis, since the second one is activated automatically when the earthquake has led the first one to failure. However, many times, the subsequent activation of the two systems with significant difference in their stiffness may prone to numerical instabilities that can cause error and/or early termination of the analysis. The possibility for these instabilities is minimized when displacement control pushover analysis is applied.

Two different pushover load patterns were applied to each direction corresponding to the first mode of the structure (mode proportional loads) and the mass contribution of the structure (mass proportional loads). Capacity curves from the non-linear static analyses of the two cases of modulus of elasticity of the ground masonry, in terms of base shear versus top displacement, are presented in Figure 34.

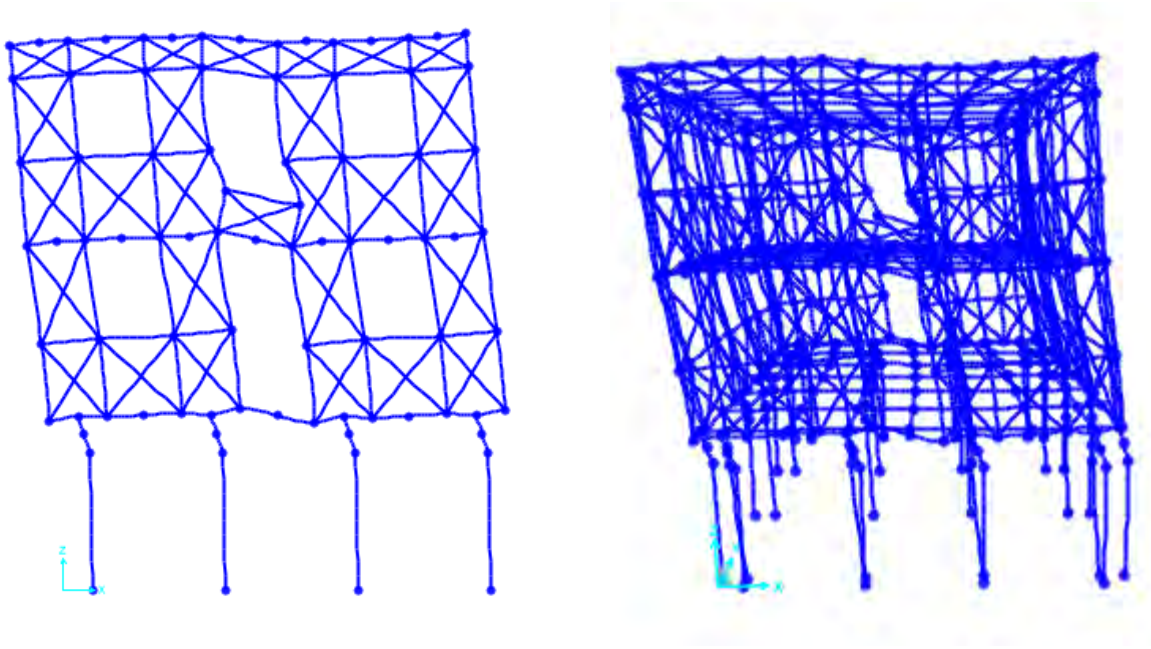

Figure 33. First eigenmode, corresponding to translation along direction *x* of the model.

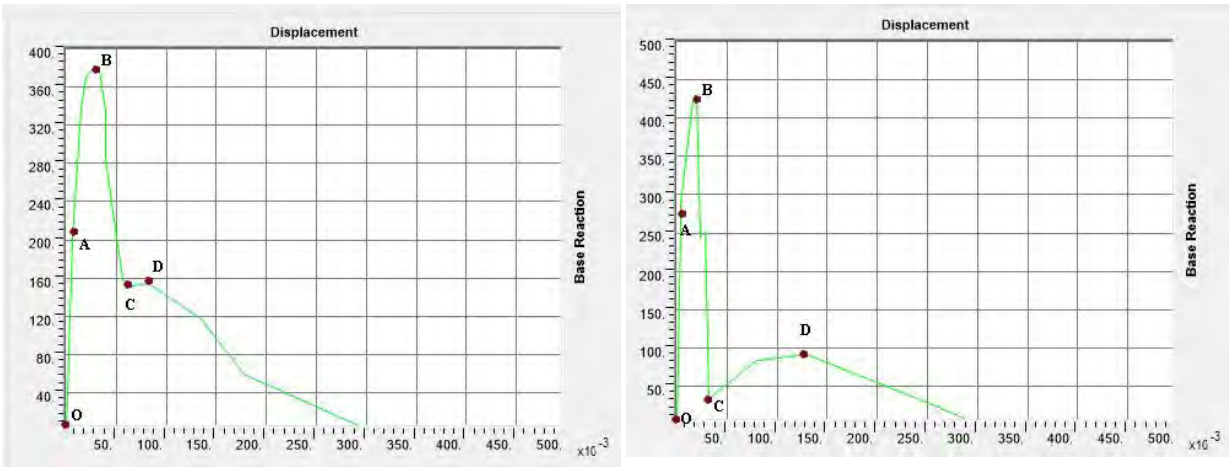

Figure 34. Capacity curves of three-storey buildings with modulus of elasticity of the masonry of the ground floor equal to: (a) *E*=2 GPa (1st case) and (b) *E*=4 GPa (2nd case).

In Figure 34, Point A on the capacity curves corresponds to the first yield of the masonry piers and therefore plastic deformations raise in the structure. The stress condition which corresponds to the point A, namely the first plastic hinges of the structural members, are presented in Figure 35, where the different colors indicate their damage state (pink color indicates the yield rotation of the cross section contrary to red color which shows the upper limit of possible rotation of the hinge).

Subsequently, due to the stress redistribution, new hinges appear in the structure. Point B on the capacity curves shown in Figure 34 corresponds to the maximum base shear that can

develop in the structure; in that state, most of the piers are already in the plastic zone (Figure 36). In fact, point B can be treated as the limit where partial collapses appear in the masonry wall of the ground floor, because although the upper limit of rotation of the plastic hinges has not been reached, the appearance of plastic deformation at the bottom and upper node of the pier can cause collapses. Finally, point C corresponds to the failure mechanism of the primary system (Figure 37). At the same time the secondary system is activated and plastic deformations start to appear at the upper nodes of the timber columns as it is depicted in Figure 38. It should be reminded that the support of the timber posts is set as free to rotate (hinged supports).

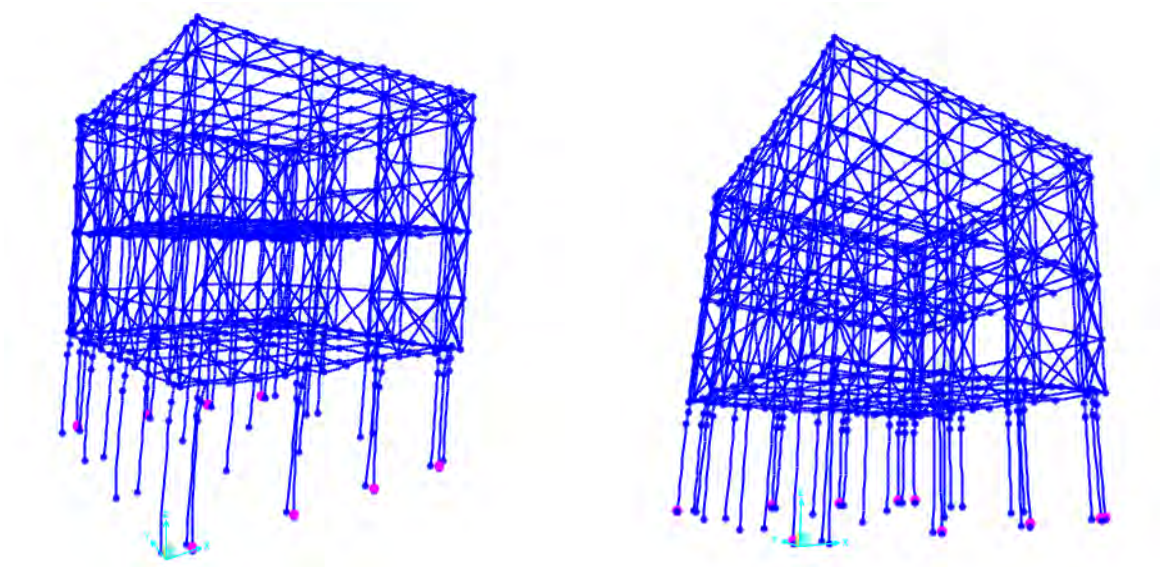

Figure 35. First hinges appearance at the base of the masonry.

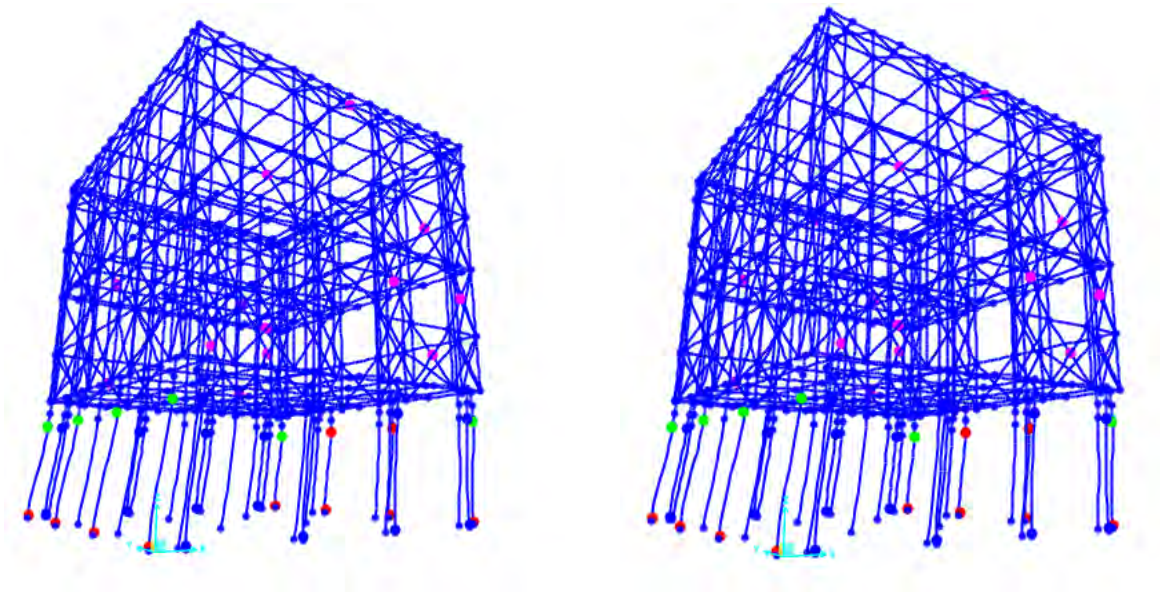

Figure 36. Hinges at the base and the top of the masonry at the time when the maximum base shear is reached.

Collapse of the building is due to the development of a ground storey mechanism. However, damages have already appeared in the upper timber-framed masonry as it is indicated by the appearance of hinges along diagonal elements (Figure 36). The evolution of the plastic deformation in the ground storey is rather quick and, finally, the failure mechanism dominates.

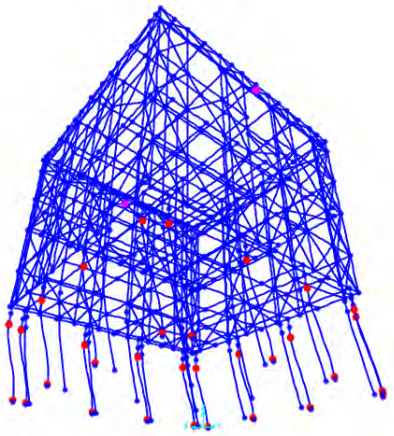

Figure 37. Failure mechanism of the ground masonry wall. Hinges correspond to point C on the capacity curves.

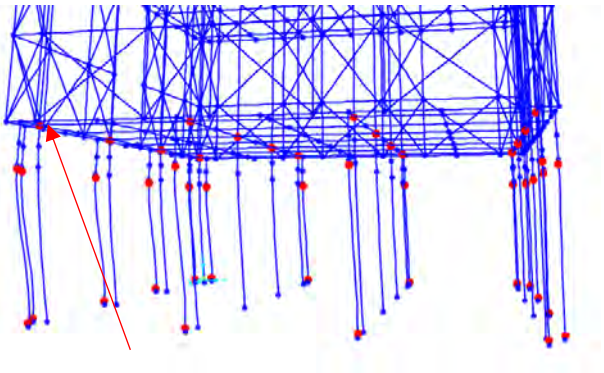

Figure 38. Activation of the secondary system and appearance of hinges in the timber elements.

The following segments are depicted in the capacity curve's diagrams: (i) the quasi-elastic part (O–A) where, in principle, no plastic deformation appears; (ii) the second part (A–B) where non-linear deformation occurs in both the ground storey and the timber-framed masonry upper storeys; (iii) the sudden drop in the base shear capacity during the third part of the capacity curve (B–C) due to the collapse of the ground storey unreinforced masonry piers; and (iv) the residual capacity during the fourth part of the response (C–D) wherein the building has a reserve displacement capacity under a small increase in the base shear. The relatively low axial force on the unreinforced masonry piers resulting from the overturning moment leads to almost simultaneous failure of the unreinforced masonry piers of the ground storey.

Based on the ATC-40 method, the capacity spectra in terms of *Sa* – *Sd* for the two examined cases of modulus of elasticity are presented in Figure 39.

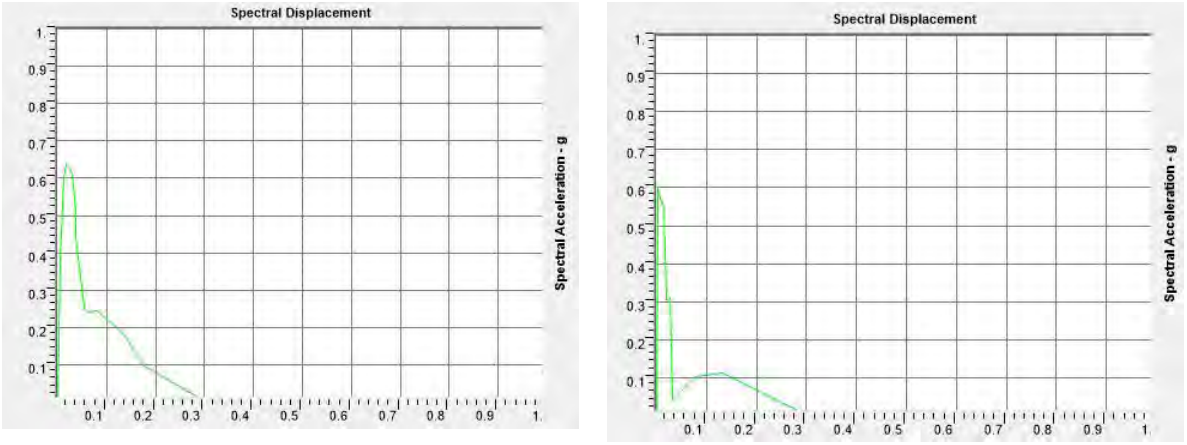

Figure 39. Capacity spectra along x direction of the three storey building for: (a) *E*=2 GPa and (b) *E*=4 GPa of the masonry walls of the ground floor.

3.3.2. Two storey building (Examined Structure No 1)

The two storey building, which was based on the Zambelion plan view, has three masonry walls at the ground floor along *y* direction and two along *x* direction of total span 22.3 m. Elastic dynamic analysis of the structure, assuming fixed supports for the masonry elements and hinges for the timber ones, was performed and the first and the fourth eigenperiods were computed equal to 0.09 sec and 0.07 sec respectively, with eigenmodes corresponding to translation along the directions *y* and *x* respectively (Figure 40). The second and the third eigenmodes also correspond to translation in direction *y*.

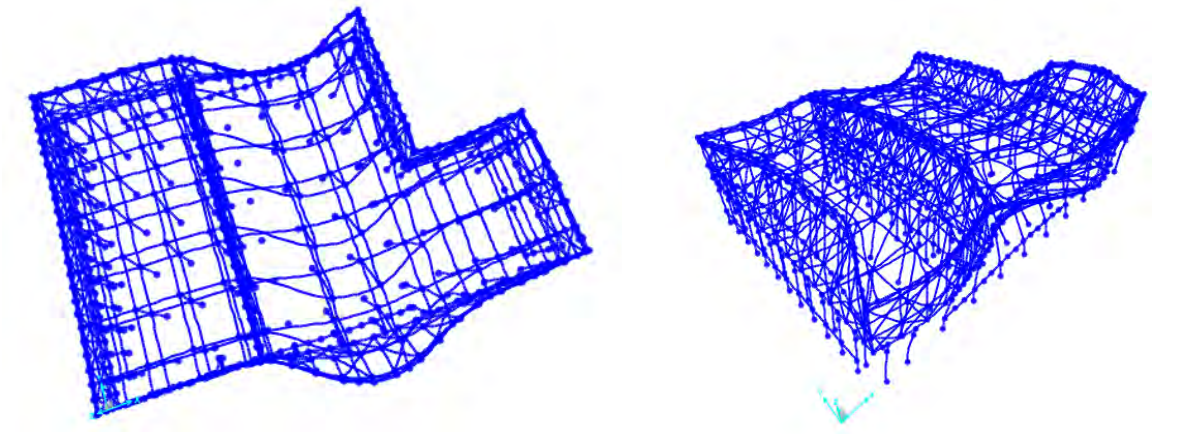

Figure 40. First and fourth eigenmodes, translational along directions y and x of the model, respectively.

It is noted that both the primary and secondary systems were included in the same structure in order to reduce the assumptions of the model and obtain results closer to the actual behaviour of the structure. Therefore, the eigenperiods calculated correspond to a structure where the two systems coexist.

Capacity curves from the non-linear static analyses of the structure along *y* and *x* direction, in terms of base shear versus top displacement, are presented in Figure 41. Due to the significant stiffness and mass of the structure, the base shear reaches higher values compared with the three-storey building. Moreover, the observed sudden reduction in the base shear corresponds to the collapse of the intermediate wall, while the remaining walls can still carry the larger horizontal zones.

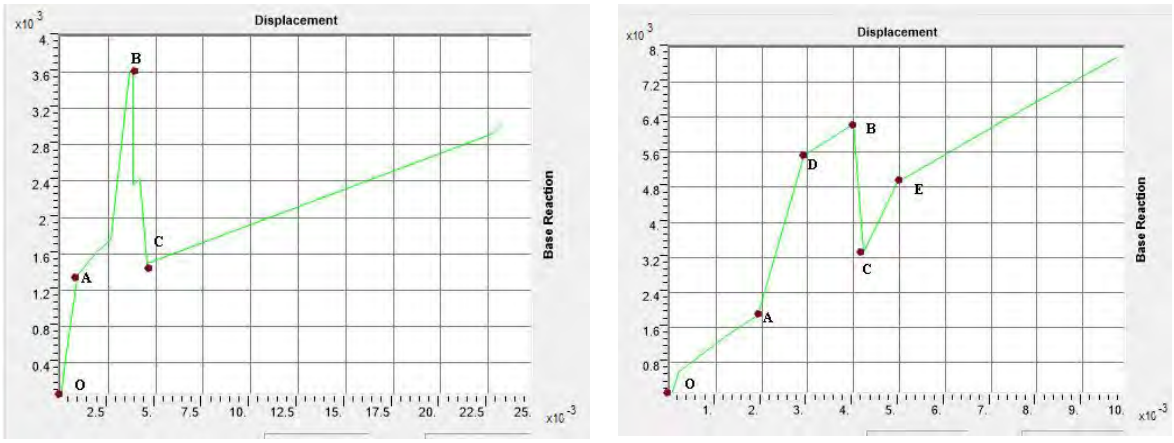

Figure 41. Capacity curves of the two-storey building in directions (a) *y* and (b) *x*.

In Figure 41, Point A corresponds to the first yield of the masonry piers and therefore plastic deformations raise in the structure. The first plastic hinges of the structural members are presented in Figure 42, where the different colors indicate their damage state (pink color indicates the yield rotation of the cross section contrary to red color which shows the upper limit of possible rotation of the hinge).

Subsequently, due to the stress redistribution, new hinges appear in the structure. Point B correspond to the maximum values of the base shears before the collapse of any of the masonry walls of the ground floor (Figure 43). In fact, point B can be treated as the limit where partial collapses appear in the masonry wall of the ground floor. It should be noted that, although the upper limit of rotation of the plastic hinges has not been reached, the appearance of plastic deformation at the bottom and the upper node of the pier can cause collapses. However, even if the middle wall collapses, the rest of the masonry walls of the ground floor can carry horizontal forces, therefore, the base shear force increases. Finally, point C corresponds to the failure mechanism of the middle wall (Figure 44) and due to the large area of the ground storey, the vertical loads are carried by the secondary system.

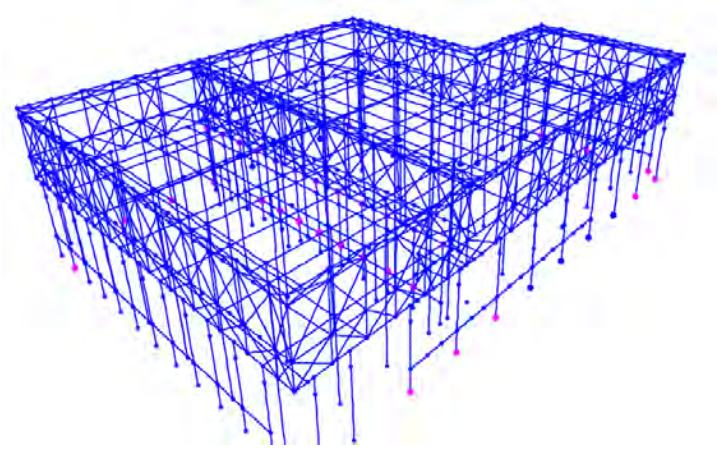

Figure 42. Deformation and distribution of hinges corresponding to point A on the capacity curve along *y* direction.

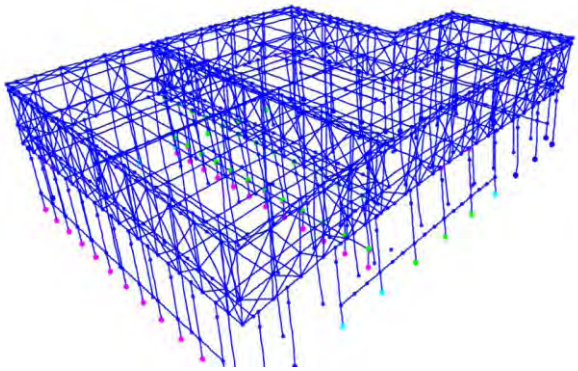

Figure 43. Deformation and distribution of hinges corresponding to point B on the capacity curve along *y* direction.

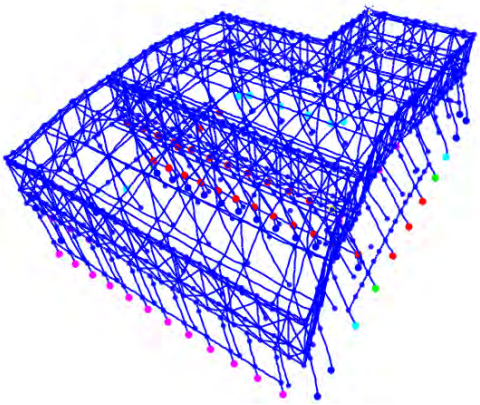

Figure 44. Deformation and distribution of hinges corresponding to point C on the capacity curve *y* along direction.

3.3.3. Two -storey building (Examined Structure No 2)

As it was mentioned in the previous paragraph, a second two storey building, having the same geometrical and material characteristics of ground and upper floor with the three storey building presented before, was analyzed for comparison reasons.

Elastic dynamic analysis of the structure, assuming fixed supports for the masonry elements and hinges for the timber ones, was performed and the first eigenperiod was computed equal to T_1=0.21 sec for elasticity modulus E=2 GPa and masonry width 0.40 m and equal to T_1=0.17 sec for elasticity modulus E=4 GPa and masonry width 0.90 m. In both cases, the first eigenmode corresponds to translation along the small side of the structure, namely direction x (Figure 45).

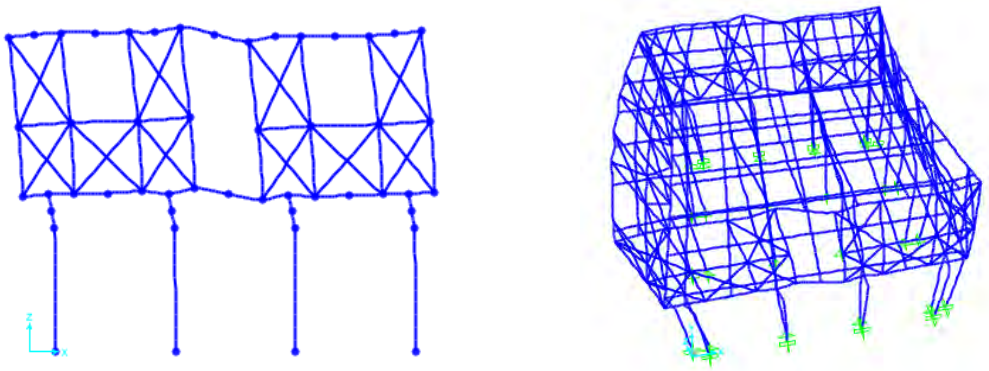

Figure 45. First eigenmode, translational along direction x of the two – storey structure.

Capacity curves from the non-linear static analyses of the two cases of modulus of elasticity of the masonry of the ground floor, in terms of base shear versus top displacement, are presented in Figure 46.

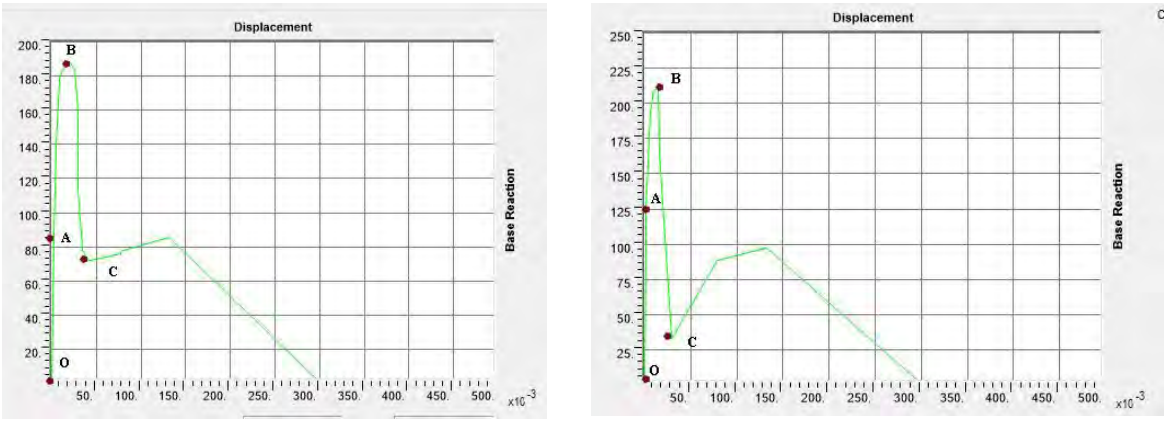

Figure 46. Capacity curves of the two-storey buildings with modulus of elasticity for the masonry of the ground floor equal to (a) E=2 GPa (1st case) and (b) E=4 GPa (2nd case).

Similar conclusions can be drawn with the analysis presented for the three-storey building (Figure 47 to Figure 50). However, it important to notice that the maximum base shear is reduced due to the reduction in vertical loads, which leads to smaller bending strength of the masonry walls of the ground floor.

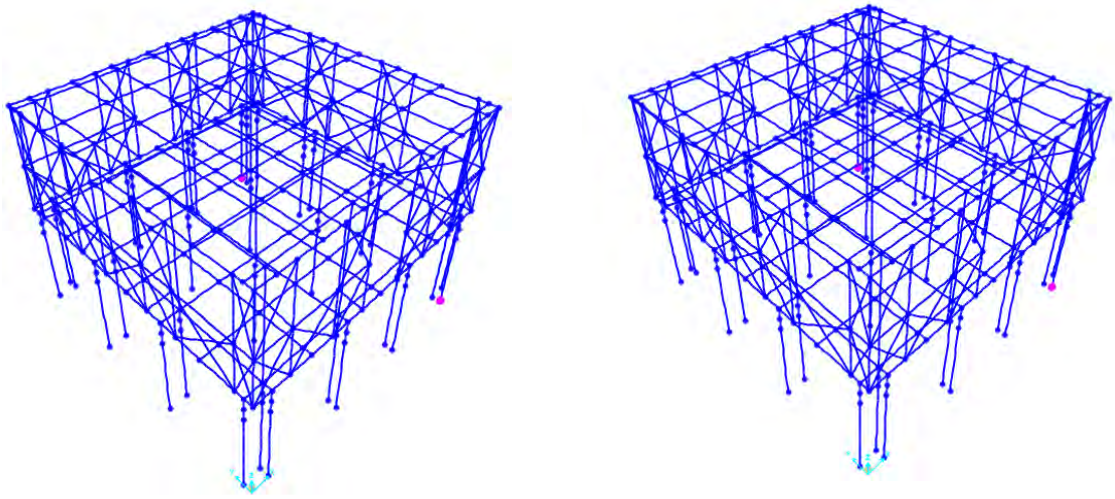

Figure 47. First hinges at the base of the ground masonry piers.

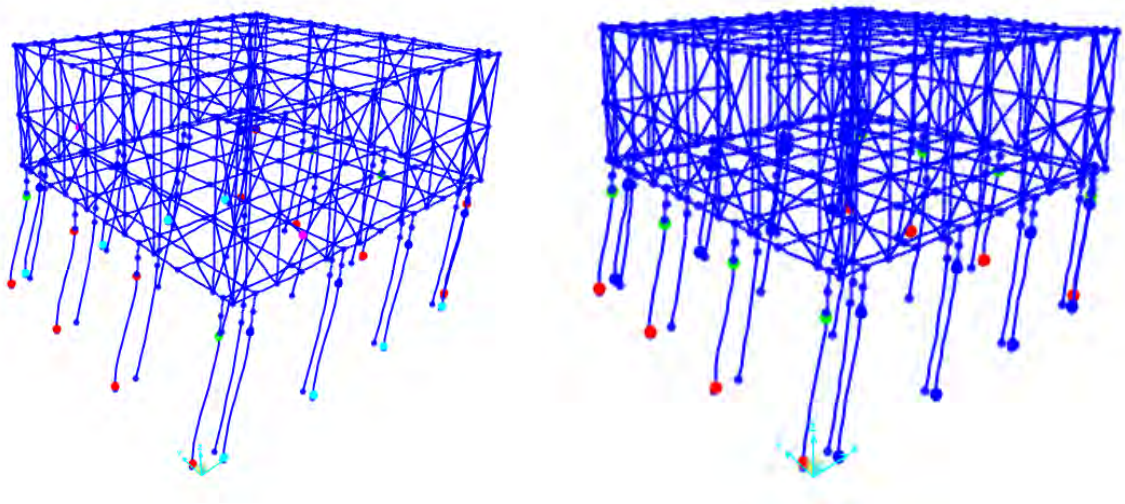

Figure 48. Hinges at the base and the top of the masonry walls of the ground floor when the maximum base shear is reached.

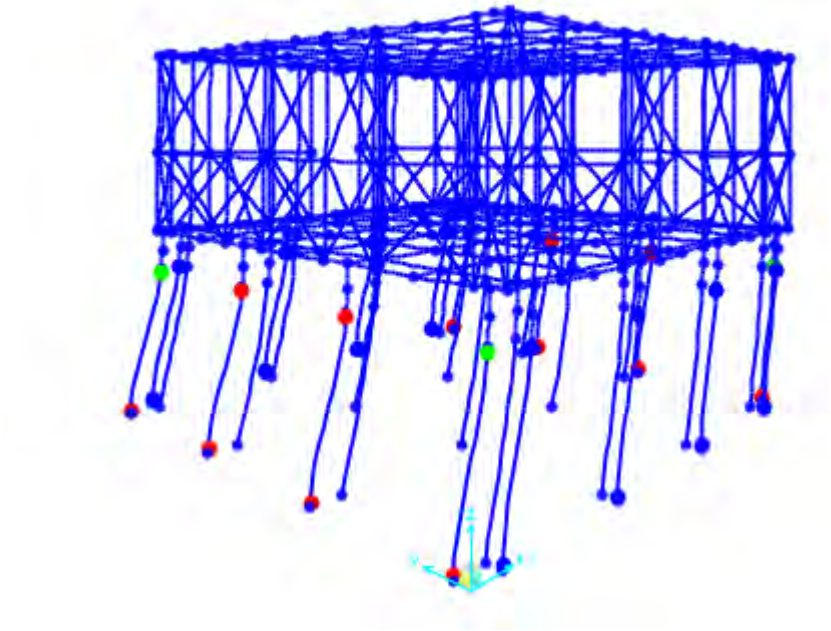

Figure 49. Failure mechanism of the masonry wall of the ground floor. The hinges correspond to point C of the capacity curves.

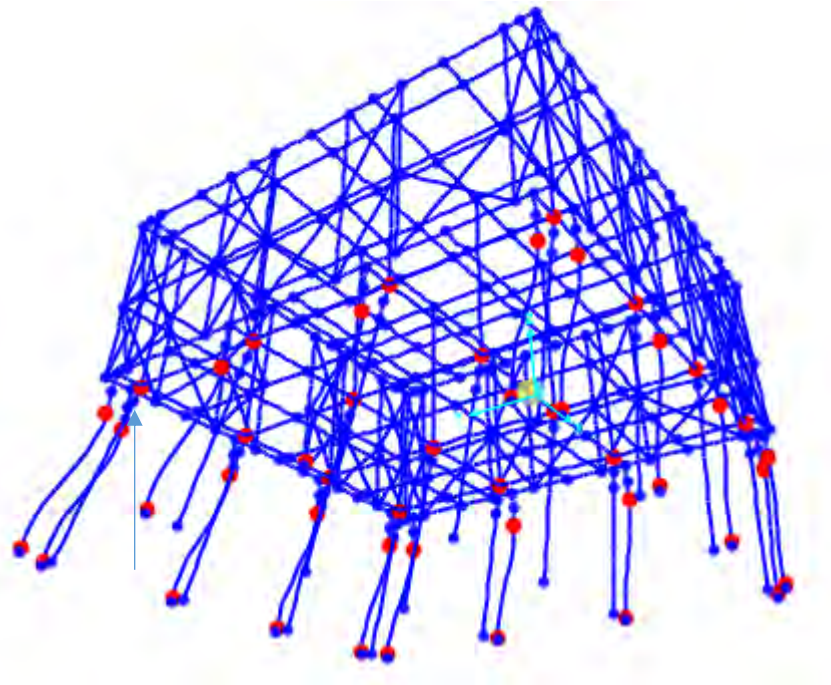

Figure 50. Activation of the secondary system and appearance of hinges at the timber elements.

Based on the ATC-40 method, the capacity spectrums in terms of *Sa* – *Sd* are presented in Figure 51 for the two examined cases of modulus of elasticity.

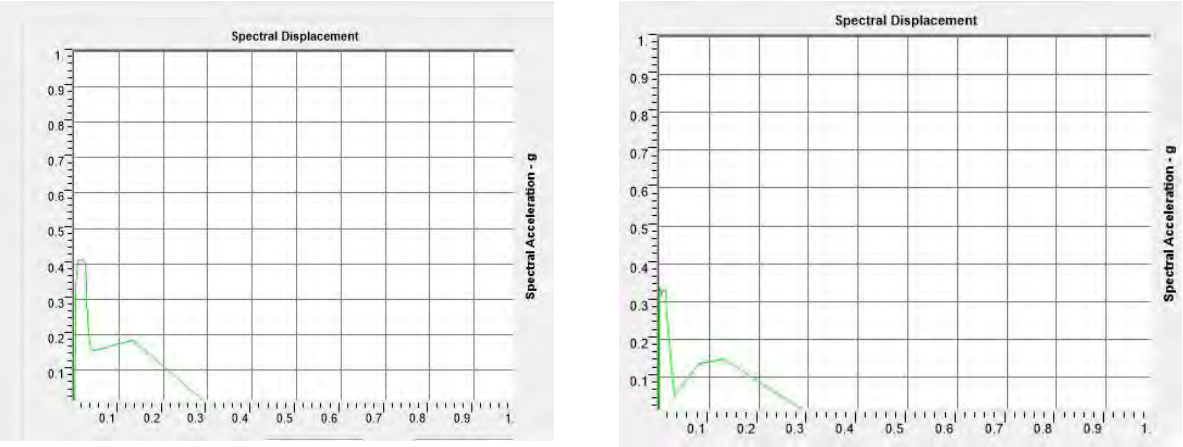

Figure 51. Capacity spectrums along *x* direction of the two storey building for (a) *E*=2 GPa and (b) *E*=4 GPa of the masonry walls of the ground floor.

4. Seismic risk assessment

4.1. Procedure

The structures considered for the assessment of the seismic risk are shown in Table 10. For each considered building two cases were examined, corresponding to directions *x* and *y*. In each case, the following limit states were set according to Giovinazzi and Lagomarsino (2006):

- Slight damage.....$d = 0.7 \cdot d_y$
- Moderate damage .....$d = 1.5 \cdot d_y$
- Extensive damage .....$d = 0.5 \cdot (d_y + d_u)$
- Collapse .....$d = d_u$

where d_y is the yield displacement and d_u is the ultimate displacement at collapse. For the types of buildings considered, the above limit states were calculated for the values of d_y and d_u that correspond to their capacity curve in the longitudinal *x* and the transverse *y* direction as shown in Figure 52, Figure 55, Figure 58, Figure 61, Figure 64 Figure 67, Figure 70 and Figure 73. The resulting limit state displacements are given in Table 11.

Table 10. Types of structures considered for the assessment of the seismic risk.

Case	Type of structure
1	Three storey building with walls of 0.4 m width and a modulus of elasticity E = 2 GPa
2	Three storey building with walls of 0.9 m width and a modulus of elasticity E = 4 GPa
3	Two storey building with walls of 0.4 m width and a modulus of elasticity E = 2 GPa
4	Two storey building with walls of 0.9 m width and a modulus of elasticity E = 4 GPa

Table 11. Capacity displacements that correspond to the considered limit states.

Case	Slight damage	Moderate damage	Extensive damage	Masonry failure
1 – dir. *x*	0.711	1.525	2.328	3.639
1 – dir. *y*	0.677	1.452	2.086	3.204
2 – dir. *x*	0.211	0.452	0.940	1.579
2 – dir. *y*	0.183	0.392	0.932	1.602
3 – dir. *x*	0.307	0.658	1.655	2.871
3 – dir. *y*	0.322	0.697	1.545	2.626
4 – dir. *x*	0.053	0.113	0.763	1.451
4 – dir. *y*	0.048	0.102	0.763	1.458

The displacement that will develop during each seismic scenario was estimated using the N2 method (Fajfar and Gašperšič 1996) and the above calculated response spectra for the probabilistic hazard and the fault-specific hazard using the different NGA methodologies.

Comparing the seismic displacement with the damage limit states, the seismic risk was assessed. The results are given in Table 12 to Table 19 and, in diagrams, in the corresponding figures in the following.

4.2. Case 1x

Three storey building: *b*=0.4 m, *E*=2 Gpa, *x* direction

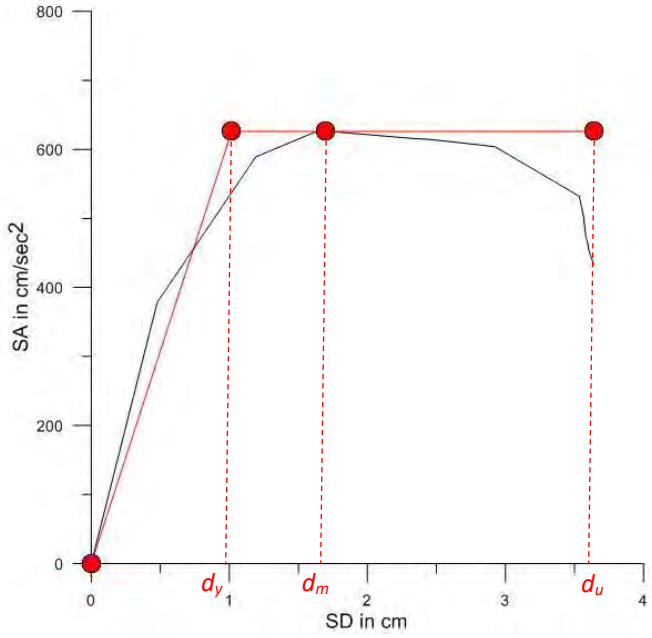

Figure 52. Capacity curve and equivalent bilinear model for case 1x. The three consecutive points at the yield acceleration level refer to the yield displacement, d_y, the displacement at the higher point of the capacity curve, d_m, which is used to define the bilinear model according to the equal energy concept, and the displacement at the masonry failure level, d_u.

Table 12. Seismic displacement and expected damage for case 1x.

Probabilistic hazard		
Probability of exceedance in 50 years	Estimated displacement [cm]	Expected damage
10%	2.73	Extensive damage to masonry failure
20%	1.98	Moderate to extensive
40%	1.31	Slight to moderate

Fault specific hazard – Scenario 1 (M_w = 7.2)		
Method	Estimated displacement [cm]	Expected damage
ABS13	1.99	Moderate to extensive
ITA10	4.93	Masonry failure
ASK14	2.06	Moderate to extensive
BSSA14	2.85	Extensive damage to masonry failure
CB14	2.23	Moderate to extensive
CY14	2.31	Moderate to extensive
IM14	3.40	Extensive damage to masonry failure
AS08	2.17	Moderate to extensive
BA08	2.76	Extensive damage to masonry failure
CB08	1.55	Moderate to extensive
CY08	2.38	Extensive damage to masonry failure
I08	1.94	Moderate to extensive
Fault specific hazard – Scenario 2 (M_w = 6.8)		
Method	Estimated displacement [cm]	Expected damage
ABS13	1.79	Moderate to extensive
ITA10	3.99	Masonry failure
ASK14	1.77	Moderate to extensive
BSSA14	2.61	Extensive damage to masonry failure
CB14	2.14	Moderate to extensive
CY14	1.81	Moderate to extensive
IM14	3.08	Extensive damage to masonry failure
AS08	1.72	Moderate to extensive
BA08	2.64	Extensive damage to masonry failure
CB08	1.46	Slight to moderate
CY08	1.98	Moderate to extensive
I08	1.24	Slight to moderate
Fault specific hazard – Scenario 3 (M_w = 6.3)		
Method	Estimated displacement [cm]	Expected damage
ABS13	1.27	Slight to moderate
ITA10	1.90	Moderate to extensive
ASK14	1.29	Slight to moderate
BSSA14	2.35	Extensive damage to masonry failure
CB14	1.55	Moderate to extensive

CY14	1.27	Slight to moderate
IM14	2.22	Moderate to extensive
AS08	1.07	Slight to moderate
BA08	1.73	Moderate to extensive
CB08	1.04	Slight to moderate
CY08	1.52	Slight to moderate
I08	0.80	Slight to moderate

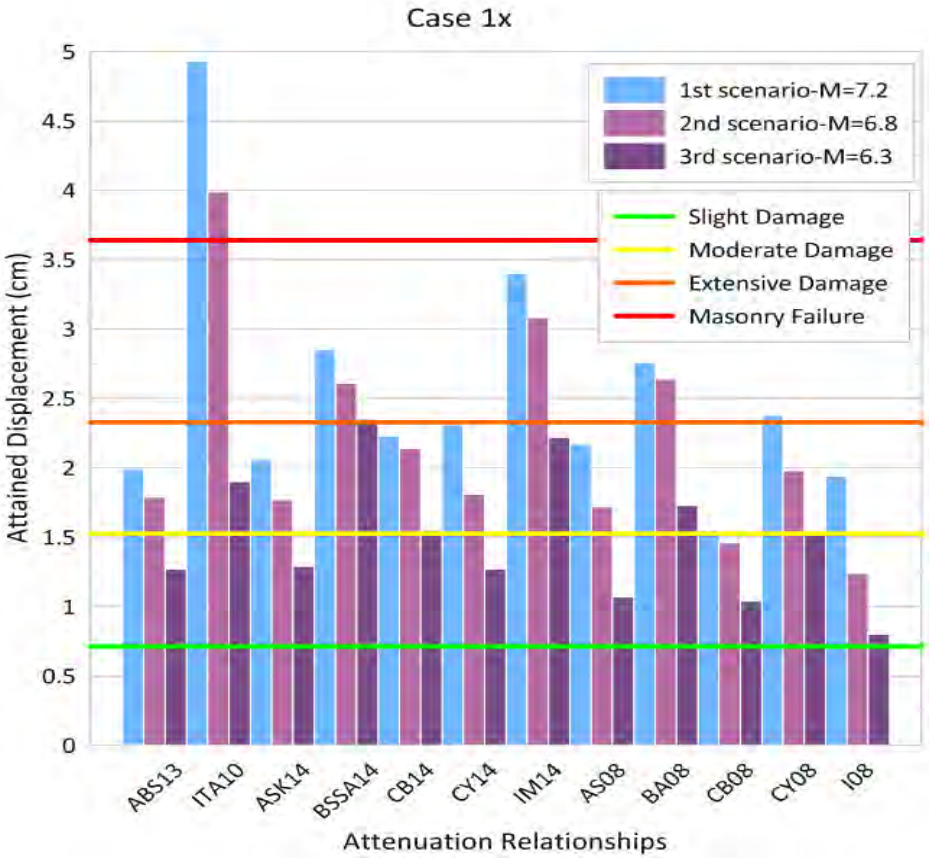

Figure 53. Attained limit states for case 1x, for fault specific hazard.

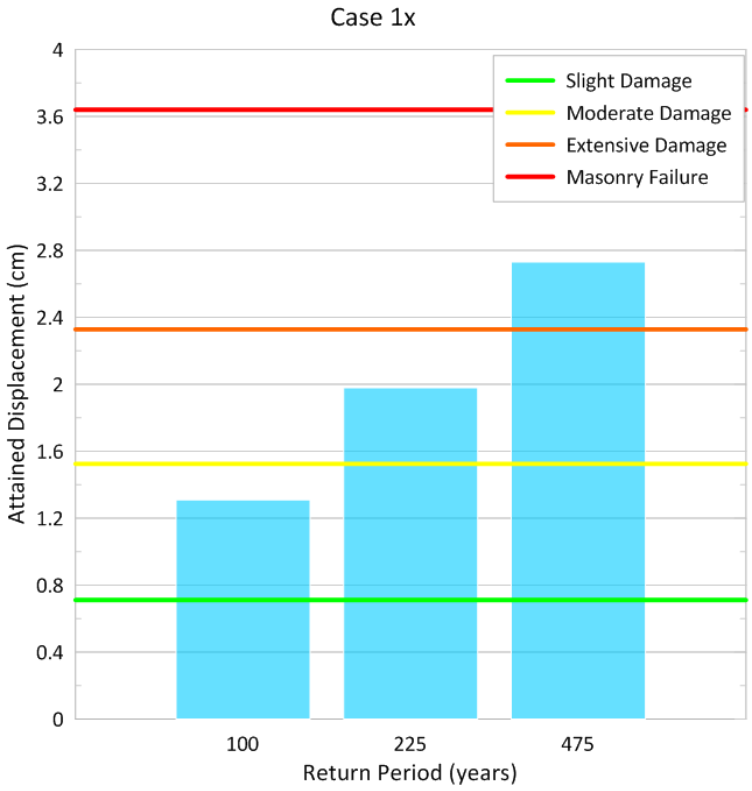

Figure 54. Attained displacement for case 1x, for probabilistic hazard.

4.3. Case 1y

Three storey building: *b*=0.4 m, *E*=2 Gpa, *y* direction

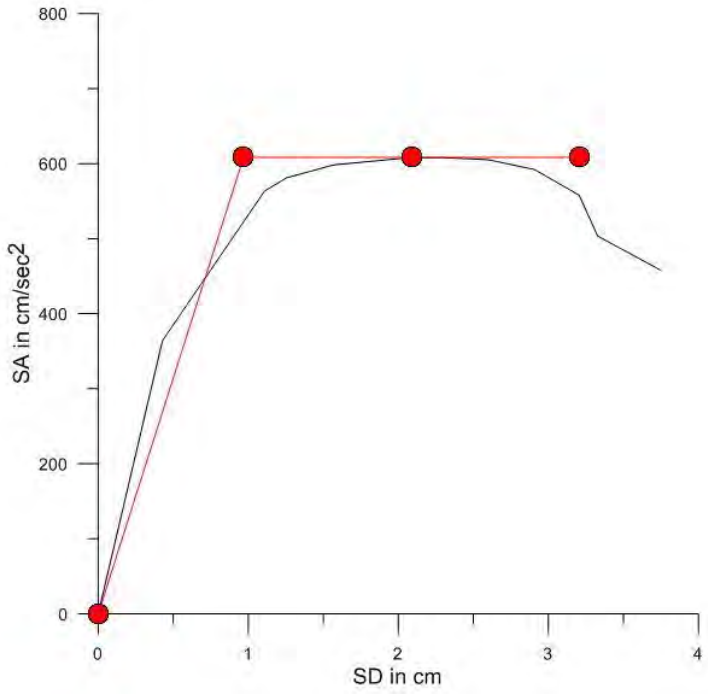

Figure 55. Capacity curve and equivalent bilinear model for case 1y.

Table 13. Seismic displacement and expected damage for case 1y.

Probabilistic hazard		
Probability of exceedance in 50 years	Estimated displacement [cm]	Expected damage
10%	2.73	Extensive damage to masonry failure
20%	1.97	Moderate to extensive
40%	1.30	Slight to moderate
Fault specific hazard – Scenario 1 (M_w = 7.2)		
Method	Estimated displacement [cm]	Expected damage
ABS13	1.98	Moderate to extensive
ITA10	4.91	Masonry failure
ASK14	2.08	Extensive damage to masonry failure
BSSA14	2.86	Extensive damage to masonry failure
CB14	2.28	Extensive damage to masonry failure
CY14	2.34	Extensive damage to masonry failure
IM14	3.36	Masonry failure
AS08	2.20	Extensive damage to masonry failure
BA08	2.76	Extensive damage to masonry failure
CB08	1.60	Moderate to extensive
CY08	2.39	Extensive damage to masonry failure
I08	1.94	Moderate to extensive
Fault specific hazard – Scenario 2 (M_w = 6.8)		
Method	Estimated displacement [cm]	Expected damage
ABS13	1.78	Moderate to extensive
ITA10	3.99	Masonry failure
ASK14	1.78	Moderate to extensive
BSSA14	2.61	Extensive damage to masonry failure
CB14	2.18	Extensive damage to masonry failure
CY14	1.83	Moderate to extensive
IM14	3.04	Extensive damage to masonry failure
AS08	1.73	Moderate to extensive
BA08	2.64	Extensive damage to masonry failure

CB08	1.48	Moderate to extensive
CY08	1.99	Moderate to extensive
I08	1.23	Slight to moderate
Fault specific hazard – Scenario 3 (M_w = 6.3)		
Method	Estimated displacement [cm]	Expected damage
ABS13	1.25	Slight to moderate
ITA10	1.89	Moderate to extensive
ASK14	1.28	Slight to moderate
BSSA14	2.35	Extensive damage to masonry failure
CB14	1.57	Moderate to extensive
CY14	1.29	Slight to moderate
IM14	2.17	Extensive damage to masonry failure
AS08	1.07	Slight to moderate
BA08	1.73	Moderate to extensive
CB08	1.05	Slight to moderate
CY08	1.52	Moderate to extensive
I08	0.78	Slight to moderate

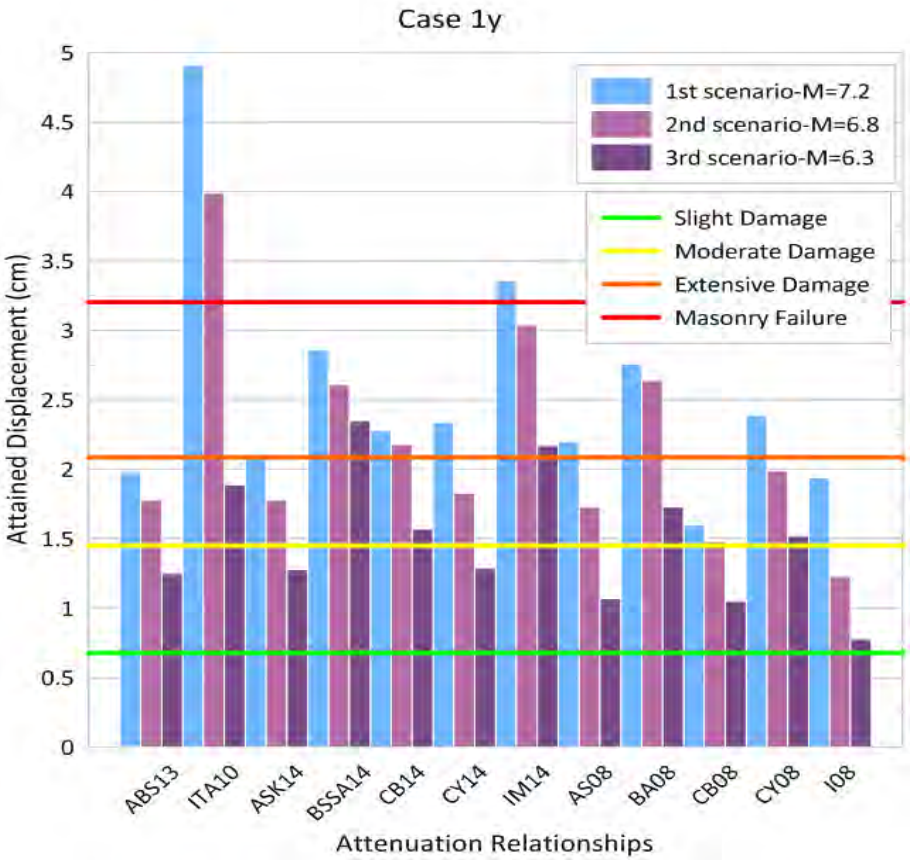

Figure 56. Attained limit states for case 1y, for fault specific hazard.

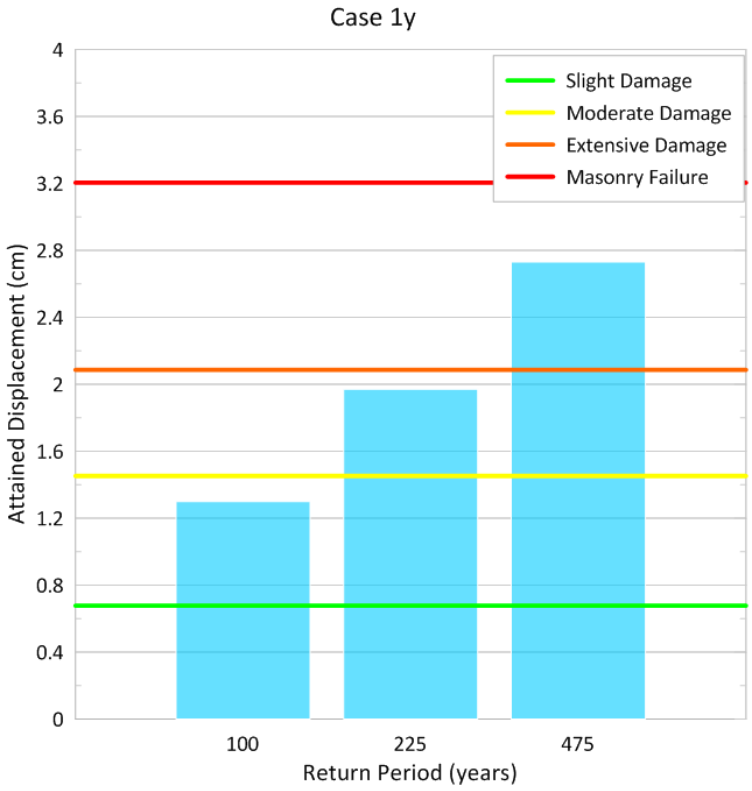

Figure 57. Attained displacement for case 1y, for probabilistic hazard.

4.4. Case 2x

Three storey building: *b*=0.9 m, *E*=4 Gpa, *x* direction

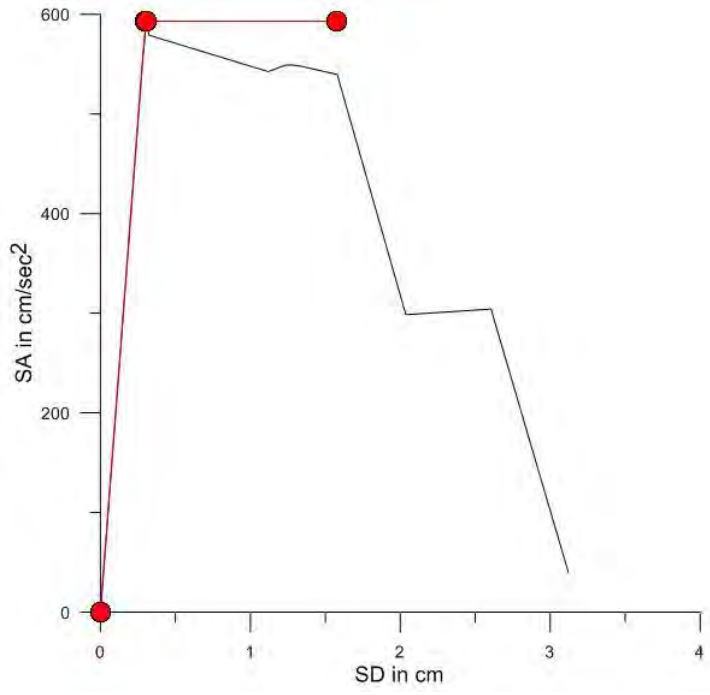

Figure 58. Capacity curve and equivalent bilinear model for case 2x.

Table 14. Seismic displacement and expected damage for case 2x.

Probabilistic hazard		
Probability of exceedance in 50 years	Estimated displacement [cm]	Expected damage
10%	1.32	Extensive damage to masonry failure
20%	0.89	Moderate to extensive
40%	0.51	Moderate to extensive
Fault specific hazard – Scenario 1 (M_w = 7.2)		
Method	Estimated displacement [cm]	Expected damage
ABS13	0.90	Moderate to extensive
ITA10	2.56	Masonry failure
ASK14	0.96	Extensive damage to masonry failure
BSSA14	1.41	Extensive damage to masonry failure
CB14	1.10	Extensive damage to masonry failure
CY14	1.12	Extensive damage to masonry failure
IM14	1.67	Masonry failure
AS08	1.04	Extensive damage to masonry failure
BA08	1.35	Extensive damage to masonry failure
CB08	0.70	Moderate to extensive
CY08	1.14	Extensive damage to masonry failure
I08	0.87	Moderate to extensive
Fault specific hazard – Scenario 2 (M_w = 6.8)		
Method	Estimated displacement [cm]	Expected damage
ABS13	0.78	Moderate to extensive
ITA10	2.05	Masonry failure
ASK14	0.79	Moderate to extensive
BSSA14	1.27	Extensive damage to masonry failure
CB14	1.03	Extensive damage to masonry failure
CY14	0.83	Moderate to extensive
IM14	1.49	Extensive damage to masonry failure
AS08	0.77	Moderate to extensive
BA08	1.28	Extensive damage to masonry failure

CB08	0.63	Moderate to extensive
CY08	0.91	Moderate to extensive
I08	0.47	Moderate to extensive
Fault specific hazard – Scenario 3 (M_w = 6.3)		
Method	Estimated displacement [cm]	Expected damage
ABS13	0.48	Moderate to extensive
ITA10	0.85	Moderate to extensive
ASK14	0.50	Moderate to extensive
BSSA14	1.11	Extensive damage to masonry failure
CB14	0.68	Moderate to extensive
CY14	0.52	Moderate to extensive
IM14	0.94	Moderate to extensive
AS08	0.39	Slight to moderate
BA08	0.76	Moderate to extensive
CB08	0.38	Slight to moderate
CY08	0.64	Moderate to extensive
I08	0.21	Slight to moderate

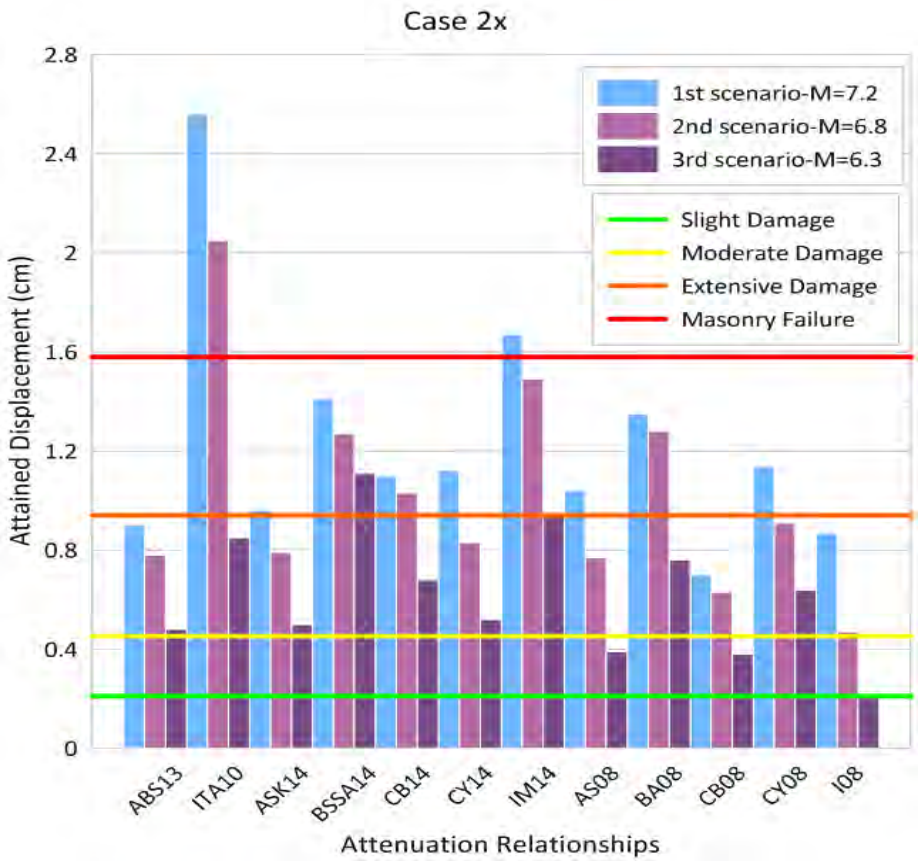

Figure 59. Attained limit states for case 2x, for fault specific hazard.

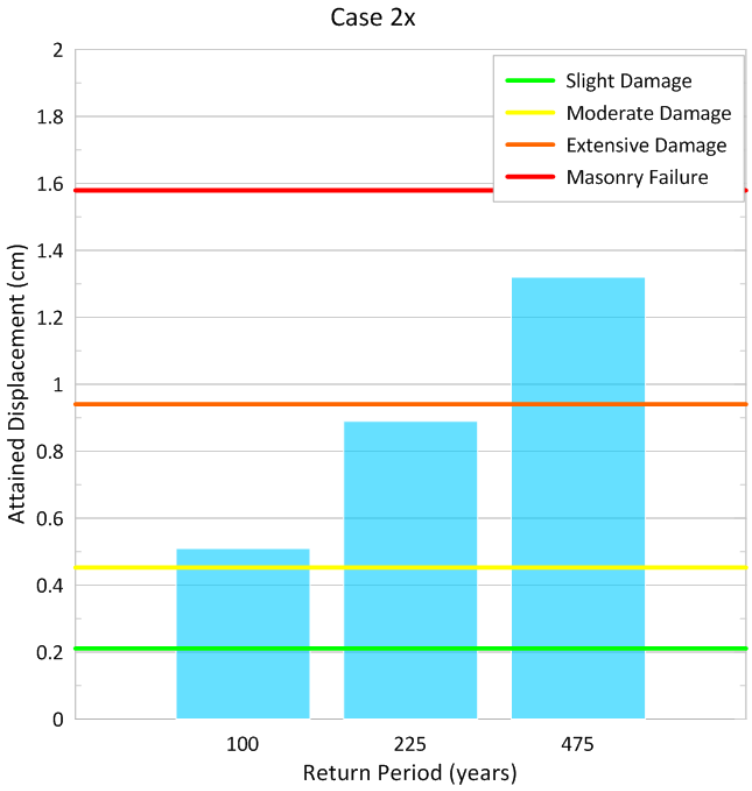

Figure 60. Attained displacement for case 2x, for probabilistic hazard.

4.5. Case 2y

Three storey building: *b*=0.9 m, *E*=2 Gpa, *y* direction

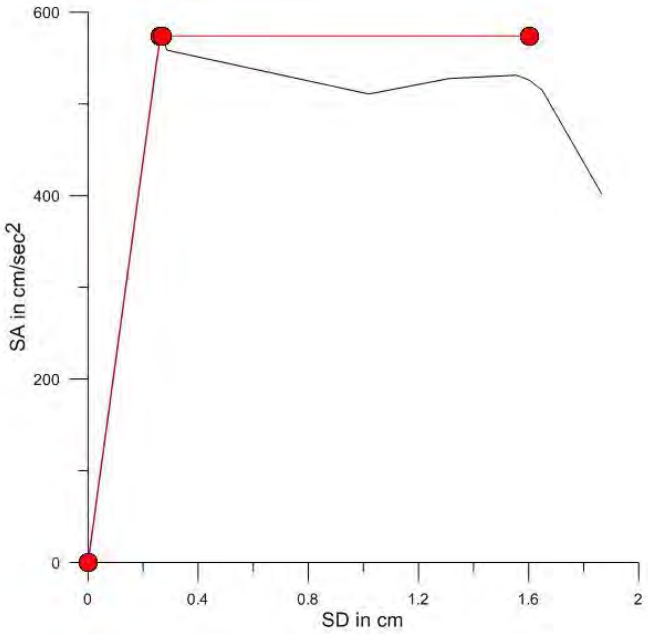

Figure 61. Capacity curve and equivalent bilinear model for case 2y.

Table 15. Seismic displacement and expected damage for case 2y.

Probabilistic hazard		
Probability of exceedance in 50 years	Estimated displacement [cm]	Expected damage
10%	1.26	Extensive damage to masonry failure
20%	0.85	Moderate to extensive
40%	0.49	Slight to moderate
Fault specific hazard – Scenario 1 (M_w = 7.2)		
Method	Estimated displacement [cm]	Expected damage
ABS13	0.86	Moderate to extensive
ITA10	2.44	Masonry failure
ASK14	0.93	Moderate to extensive
BSSA14	1.36	Extensive damage to masonry failure
CB14	1.08	Extensive damage to masonry failure
CY14	1.09	Extensive damage to masonry failure
IM14	1.57	Extensive damage to masonry failure
AS08	1.00	Extensive damage to masonry failure
BA08	1.29	Extensive damage to masonry failure
CB08	0.70	Moderate to extensive
CY08	1.10	Extensive damage to masonry failure
I08	0.83	Moderate to extensive
Fault specific hazard – Scenario 2 (M_w = 6.8)		
Method	Estimated displacement [cm]	Expected damage
ABS13	0.74	Moderate to extensive
ITA10	1.96	Masonry failure
ASK14	0.76	Moderate to extensive
BSSA14	1.22	Extensive damage to masonry failure
CB14	1.01	Extensive damage to masonry failure
CY14	0.81	Moderate to extensive
IM14	1.40	Extensive damage to masonry failure
AS08	0.74	Moderate to extensive

BA08	1.23	Extensive damage to masonry failure
CB08	0.62	Moderate to extensive
CY08	0.88	Moderate to extensive
I08	0.45	Moderate to extensive
Fault specific hazard – Scenario 3 (M_w = 6.3)		
Method	Estimated displacement [cm]	Expected damage
ABS13	0.45	Moderate to extensive
ITA10	0.81	Moderate to extensive
ASK14	0.48	Moderate to extensive
BSSA14	1.06	Extensive damage to masonry failure
CB14	0.66	Moderate to extensive
CY14	0.51	Moderate to extensive
IM14	0.88	Moderate to extensive
AS08	0.37	Slight to moderate
BA08	0.73	Moderate to extensive
CB08	0.37	Slight to moderate
CY08	0.62	Moderate to extensive
I08	0.20	Slight to moderate

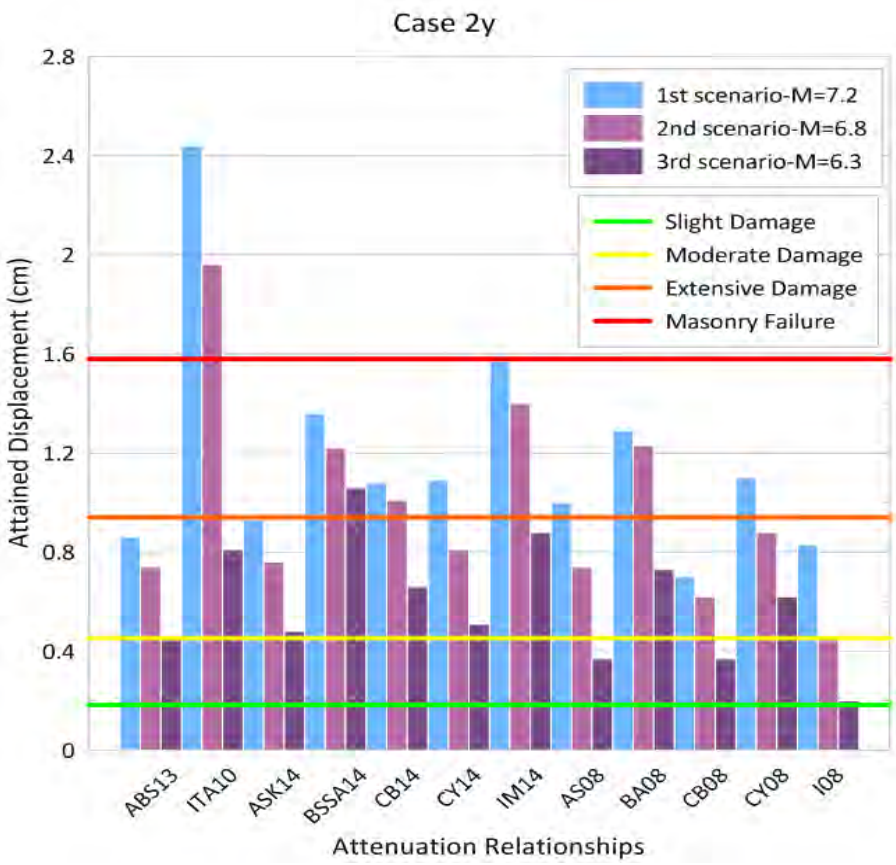

Figure 62. Attained limit states for case 2y, for fault specific hazard.

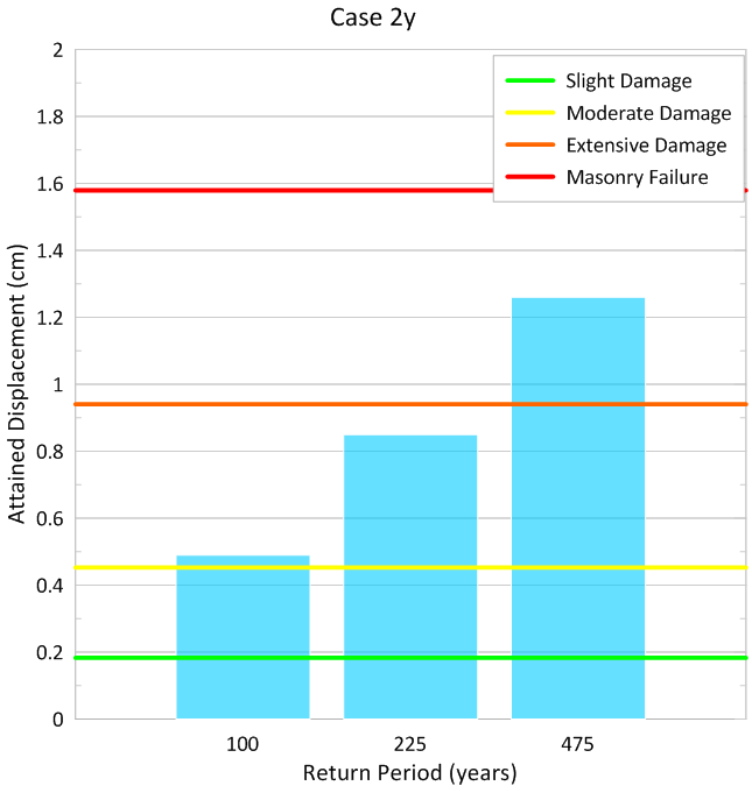

Figure 63. Attained displacement for case 2y, for probabilistic hazard.

4.6. Case 3x

Two storey building: *b*=0.4 m, *E*=2 Gpa, *x* direction

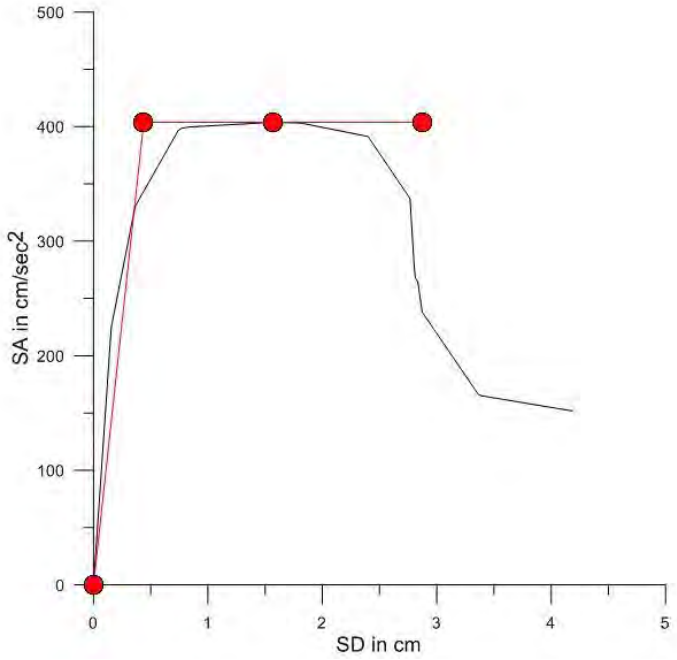

Figure 64. Capacity curve and equivalent bilinear model for case 3x.

Table 16. Seismic displacement and expected damage for Case 3x.

Probabilistic hazard		
Probability of exceedance in 50 years	Estimated displacement [cm]	Expected damage
10%	2.44	Extensive damage to masonry failure
20%	1.73	Extensive damage to masonry failure
40%	1.16	Moderate to extensive
Fault specific hazard – Scenario 1 (M_w = 7.2)		
Method	Estimated displacement [cm]	Expected damage
ABS13	1.55	Moderate to extensive
ITA10	3.69	Masonry failure
ASK14	1.72	Extensive damage to masonry failure
BSSA14	2.46	Extensive damage to masonry failure
CB14	2.39	Extensive damage to masonry failure
CY14	1.92	Extensive damage to masonry failure
IM14	2.43	Extensive damage to masonry failure
AS08	1.72	Extensive damage to masonry failure
BA08	2.44	Extensive damage to masonry failure
CB08	1.62	Extensive damage to masonry failure
CY08	1.90	Extensive damage to masonry failure
I08	1.06	Moderate to extensive
Fault specific hazard – Scenario 2 (M_w = 6.8)		
Method	Estimated displacement [cm]	Expected damage
ABS13	1.55	Moderate to extensive
ITA10	3.69	Masonry failure
ASK14	1.72	Moderate to extensive
BSSA14	2.46	Extensive damage to masonry failure
CB14	2.39	Extensive damage to masonry failure
CY14	1.92	Extensive damage to masonry failure
IM14	2.43	Extensive damage to masonry failure

AS08	1.72	Extensive damage to masonry failure
BA08	2.44	Extensive damage to masonry failure
CB08	1.62	Extensive damage to masonry failure
CY08	1.90	Extensive damage to masonry failure
I08	1.06	Moderate to extensive
Fault specific hazard – Scenario 3 (M_w = 6.3)		
Method	Estimated displacement [cm]	Expected damage
ABS13	1.02	Moderate to extensive
ITA10	1.70	Extensive damage to masonry failure
ASK14	1.16	Moderate to extensive
BSSA14	2.14	Extensive damage to masonry failure
CB14	1.65	Moderate to extensive
CY14	1.37	Moderate to extensive
IM14	1.61	Moderate to extensive
AS08	1.02	Moderate to extensive
BA08	1.61	Moderate to extensive
CB08	1.08	Moderate to extensive
CY08	1.42	Moderate to extensive
I08	0.61	Slight to moderate

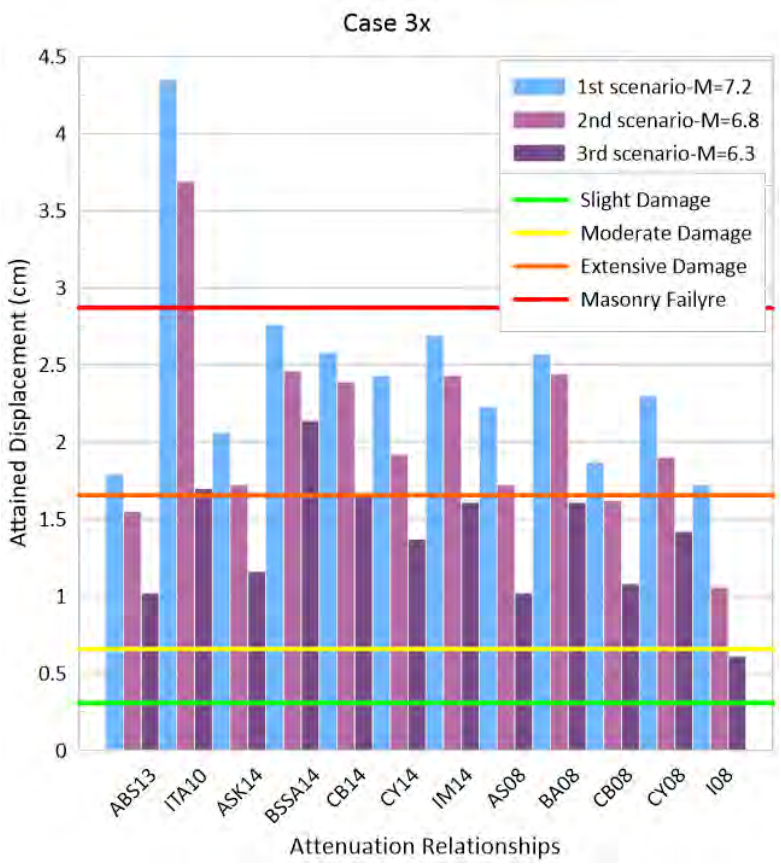

Figure 65. Attained limit states for case 3x, for fault specific hazard.

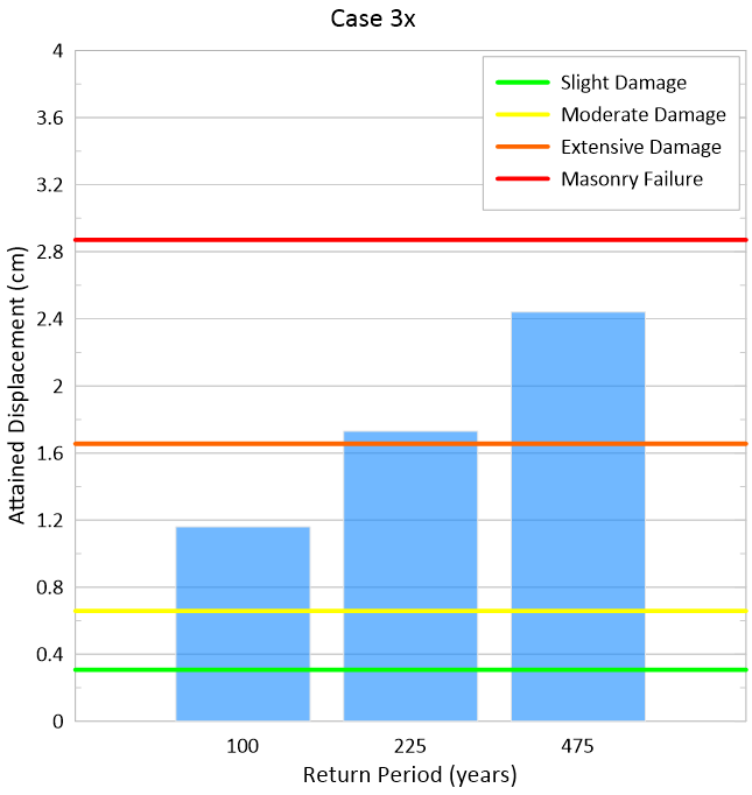

Figure 66. Attained displacement for case 3x, for probabilistic hazard.

4.7. Case 3y

Two storey building: *b*=0.4 m, *E*=2 Gpa, *y* direction

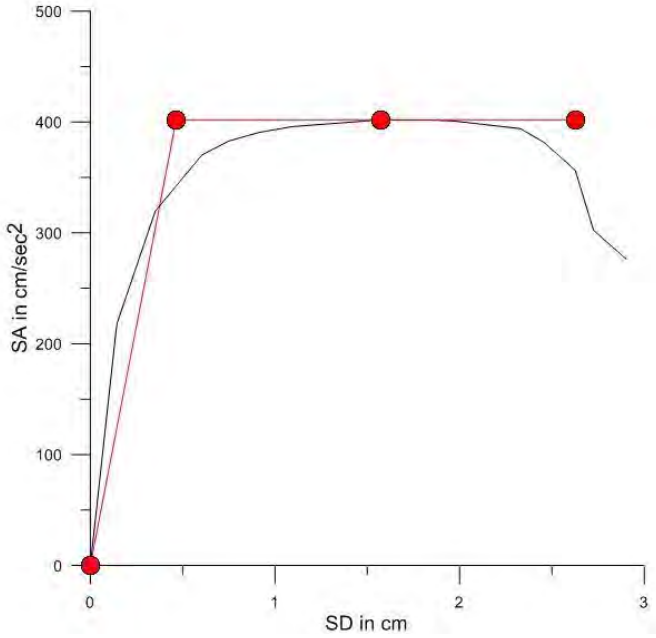

Figure 67. Capacity curve and equivalent bilinear model for case 3y.

Table 17. Seismic displacement and expected damage for Case 3y.

Probabilistic hazard		
Probability of exceedance in 50 years	Estimated displacement [cm]	Expected damage
10%	2.54	Extensive damage to masonry failure
20%	1.80	Extensive damage to masonry failure
40%	1.21	Moderate to extensive
Fault specific hazard – Scenario 1 (M_w = 7.2)		
Method	Estimated displacement [cm]	Expected damage
ABS13	1.85	Extensive damage to masonry failure
ITA10	4.50	Masonry failure
ASK14	2.14	Extensive damage to masonry failure
BSSA14	2.86	Extensive damage to masonry failure
CB14	2.68	Extensive damage to masonry failure
CY14	2.52	Extensive damage to masonry failure

IM14	2.79	Extensive damage to masonry failure
AS08	2.32	Extensive damage to masonry failure
BA08	2.67	Extensive damage to masonry failure
CB08	1.94	Extensive damage to masonry failure
CY08	2.39	Extensive damage to masonry failure
I08	1.79	Extensive damage to masonry failure
Fault specific hazard – Scenario 2 (M_w = 6.8)		
Method	Estimated displacement [cm]	Expected damage
ABS13	1.61	Moderate to extensive
ITA10	3.83	Masonry failure
ASK14	1.79	Extensive damage to masonry failure
BSSA14	2.56	Extensive damage to masonry failure
CB14	2.49	Extensive damage to masonry failure
CY14	2.00	Extensive damage to masonry failure
IM14	2.52	Extensive damage to masonry failure
AS08	1.79	Extensive damage to masonry failure
BA08	2.54	Extensive damage to masonry failure
CB08	1.69	Extensive damage to masonry failure
CY08	1.98	Extensive damage to masonry failure
I08	1.11	Moderate to extensive
Fault specific hazard – Scenario 3 (M_w = 6.3)		
Method	Estimated displacement [cm]	Expected damage
ABS13	1.06	Moderate to extensive
ITA10	1.77	Extensive damage to masonry failure
ASK14	1.22	Moderate to extensive
BSSA14	2.23	Extensive damage to masonry failure
CB14	1.72	Extensive damage to masonry failure
CY14	1.43	Moderate to extensive

IM14	1.67	Extensive damage to masonry failure
AS08	1.07	Moderate to extensive
BA08	1.68	Extensive damage to masonry failure
CB08	1.13	Moderate to extensive
CY08	1.49	Moderate to extensive
I08	0.64	Slight to moderate

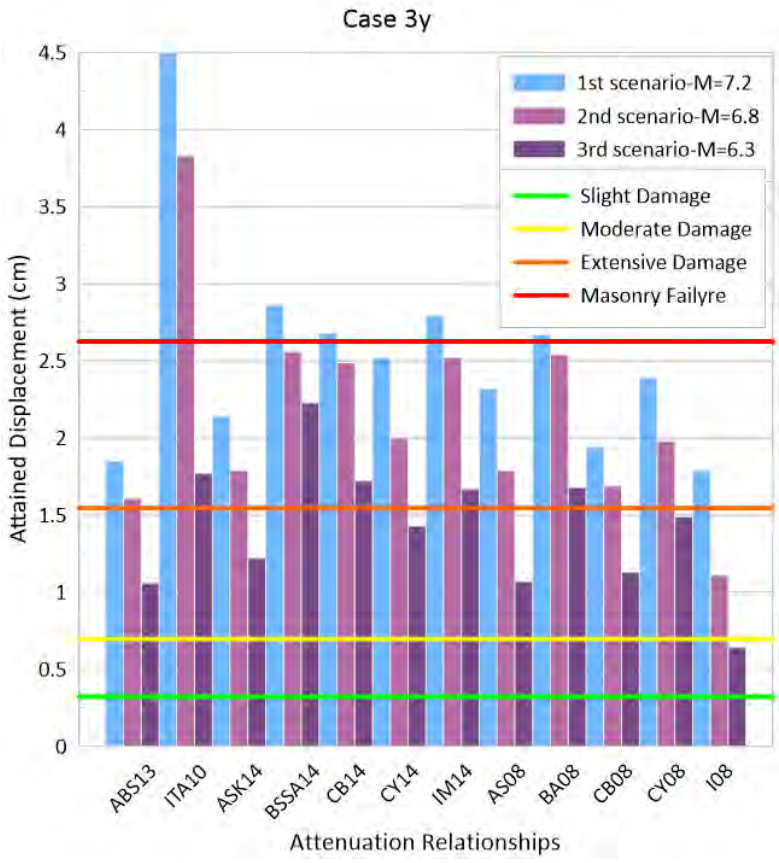

Figure 68. Attained limit states for case 3y, for fault specific hazard.

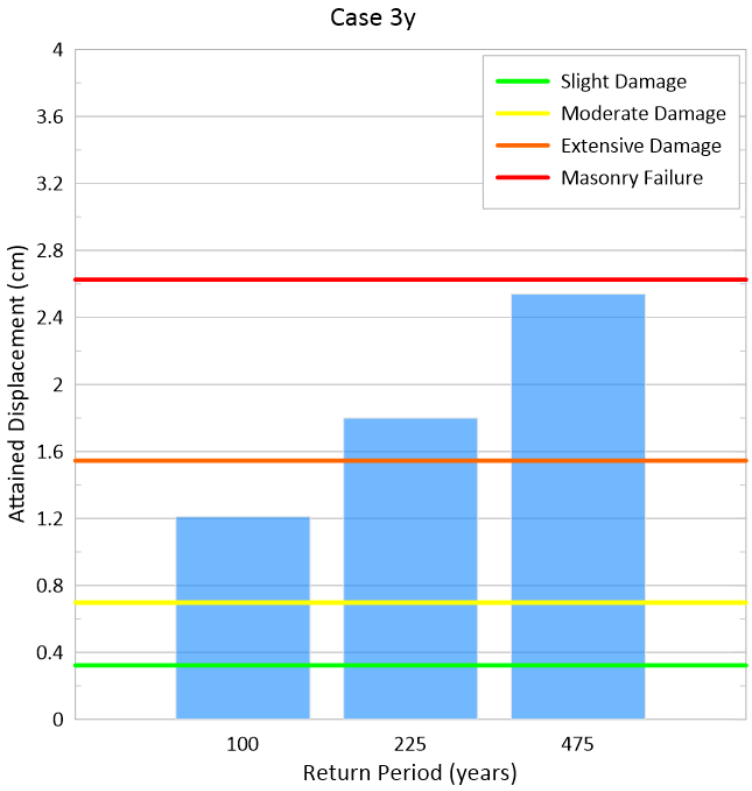

Figure 69. Attained displacement for 3y, for fault specific hazard.

4.8. Case 4x

Two storey building: *b*=0.9 m, *E*=4 Gpa, *x* direction

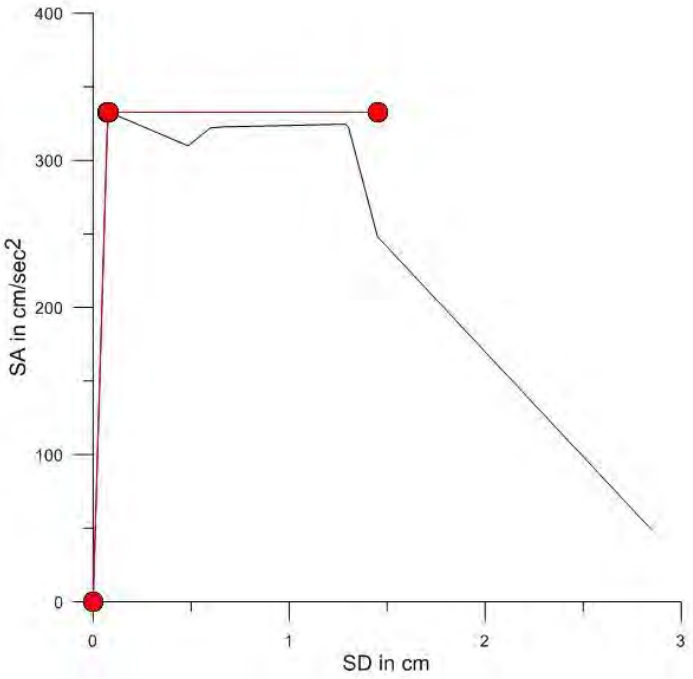

Figure 70. Capacity curve and equivalent bilinear model for case 4x.

Table 18. Seismic displacement and expected damage for Case 4x.

Probabilistic hazard		
Probability of exceedance in 50 years	Estimated displacement [cm]	Expected damage
10%	1.07	Extensive damage to masonry failure
20%	0.74	Extensive damage to masonry failure
40%	0.47	Moderate to extensive
Fault specific hazard – Scenario 1 (M_w = 7.2)		
Method	Estimated displacement [cm]	Expected damage
ABS13	0.76	Moderate to extensive
ITA10	1.96	Masonry failure
ASK14	0.92	Extensive damage to masonry failure
BSSA14	1.25	Extensive damage to masonry failure
CB14	1.21	Extensive damage to masonry failure
CY14	1.11	Extensive damage to masonry failure
IM14	1.14	Extensive damage to masonry failure
AS08	1.01	Extensive damage to masonry failure
BA08	1.15	Extensive damage to masonry failure
CB08	0.87	Extensive damage to masonry failure
CY08	1.03	Extensive damage to masonry failure
I08	0.73	Moderate to extensive
Fault specific hazard – Scenario 2 (M_w = 6.8)		
Method	Estimated displacement [cm]	Expected damage
ABS13	0.65	Moderate to extensive
ITA10	1.67	Masonry failure
ASK14	0.75	Moderate to extensive
BSSA14	1.10	Extensive damage to masonry failure
CB14	1.11	Extensive damage to masonry failure

CY14	0.87	Extensive damage to masonry failure
IM14	1.03	Extensive damage to masonry failure
AS08	0.76	Moderate to extensive
BA08	1.09	Extensive damage to masonry failure
CB08	0.73	Moderate to extensive
CY08	0.84	Extensive damage to masonry failure
I08	0.42	Moderate to extensive
Fault specific hazard – Scenario 3 (M_w = 6.3)		
Method	Estimated displacement [cm]	Expected damage
ABS13	0.39	Moderate to extensive
ITA10	0.73	Moderate to extensive
ASK14	0.48	Moderate to extensive
BSSA14	0.94	Extensive damage to masonry failure
CB14	0.74	Moderate to extensive
CY14	0.60	Moderate to extensive
IM14	0.65	Moderate to extensive
AS08	0.42	Moderate to extensive
BA08	0.69	Moderate to extensive
CB08	0.46	Moderate to extensive
CY08	0.61	Moderate to extensive
I08	0.20	Moderate to extensive

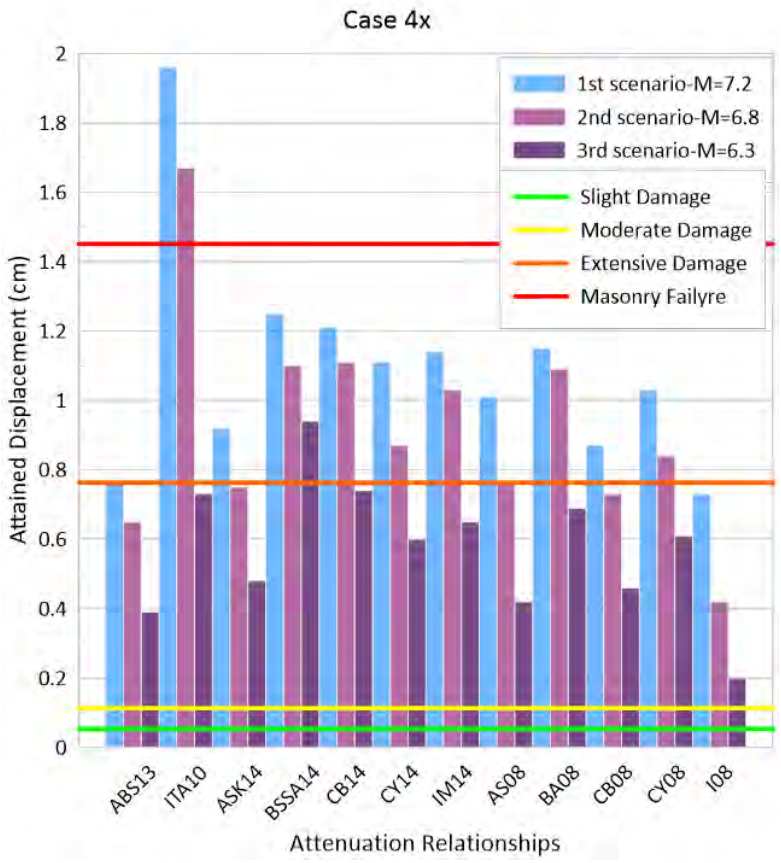

Figure 71. Attained limit states for case 4x, for fault specific hazard.

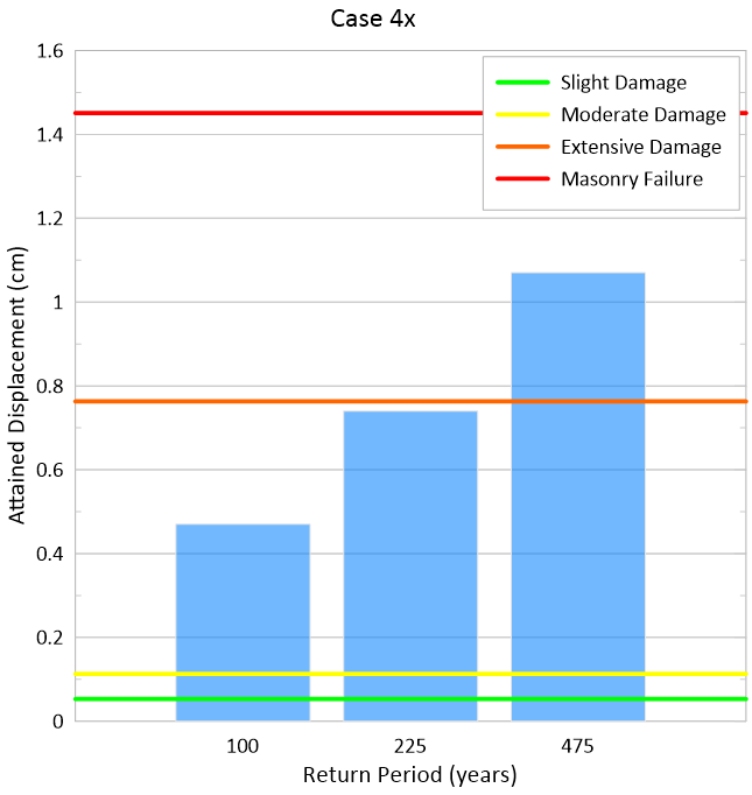

Figure 72. Attained displacement for case 4x, for probabilistic hazard.

4.9. Case 4y

Two storey building: *b*=0.9 m, *E*=4 Gpa, *y* direction

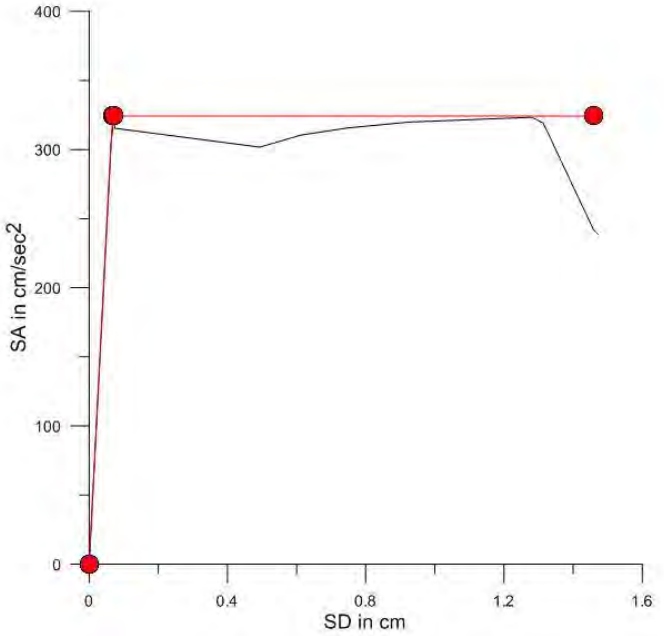

Figure 73. Capacity curve and equivalent bilinear model for case 4y.

Table 19. Seismic displacement and expected damage for Case 4y.

Probabilistic hazard		
Probability of exceedance in 50 years	Estimated displacement [cm]	Expected damage
10%	1.04	Extensive damage to masonry failure
20%	0.71	Extensive damage to masonry failure
40%	0.46	Moderate to extensive
Fault specific hazard – Scenario 1 (M_w = 7.2)		
Method	Estimated displacement [cm]	Expected damage
ABS13	0.74	Moderate to extensive
ITA10	1.89	Masonry failure
ASK14	0.89	Extensive damage to masonry failure
BSSA14	1.21	Extensive damage to masonry failure
CB14	1.18	Extensive damage to masonry failure
CY14	1.08	Extensive damage to masonry failure
IM14	1.10	Extensive damage to masonry failure

AS08	0.98	Extensive damage to masonry failure
BA08	1.11	Extensive damage to masonry failure
CB08	0.85	Extensive damage to masonry failure
CY08	1.00	Extensive damage to masonry failure
I08	0.71	Moderate to extensive
Fault specific hazard – Scenario 2 (M_w = 6.8)		
Method	Estimated displacement [cm]	Expected damage
ABS13	0.63	Moderate to extensive
ITA10	1.62	Masonry failure
ASK14	0.73	Moderate to extensive
BSSA14	1.07	Extensive damage to masonry failure
CB14	1.09	Extensive damage to masonry failure
CY14	0.85	Extensive damage to masonry failure
IM14	0.99	Extensive damage to masonry failure
AS08	0.74	Moderate to extensive
BA08	1.05	Extensive damage to masonry failure
CB08	0.72	Moderate to extensive
CY08	0.81	Extensive damage to masonry failure
I08	0.41	Moderate to extensive
Fault specific hazard – Scenario 3 (M_w = 6.3)		
Method	Estimated displacement [cm]	Expected damage
ABS13	0.38	Moderate to extensive
ITA10	0.71	Moderate to extensive
ASK14	0.46	Moderate to extensive
BSSA14	0.91	Extensive damage to masonry failure
CB14	0.72	Moderate to extensive
CY14	0.59	Moderate to extensive
IM14	0.62	Moderate to extensive
AS08	0.41	Moderate to extensive
BA08	0.67	Moderate to extensive
CB08	0.44	Moderate to extensive
CY08	0.59	Moderate to extensive
I08	0.20	Moderate to extensive

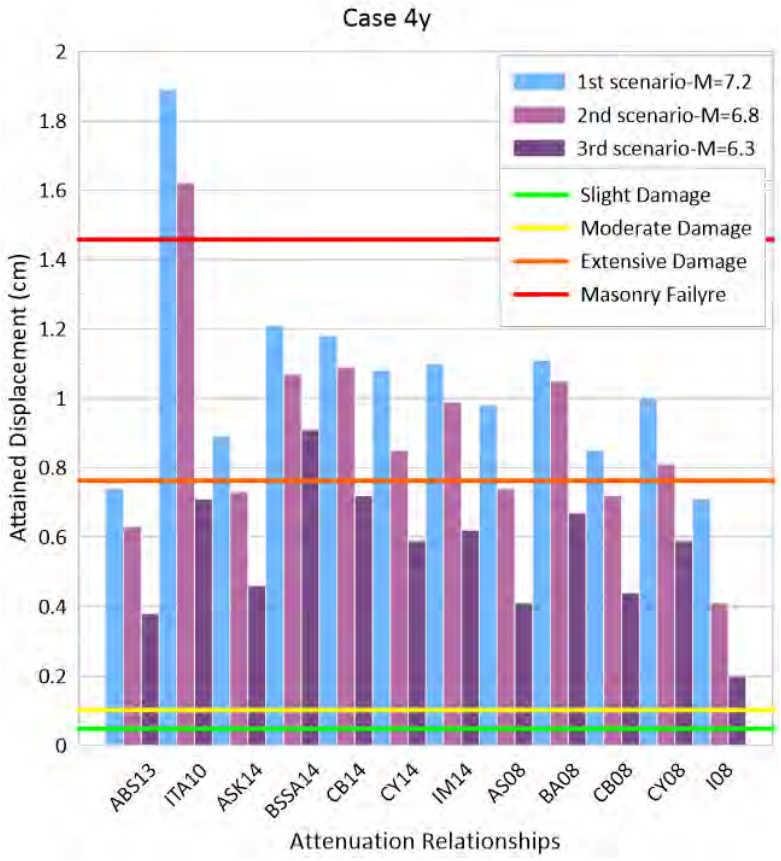

Figure 74. Attained limit states for case 4y, for fault specific hazard.

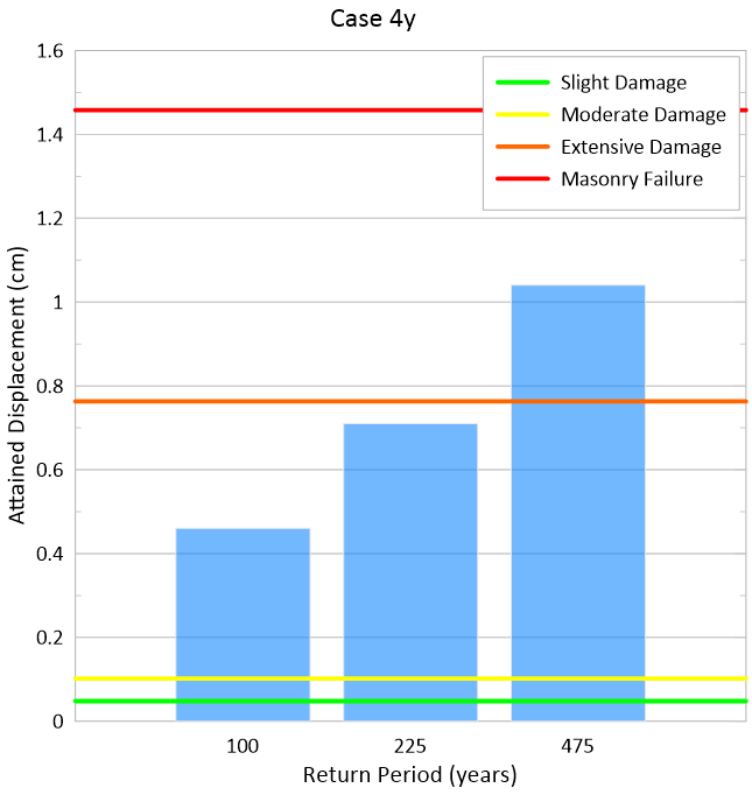

Figure 75. Attained displacements for case 4y, for probabilistic hazard.

5. Conclusions

The seismicity of Lefkas is dominated by the Northern segment of the Cephalonia Transform fault. For the estimation of the seismic hazard a probabilistic and a deterministic approach were considered. According to the probabilistic approach three levels of hazard were evaluated for a return period of 100, 225 and 475 years accordingly. The hazard values were given for a rock site and through the use of amplification parameters given by IBC for different soil types and levels of rock ground motion these values were translated in ground and spectral accelerations for a soil of V_{s30} velocity of 250m/sec accounting for the soil type at the site of Lefkas city center. The values for 0.2 structural period approximating the constant spectral acceleration period range, and 1.0 sec period accounting for the constant velocity period range, permitted the construction of demand spectra for the probabilistic scenarios. The deterministic approach was based on the characteristics of the Lefkas segment of CFT for three levels of event magnitude, a) an event of 7.2 magnitude considered as the extreme case of an event on the fault, similar to the assumptions inherent in the already referred probabilistic approach, b) a 6.8 event considered as the maximum magnitude occurring at the fault during the last four hundred years and c) a 6.3 magnitude event compatible with a 100 years return period and considered as comparatively a common event for the considered site. For each of the referred deterministic cases a set of attenuation relationships were used. Most of them were taken from the NGA 2008 and NGA 2014 research programs The main exception is the ITA10 attenuation relationship compiled in 1910 for the events of the Italian peninsula and used by the probabilistic EFEHR methodology for the Lefkas fault. Accordingly, the relationship was used in order to associate the probabilistic and deterministic approaches. From the attenuation relationships peak ground accelerations as well as spectral accelerations for 0.2 and 1.0 periods were evaluated. The spectral values for the constant acceleration and constant velocity regions permitted the compilation of demand spectra to be used with the structural capacity curves for the estimation of the expected risk.

The methodology for the estimation of the attained structural risk is the following. For each of the four structural types an estimated pushover curve is translated to a capacity curve in terms of spectral acceleration versus spectral displacement. A characteristic of the capacity curves is that at a displacement close to that of the maximum attained acceleration, considered as the yield acceleration S_{ay}, the masonry fails with a degradation of its bearing capacity of more than 30%. This point is considered associated with masonry failure and the relevant displacement is considered as the ultimate masonry displacement du. The yield displacement dy is evaluated from a bilinear approximation of the capacity curve up to the point of maximum attained acceleration S_{ay}. The upper point of the approximated elasti branch defines the yield displacement dy. The values of the considered limit states of slight, moderate, extensive masonry damage and masonry failure are evaluated from the relationships given by Lagomarsino and Giovinazzi. After the point of masonry failure and the following bearing capacity degradation the timber framing stabilizes the structural capacity for further deformation avoiding structural collapse up to its consequent failure. This final state of timber frame failure is never reached even in the cases of extreme calculated risk values. The N2 method proposed by Fajfar is used for the estimation of the attained displacement with the use of the demand and capacity curves. The results

produced for the probabilistic hazard refer to the three return periods for each of the structural cases. The results show that:

- For cases 1x and 1y, the structural risk exceeds slight damage for the 100 years period earthquake, moderate damage for the 225 years period earthquake and extensive damage for the 475 years period earthquake.
- For cases 2x, 2y, 4x and 4y, the structural risk exceeds moderate damage for the 100 years period and the 225 years period earthquakes and extensive damage for the 475 years period earthquake.
- For cases 3x, and 3y, the structural risk exceeds moderate damage for the 100 years period earthquake and extensive damage and for the 225 years and the 475 years period earthquakes.

For the deterministic risk assessment, the following results were obtained:

- Case 1x. The only attenuation relationship that presents constantly extreme values of risk, exceeding the masonry failure limit state for the 7.2 and 6.8 events, is the ITA10 relationship which can be finally disregarded. According to the remaining attenuation relationships, for the extreme case of a 7.2 event, masonry failure occurs in one case, the extensive damage limit state is exceeded in six cases and the moderate limit state is exceeded in four cases. For the 6.8 event, the extensive damage limit state is exceeded in four cases, the moderate limit state is exceeded in six cases and the slight damage limit state is exceeded in one case. For the 6.3 event, the extensive damage limit state is exceeded in two cases, the moderate limit state is exceeded in three cases and the slight damage limit state is exceeded in six cases.
- Case 1y. Disregarding the extreme case of ITA10, for the remaining relationships the following limit states are attained: For the extreme case of a 7.2 event, the extensive damage limit state is exceeded in seven cases and the moderate limit state is exceeded in four cases. For the 6.8 event, the extensive damage is exceeded four times, the moderate damage is exceeded six times and the slight damage is exceeded once. For the 6.3 event, the extensive damage is exceeded twice, the moderate damage is exceeded three times and the slight damage is exceeded six times.
- Case 2x. Disregarding the extreme case of ITA10, for the remaining relationships the following limit states are attained: For the extreme case of a 7.2 event, the masonry fails in one case, the extensive damage limit state is exceeded in six cases and the moderate limit state is exceeded in four cases. For the 6.8 event, the extensive damage is exceeded four times and the moderate damage is exceeded seven times. For the 6.3 event, the extensive damage is exceeded once, the moderate damage is exceeded seven times and the slight damage is exceeded three times.
- Case 2y. Disregarding the extreme case of ITA10, for the remaining relationships the following limit states are attained: For the extreme case of a 7.2 event, the extensive damage limit state is exceeded in seven cases and the moderate limit state is exceeded in four cases. For the 6.8 event, the extensive damage is exceeded four times, the moderate damage is exceeded six times and the slight damage is exceeded once. For the 6.3 event, the extensive damage is exceeded once, the moderate damage is exceeded seven times and the slight damage is exceeded three times.

- Case 3x. Disregarding the extreme case of ITA10, for the remaining relationships the following limit states are attained: For the extreme case of a 7.2 event, the extensive damage limit state is exceeded in all eleven cases. For the 6.8 event, the extensive damage is exceeded eight times and the moderate damage is exceeded three times and the slight damage is exceeded once. For the 6.3 event, the extensive damage is exceeded twice and the moderate damage is exceeded nine times.
- Case 3y. Disregarding the extreme case of ITA10, for the remaining relationships the following limit states are attained: For the extreme case of a 7.2 event, masonry failure occurs in four cases and the extensive damage limit state is exceeded in seven cases. For the 6.8 event, the extensive damage is exceeded ten times and the moderate damage is exceeded once. For the 6.3 event, the extensive damage is exceeded five times, the moderate damage is exceeded six times and the slight damage is exceeded once.
- Case 4x. Disregarding the extreme case of ITA10, for the remaining relationships the following limit states are attained. For the extreme case of a 7.2 event, the extensive damage limit state is exceeded in nine cases and the moderate limit state is exceeded in two cases. For the 6.8 event, the extensive damage is exceeded six times and the moderate damage is exceeded five times. For the 6.3 event, the extensive damage is exceeded once and the moderate damage is exceeded ten times.
- Case 4y. Disregarding the extreme case of ITA10, for the remaining relationships the following limit states are attained: For the extreme case of a 7.2 event, the extensive damage limit state is exceeded in nine cases and the moderate limit state is exceeded in two cases. For the 6.8 event, the extensive damage is exceeded six times and the moderate damage is exceeded five times. For the 6.3 event, the extensive damage is exceeded once and the moderate damage is exceeded ten times.

From the referred observations it can be stated that, generally, the structural risk is below the limit of masonry failure and, even in few cases in which this limit state is attained, the timber frame remains intact and, thus, preserves structural collapse. This conclusion is compatible with post event recent reports, as well as chroniclers' descriptions.

6. References

Bie L, Gonzalez P, Rietbrock A (2017). Slip distribution of the 2015 Lefkada earthquake and its implications for fault segmentation, *Geophysical J. Int*., 210(1): 420-427.

Fajfar, P. and Gašperšič, P. (1996). N2 – A method for non-linear seismic analysis for RC buildings, *Earthquake Engineering and Structural Dynamics*, 25, 23-67.

Fokaefs A. and Papadopoulos G.A. (2004). Historical earthquakes in the region of Lefkada Island, Ionian Sea – Estimation of magnitudes from epicentral intensities. *Bull. Geological Soc. of Greece*, 1389-1396.

Kappos AJ, Penelis GG, Drakopoulos CG (2002). Evaluation of simplified models for lateral load analysis of unreinforced masonry buildings. *J. Struct. Eng*., 128: 890–897.

Karakostas C, Lekidis V, Makarios T, Salonikios T, Sous I, Demosthenous M (2005). Seismic response of structures and infrastructure facilities during the Lefkada, Greece earthquake of 14/8/2003, *Eng. Struct*. 27: 213–227.

Kouris L.A. (2015). *Fragility curves and loss estimation for Traditional timber-framed masonry buildings in Lefkas, Greece*.

Kouris LAS, Meireles H, Bento R, Kappos AJ (2014). Simple and complex modelling of timber-framed masonry walls in Pombalino buildings. *Bull. Earthq. Eng*. 1–27.

Kouris LAS, Kappos AJ (2012). Detailed and simplified non-linear models for timber-framed masonry structures, *J. Cult. Heritage*, 13: 47–58.

Kouris LAS (2012). *Assessment of the seismic behaviour of timber-framed masonry buildings*. PhD thesis, Department of Civil Engineering, Aristotle University of Thessaloniki (in Greek).

Kouris LA, Kappos A (2009) Seismic performance of ancient timber-framed walls. In: Ferrari A (ed) 4th International congress: science and technology for the safeguard of cultural heritage of the Mediterranean Basin, Cairo, Egypt, vol I, pp 119–127, 6th–8th Dec.

Lagomarsino S and Giovinazzi S (2006). Macroseismic and mechanical models for the vulnerability and damage assessment of current buildings. *Bull. Earthq. Eng*., 4: 415–443.

Makarios T, Demosthenous M (2006). Seismic response of traditional buildings of Lefkas Island, Greece. *Eng. Struct.*, 28: 264–278.

Papadatou-Giannopoulou Ch. (2014). *Stability Techniques of Traditional Architecture and Glossary of Lefkada's Structural Terms*.

Penelis GG (2006). An efficient approach for pushover analysis of unreinforced masonry (URM) structures. *J. Earthq. Eng*., 10: 359–379.

Touliatos, P., Gante, D. (1995). *Local historic antiseismic constructions; The example of Lefkada*, NTUA, Athens (in Greek).

Touliatos P, Gante D (1995) *Local traditional earthquake-resistant construction: the paradigm of Lefkas*. National Technical University of Athens, Athens (in Greek)

Vieux-Champagne F, Sieffert Y, Grange S, Polastri A, Ceccotti A, Daudeville L (2014). Experimental analysis of seismic resistance of timber-framed structures with stones and earth infill. *Eng. Struct*., 69: 102–115.

Vintzileou E, Zagkotsis A, Repapis C, Zeris C (2007). Seismic behaviour of the historical structural system of the island of Lefkada, Greece. *Constr. Build. Mat*., 21: 225–236.

Vintzileou E, Touliatos P (2005). Seismic behaviour of the historical structural system of the island of Lefkada, Greece. *Adv. Archit. Ser*., 20: 291–300.

Vintzileou E. (2003). *Compilation package for the restoration of buildings of traditional settlement town of Lefkada after earthquake* (in Greek), The Earthquake Planning and Protection Organization (EPPO).

APPENDIX A
NGA relationships

The NGA database, used by the developers, consisted of 3,551 publicly available multi-component records from 173 shallow crustal earthquakes by 1,456 recording stations. The aforementioned numbers were significantly raised in 2014 with 21,336 three-component records from 600 earthquakes by 4,147 recording stations. Apart from the earthquakes records, the database contains supporting information about the location of the recording stations, source parameters, source-to-site distance and local site conditions at the recording stations.

All the attenuation models estimate peak ground acceleration (PGA), peak ground velocity (PGV), 5% damped elastic pseudo-response spectral accelerations (Sa) in the period range of 0 to 10 seconds and the corresponding standard deviations. Ground motion prediction equations can be applied for the average horizontal component ground motions. The applications thresholds and the independent parameters that are involved in the prediction equations differ among the five models. For the development of the NGA relations database, records were analyzed in combination with basic seismological theory, simple seismological models and supplemental analyses. The following effects on ground motions were taken into account:

- moderate to large magnitude scaling at close distances
- distance scaling at both close and far distances
- rupture directivity
- footwall and hanging wall for dipping faults
- style of faulting
- depth to faulting
- static stress drop
- site amplification relative to a reference 'rock' condition
- sedimentary basin amplification and depth to basement rock

The consideration in the statistical analysis of data pertained to the following:

- uncertainties in predictor variables
- dependence of standard errors on magnitude
- distance
- soil type
- shaking level

Each developer decided which effects should be incorporated in the attenuation model and which parameters should be included in the ground motion prediction equations. The directivity effect is not yet adequately analyzed in order to be inserted in the attenuation models. The developers of the attenuation models in 2008 version were:

- Norman Abrahamson and Water Silva (AS08 model)
- David Boore and Gail Atkinson (BA08 model)
- Kenneth Campbell and Yousef Bozorgnia (CB08 model)

- Brian Chiou and Robert Youngs (CY08 model)
- Izzat Idriss (I08 model)

In the latest version of 2014, in the first team, participated Ronnie Kamai (ASK14 model), and in the second team Jonathan Stewart and Emel Seyhan were added (BSSA14 model). The other teams remained unchanged (CB14 model, CY14 model and IM14 model respectively).

Ground motion prediction equations include parameters for a particular seismic scenario. The definitions of the parameters are given in Table A10 and Table A11. The number of used parameters as well as the complexity varies for the different attenuation models (Abrahamson and Silva 2008, Boore and Atkinson 2008, Campbell and Bozorgnia 2008, Chiou and Youngs 2008, Idriss 2008, Abrahamson et al. 2014, Boore et al. 2014, Campbell and Bozorgnia 2014, Chiou and Youngs 2014, Idriss 2014). The models with greater complexity and number of parameters are ASK, CB and CY while BSSA and IM have a simpler form. Furthermore, the model of Akkar and Bommer as well that developed for Italy in 2010 are included. The parameters can be divided in the following categories:

- Earthquake's magnitude (M)
- Fault style and geometry (strike-slip/normal/reverse fault, δ, λ)
- Distance between fault and examined site (R_{JB}, R_{RUP}, R_{Y0}, R_X, CRJB)
- Soil type and depth to basement bedrock (V_{S30}, $Z_{1.0}$, $Z_{2.5}$)
- Depth of the rupture (Z_{TOR}, Z_{HYPO})
- Hanging wall effect (F_{HW})
- Earthquake classification (mainshock/aftershock)
- Modeling region (California/Japan/China/Taiwan/Italy/Turkey)

Table A-1. Abbreviations of ground motion prediction equations' names.

Abbreviation	Name of the model
AS08	Norman Abrahamson & Water Silva , 2008
BA08	David Boore & Gail Atkinson , 2008
CB08	Kenneth Campbell & Yousef Bozorgnia , 2008
CY08	Brian Chiou & Robert Youngs , 2008
I08	Izzat Idriss , 2008
ASK14	Norman Abrahamson, Water Silva & Ronnie Kamai , 2014
BSSA14	David Boore, Jonathan Stewart, Emel Seyhan & Gail Atkinson , 2014
CB14	Kenneth Campbell & Yousef Bozorgnia , 2014
CY14	Brian Chiou & Robert Youngs , 2014
IM14	Izzat Idriss , 2014
ABS13	Sinan Akkar, bbdulah Sndikkaya & Julian Bommer , 2013
ITA10	Bindi et al. , 2010

Table A-2. Parameters used by the new generation attenuation relations (NGA 2008).

Parameter/Model		AS08	BA08	CB08	CY08	I08
Moment Magnitude	M	X	X	X	X	X
Soil Classification	V_{S30} (m/s)	X	X	X	X	X
Fault's characteristics	U	-	X	-	-	-
	SS	-	X	-	-	-
	NS	-	X	-	-	-
	RS	-	X	-	-	-
	F_{RV}	X	-	X	X	-
	F_{NM}	X	-	X	X	-
	F	-	-	-	-	X
Distance between site and fault	W (km)	X	-	-	-	-
	Dip/δ (°)	X	-	X	X	-
	λ (°)	-	-	-	-	-
	R_{JB} (km)	X	X	X	X	-
	R_{RUP} (km)	X	-	X	X	X
	R_X (km)	X	-	-	X	-
	CR_{JB} (km)	-	-	-	-	-
	R_{Y0} (km)	-	-	-	-	-
	R_{EPI} (km)	-	-	-	-	-
	R_{HYPO} (km)	-	-	-	-	-
	Z_{TOR} (km)	X	-	X	X	-
	$Z_{1,0}$ (m)	X	-	-	X	-
	$Z_{2,5}$ (km)	-	-	X	-	-
	ΔZ_{TOR} (km)	-	-	-	-	-
	$\Delta Z_{1,0}$ (m)	-	-	-	-	-
	Z_{HYPO} (km)	-	-	-	-	-

Table A-3. Parameters used by the new generation attenuation relations (NGA 2008).

Parameter/Model		AS08	BA08	CB08	CY08	I08
Directivity	DPP	-	-	-	-	-
	ΔDPP	-	-	-	-	-
Earthquake's classification	F_{AS}	X	-	-	X	-
	Event Type	-	-	-	-	-
Hanging wall	F_{HW}	X	-	-	X	-
	HW Taper	X	-	-	-	-
Region	Region	-	-	-	-	-
	F_{CL}	-	-	-	-	-
	F_{CN}	-	-	-	-	-
	F_{JP}	-	-	-	-	-
	F_{TW}	-	-	-	-	-
	S_J	-	-	-	-	-
Estimation of V_{S30}	F_{INF}	-	-	-	X	-
	F_{MEAS}	X	-	-	X	-

Table A-4. Parameters used by the new generation attenuation relations (NGA 2014).

Parameter/Model		ASK14	BSSA14	CB14	CY14	IM14
Moment Magnitude	M	X	X	X	X	X
Soil Classification	V_{S30} (m/s)	X	X	X	X	X
Fault's characteristics	U	-	X	-	-	-
	SS	-	X	-	-	-
	NS	-	X	-	-	-
	RS	-	X	-	-	-
	F_{RV}	X	-	X	X	-
	F_{NM}	X	-	X	X	-
	F	-	-	-	-	X
Distance between site and fault	W (km)	X	-	X	-	-
	Dip/δ (°)	X	-	X	X	-
	λ (°)	-	-	X	-	-
	R_{JB} (km)	X	X	X	X	-
	R_{RUP} (km)	X	-	X	X	X
	R_X (km)	X	-	X	X	-
	CR_{JB} (km)	X	-	-	-	-
	R_{Y0} (km)	X	-	-	-	-
	R_{EPI} (km)	-	-	-	-	-
	R_{HYPO} (km)	-	-	-	-	-
	Z_{TOR} (km)	X	X	X	X	-
	$Z_{1,0}$ (m)	X	X	-	X	-
	$Z_{2,5}$ (km)	-	-	X	-	-
	ΔZ_{TOR} (km)	-	-	-	X	-
	$\Delta Z_{1,0}$ (m)	-	-	-	X	-
	Z_{HYPO} (km)	-	X	X	-	-

Table A-5. Parameters used by the new generation attenuation relations (NGA 2014).

Parameter/Model		ASK14	BSSA14	CB14	CY14	IM14
Directivity	DPP	-	-	-	X	-
	ΔDPP	-	-	-	X	-
Earthquake's classification	F_{AS}	X	-	-	-	-
	Event Type	-	X	-	-	-
Hanging wall	F_{HW}	X	-	-	X	-
	HW Taper	-	-	-	-	-
Region	Region	-	X	-	X	-
	F_{CL}	X	-	-	-	-
	F_{CN}	X	-	-	-	-
	F_{JP}	X	-	-	-	-
	F_{TW}	X	-	-	-	-
	S_J	-	-	X	-	-
Estimation of V_{S30}	F_{INF}	X	-	-	X	-
	F_{MEAS}	-	-	-	X	-

Table A-6. Parameters used by Italian ground motion prediction models.

Parameter/Model		ITA10	ABS13
Moment Magnitude	M	X	X
Soil Classification	V_{S30} (m/s)	X	X
Fault's characteristics	U	X	X
	SS	X	X
	NS	X	X
	RS	X	X
	F_{RV}	-	-
	F_{NM}	-	-
	F	-	-
	W (km)	-	-
	Dip/δ (°)	-	-
	λ (°)	-	-
Distance between site and fault	R_{JB} (km)	X	X
	R_{RUP} (km)	-	-
	R_X (km)	-	-
	CR_{JB} (km)	-	-
	R_{Y0} (km)	-	-
	R_{EPI} (km)	-	X
	R_{HYPO} (km)	-	X
	Z_{TOR} (km)	-	-
	$Z_{1,0}$ (m)	-	-
	$Z_{2,5}$ (km)	-	-
	ΔZ_{TOR} (km)	-	-
	$\Delta Z_{1,0}$ (m)	-	-
	Z_{HYPO} (km)	-	-

Table A-7. Parameters used by Italian ground motion prediction models.

Parameter/Model		ITA10	ABS13
Directivity	DPP	-	-
	ΔDPP	-	-
Earthquake's classification	F_{AS}	-	-
	Event Type	-	-
Hanging wall	F_{HW}	-	-
	HW Taper	-	-
Region	Region	-	-
	F_{CL}	-	-
	F_{CN}	-	-
	F_{JP}	-	-
	F_{TW}	-	-
	S_J	-	-
Estimation of V_{S30}	F_{INF}	-	-
	F_{MEAS}	-	-

Table A-8. Limits for new generation attenuation models' implementation (NGA 2008).

Parameter/Model	AS08	BA08	CB08	CY08	I08
Moment Magnitude M (Strike slip fault)	$5 \le M \le 8,5$		$4 < M < 8,5$	$4 \le M \le 8,5$	$5 \le M \le 8,5$
Moment Magnitude M (Reverse fault)	$5 \le M \le 8$	$5 \le M \le 8$	$4 < M < 8$	$4 \le M \le 8$	$5 \le M \le 8$
Moment Magnitude M (Normal fault)			$4 < M < 7,5$		$5 \le M \le 8,5$
Rupture Distance R_{RUP} (km)	$0 \le R_{RUP} \le 200$	-	$0 \le R_{RUP} \le 200$	$0 \le R_{RUP} \le 200$	$0 \le R_{RUP} \le 200$
Joyner-Boore Distance R_{JB} (km)	-	$0 \le R_{JB} \le 200$	-	-	-
Velocity V_{S30} (m/s)	$150 \le V_{S30} \le 2000$	$180 \le V_{S30} \le 1300$	$150 \le V_{S30} \le 1500$	$150 \le V_{S30} \le 1500$	$450 \le V_{S30} \le 900$ και $V_{S30} > 900$
Depth $Z_{2,5}$ (km)	-	-	$0 \le Z_{2,5} \le 10$	-	-
Depth Z_{TOR} (km)	-	-	$0 \le Z_{TOR} \le 15$	-	-
Dip angle δ (°)	-	-	$15 \le \delta \le 90$	-	-
Reference Velocity *Vref* (m/s)	1100	760	1100	1130	-

Table A-9. Limits for new generation attenuation models' implementation (NGA 2014).

Parameter/Model	ASK14	BSSA14	CB14	CY14	IM14
Moment Magnitude M (Strike slip)	$3 \le M \le 8,5$	$3 \le M \le 8,5$	$3,3 \le M < 8,5$	$3,5 \le M \le 8,5$	$5 \le M \le 8$
Moment Magnitude M (Reverse fault)			$3,3 \le M \le 8$	$3,5 \le M \le 8$	
Moment Magnitude M (Normal fault)		$3,3 \le M \le 7$	$3,3 \le M < 7$		
Rupture Distance R_{RUP} (km)	$0 \le R_{RUP} \le 300$	$0 \le R_{RUP} \le 400$	$0 \le R_{RUP} \le 300$	$0 \le R_{RUP} \le 300$	$0 \le R_{RUP} \le 150$
Velocity V_{S30} (m/s)	$180 \le V_{S30} \le 1500$	$150 \le V_{S30} \le 1500$	$150 \le V_{S30} \le 1500$	$180 \le V_{S30} \le 1500$	$450 \le V_{S30} \le 2000$
Depth Z_{TOR} (km)	-	-	-	$Z_{TOR} \le 20$	-
Reference Velocity *Vref* (m/s)	1100	760	1100	1130	-

Table A-10. Limits for European attenuation models' implementation.

Moment Magnitude M (Strike slip)	ITA10	ABS13
Moment Magnitude M (Reverse slip)	$4 \leq M \leq 6.9$	$4 \leq M \leq 8$
Moment Magnitude M (Normal fault)		
Rupture Distance R_{RUP} (km)		
Joyner-Boore Distance R_{JB} (km)	$0 \leq R_{JB} \leq 200$	$0 \leq R_{JB} \leq 200$
Velocity V_{S30} (m/s)	-	$0 \leq R_{HYPO} \leq 200$
Depth $Z_{2,5}$ (km)	-	$0 \leq R_{EPI} \leq 200$
Depth Z_{TOR} (km)	$180 \leq V_{S30} \leq 1500$	$150 \leq V_{S30} \leq 1500$
Dip angle δ (°)	-	-
Reference Velocity *Vref* (m/s)	1100	750

Table A-11. Definitions of the parameters used by attenuation relations.

Parameter		Definition
Moment Magnitude	M	Moment Magnitude
Soil Classification	V_{S30} (m/s)	"Average" shear wave velocity for the upper 30m at the site
Fault's characteristics	U	Flag for unspecified fault type
	SS	Flag for strike-slip fault type
	NS	Flag for normal-slip fault type
	RS	Flag for reverse-slip fault type
	F_{RV}	Flag for reverse and reverse/oblique fault type
	F_{NM}	Flag for normal fault type
	F	Refers to source mechanism, 0 for stike-slip and normal mechanisms and 1 for reverse and oblique mechanisms
	W (km)	Fault's width
	Dip/δ (°)	Fault's dip angle
	λ (°)	Fault's rake angle
Distance between site and fault	R_{JB} (km)	Joyner-Boore distance, the shortest distance from a site to the surface projection of the rupture surface.
	R_{RUP} (km)	Rupture distance, the shortest distance from a site to a rupture surface.
	R_X (km)	Distance Rx, the shortest horizontal distance from a Site to a line defined by extending the fault trace (or the top edge of the rupture) to infinity in both directions. Values on the hanging-wall are positive and those on the foot-wall are negative.
	CR_{JB} (km)	Centroid Joyner-Boore distance, which is the shortest distance between the centroid of Joyner-Boore rupture surface of the potential Class 2 earthquakes and the closest point on the edge of the Joyner-Boore rupture surface of the main shock
	R_{Y0} (km)	R_{Y0} distance, the horizontal distance off the end of rupture measured parallel to strike, only for sites on the hanging wall side
	R_{EPI} (km)	Epicentral distance, the distance between the site and the earthquake's epicenter
	R_{HYPO} (km)	Hypocentral distance, the distance between the site and the earthquake's focus
	Z_{TOR} (km)	Depth to top of rupture
	$Z_{1,0}$ (m)	Depth to rock with shear wave velocity = 1.0 km/sec
	$Z_{2,5}$ (km)	Depth to rock with shear wave velocity = 2.5 km/sec
	ΔZ_{TOR} (km)	Z_{TOR} centered on the M-dependent average
	$\Delta Z_{1,0}$ (m)	$Z_{1.0}$ centered on the VS30-dependent average
	Z_{HYPO} (km)	The hypocentral depth of the earthquake measured from sea level

Table A-12. Definitions of the parameters used by attenuation relations.

Parameter		Definition
Directivity	DPP	Direct point parameter for directivity effect
Earthquake classification	ΔDPP	DPP centered on the site- and earthquake specific average DPP
Earthquake's classification	F_{AS}	Flag for aftershocks,0 for main shock (Class 1) and 1 for aftershock (Class 2)
	Event Type	Flag for aftershocks,0 for main shock (Class 1) and 1 for aftershock (Class 2)
Hanging wall	F_{HW}	Flag for hanging wall sites, 1 for sites on the hanging wall side (HW) of the fault, 0 otherwise. The boundary between the foot wall (FW) and HW is defined by the vertical projection of the top of the rupture. For dip of 90 degrees is 0.
	HW Taper	To choose the hanging wall taper to be used in AS08. Enter 0 to use the hanging wall taper as published in Abrahamson and Silva (2008) or enter 1 to use the hanging wall taper suggested by Norm Abrahamson.
Region	Region	Flag for region, is 0 if no regional correction is to be made(default value),1 for California, New Zealand (this also provides no correction), 2 for China and Turkey and 3 for Italy, 4 for Japan and 5 for Taiwan
	F_{CL}	Is an indicator variable representing regional effects, where 1 is for sites located in California and 0 otherwise
	F_{CN}	Is an indicator variable representing regional effects, where 1 is for sites located in China and 0 otherwise
	F_{JP}	Is an indicator variable representing regional effects, where 1 is for sites located in Japan and 0 otherwise
	F_{TW}	Is an indicator variable representing regional effects, where 1 is for sites located in Taiwan and 0 otherwise
	S_J	Is an indicator variable representing regional effects, where 1 is for sites located in Japan and 0 otherwise
Estimation of V_{S30}	F_{INF}	Is an indicator variable which shows if V_{S30} is estimated or measured. 1 for estimated V_{S30} and 0 otherwise
	F_{MEAS}	Is an indicator variable which shows if V_{S30} is estimated or measured. 1 for measured V_{S30} and 0 otherwise

Literature

Abrahamson Norman A., Walter J. Silva and Ronnie Kamai, 2014, Summary of the ASK14 Ground Motion Relation for Active Crustal Regions.

Abrahamson Norman and Walter Silva, 2008, Summary of the Abrahamson & Silva NGA Ground-Motion Relations.

Akkar, S. M., Sandikkaya A. and. Bommer, J. J., 2013, Empirical ground-motion models for point- and extended-source crustal earthquake scenarios in Europe and the Middle East.

Ambraseys, N., 2009. Earthquakes in the eastern Mediterranean and the Middle East: a multidisciplinary study of 2000years of seismicity, Cambridge University Press, ISBN 9780521872928, 947pp

Andizei M., Baldi P., Casula G., Galvani A., Mantovani E., Pesci A., Riguzzi F., Serpelloni E. (2001), «Insights Into Present-Day Crustal Motion in the Central Mediterranean Area From GPS Surveys», Geophys. J. Int. 146 (1), 98– 110

Benetatos, C., Dreger, D.,Kiratzi, A., Complex and Segmented Rupture Associated with the 14 August 2003 Mw 6.2 Lefkada, Ionian Islands, Earthquake,Bulletin of the Seismological Society of America, 97(1B),https://doi.org/10.1785/0120060123, 2007.

Benetatos, C., Kiratzi, A., Roumelioti, Z., Stavrakakis, G., Drakatos, G., Latoussakis, I., 2005. The 14 August 2003 Lefkada Island (Greece) earthquake: focal mechanisms of the mainshock and of the aftershock sequence. Journal of Seismology v.9, pp.:171–190

Bindi, D., Pacor, F. ,Luzi, L., Puglia, R., Massa, M., Ameri, G., Paolucci, R.,2011, Ground motion prediction equations derived from the Italian strong motion database.

Boore David M. and Gail M. Atkinson, 2008, Ground-Motion Prediction Equations for the Average Horizontal Component of PGA, PGV, and 5%-Damped PSA at Spectral Periods between 0.01 s and 10.0 s.

Boore David M., Jonathan P. Stewart, Emel Seyhan and Gail M. Atkinson, 2014, NGA-West2 Equations for Predicting PGA, PGV, and 5% Damped PSA for Shallow Crustal Earthquakes.

Bozorgnia, Y., Abrahamson, N. A., Al Atik, L., Ancheta, T. D., Atkinson, G. M., Baker, J. W., Baltay, A., Boore, D. M., Campbell, K. W., Chiou, B. S.-J., Darragh, R., Day, S., Donahue, J., Graves, R. W., Gregor, N., Hanks, T., Idriss, I. M., Kamai, R., Kishida, T., Kottke, A., Mahin, S. A., Rezaeian, S., Rowshandel, B., Seyhan, E., Shahi, S., Shantz, T., Silva, W., Spudich, P., Stewart, J. P., Watson-Lamprey, J., Wooddell, K., and Youngs, R., 2014. NGA-West2 research project, Earthquake Spectra 30, 973–987. (16) (PDF) NGA-West2 Ground Motion Model for the Average Horizontal Components of PGA, PGV, and 5% Damped Linear Acceleration Response Spectra.

Bournovas, 1964, Geological study of Lefkada island, Institute of geology and mineral exploration.

Campbell Kenneth W. and Yousef Bozorgnia, 2008, NGA Ground Motion Model for the Geometric Mean Horizontal Component of PGA, PGV, PGD and 5% Damped Linear Elastic Response Spectra for Periods Ranging from 0.01 to 10 s.

Campbell Kenneth W. and Yousef Bozorgnia, 2014, NGA-West2 Ground Motion Model for the Average Horizontal Components of PGA, PGV, and 5% Damped Linear Acceleration Response Spectra.

Chiou Brian S.-J. and Robert R. Youngs, 2008, An NGA Model for the Average Horizontal Component of Peak Ground Motion and Response Spectra.

Chiou Brian S.-J. and Robert R. Youngs, 2014, Update of the Chiou and Youngs NGA Model for the Average Horizontal Component of Peak Ground Motion and Response Spectra.

Cushing, E. 1985. Evolution structurale de la marge Nord Ouest Hellénique dans l'île de Levkas et ses environs (Grèce Nord occidentale). Thèse 3ème Cycle, Univ. Paris Sud, Orsay, 297 pp.

Ganas A., Marinou A., Anastasiou D., Paradissis D., Papazissi K., Tzavaras P., Drakatos G (2013), «GPS-Derived Estimates of Crustal Deformation in the Central and North Ionian Sea, Greece: 3-yr Results *From NOA NET Continuous Network Data», Journal* of Geodynamics, 67, 62–71

Gazetas, G., 2004. Geotechnical aspects of the Ms 6.4 Lefkada Island, Greece, 2003 earthquake: preliminary assessment. In: Proc. of the 5th Int. Conf. on Case Histories in Geotechnical Engineering, 13–17 April 2004,New York, paper no. 13

Giardini, D., Wössner, J. and Danciu, L. (2014), Mapping Europe's Seismic Hazard, Eos Trans. AGU, 95(29), 261.

Haslinger, H., Kissling, E., Ansorge, J., Hatzfeld, D., Papadimitriou, E., Karakostas, V., Makropoulos, K., Kahle, H.-G., and Peter, Y., 1999. 3D Crustal Structure from Local Earthquake Tomography Around the Gulf of Arta (Ionian region, NW Greece). Tectonophysics, 304, 201-218.

Hatzfeld, D., Kassaras, I., Panagiotopoulos, D.G., Amorese, D., Makropoulos, K., Karakaisis, G.F., Coutant, O., 1995. Microseismicity and strain pattern in NW Greece. Tectonics 14:773–785

Idriss I. M., 2008, An NGA Empirical Model for Estimating the Horizontal Spectral Values Generated By Shallow Crustal Earthquakes.

Idriss I. M., 2014, An NGA-West2 Empirical Model for Estimating the Horizontal Spectral Values Generated by Shallow Crustal Earthquakes.

ITSAK, 2003. The earthquake of Lefkada (M = 6.4), August 14, 2003, Technical Chamber of Greece, Athens.

ITSAK (2004), "The Lehkada earthquake (M = 6.2), 14 August 2003", Technical Chamber of Greece, Athens

Kalantoni, D., Pomonis, A., Kassaras, I., Kouskouna, V., Pavlou, K., Vassilopoulou, S., Karababa, F. and Makropoulos, K. 2013. Vulnerability assessment in Lefkas old town (W. Greece) with the use of EMS-98; comparison with the 14-8-2003, Mw=6.2, earthquake

effects. First results, Proc. of Congress on Recent Advances in Earthquake Engineering and Structural Dynamics 2013 (VEESD 2013), Vienna, Paper No. 356. 28–30 Aug 2013

Karakostas, V. et al. “Properties of the 2003 Lefkada, Ionian Islands, Greece, Earthquake Seismic Sequence and Seismicity Triggering.”, 2004.

Karakostas, V., Papadimitriou, E., 2010. Fault complexity associated with the 14 August 2003 Mw6.2 Lefkada, Greece,aftershock sequence. Acta Geophysica, 58, 5, 838-854. doi: 10.2478/s11600-010-0009-6

Kassaras, I., Karakonstantis, A., Vlachou, K., Kapetanidis, V., Kaviris, G., Papadimitriou, P., Voulgaris, N., Lagios, E., Makropoulos, K., 2012. Study of the Geodynamics in Aitoloakarnania (W. Greece) based on joint Seismological and GPS Data, Book of Abstracts, 33 ESC General Assembly, Moscow, pp 164–165

Kassaras, I., Makropoulos, K.C., Papadimitriou, P., Drakopoulos, J., Amorese, D., Hatzfeld, D., Coutant, O., Panagiotopoulos, D., Karakaisis, G. and Scordilis, M., 1993. Seismotectonic analysis in Kefallinia-Lefkas (Greece). 2nd International Geophysicsl Congress, Florina, Greece, v1, 427-438.

Kassaras, I., Karakonstantis, A., Vlachou, K., Kapetanidis, V., Kaviris, G., Papadimitriou, P., Voulgaris, N., Makropoulos, K., 2013. On the geodynamics of western Greece deduced by massive seismological observations, AHS/IAPSO/IASPEI Joint Assembly, Gothenburg, Sweden, 22-26 July 2013

Kassaras, I., Kalantoni, D., Pomonis, A., Kouskouna, V., Karababa, F., Makropoulos, K. 2014a. Development of seismic damage scenarios in Lefkas old town (W. Greece). Part I: Vulnerability assessment of local constructions with the use of EMS-98. Bull Earthq Eng. doi:10.1007/s10518-014-9643-8

Le Pichon, X. and Angelier, J., 1979. The Hellenic Arc and Trench System: A Key to the Neotectonic Evolution of the Eastern Mediterranean Area, Tectonophysics, 60, 1-42

Louvari, E., Kiratzi, A., Papazachos, B., 1999. The Cephalonia Transform Fault and its extension to western Lefkas Island (Greece), Tectonophysics, 308, 223–236

Makropoulos, K., Diagourtas, D., Kassaras, I., Kouskouna, V., Papadimitriou, P. and Ziazia, M., 1996. The November-December 1994 Lefkas (W. Greece) earthquake sequence: Results from in situ seismological survey, First Congress of the Balkan Geophysical Society, Athens, September 23-27, pp. 10-11.

Makropoulos, K., Kaviris, G. and Kouskouna, V., 2012. An updated and extended earthquake catalogue for Greece and adjacent areas since 1900, Nat. Hazards Earth Syst. Sci., 12:1425-1430

Makropoulos, K.C., Kouskouna, V., 1994. The Ionian Islands earthquakes of 1767 and 1769: seismological aspects.Contribution of historical information to a realistic seismicity and hazard assessment of an area. In: P. Albini and A. Moroni (eds), Materials of CEC Project Review of Historical Seismicity in Europe, CNR, Milano, 2: 254 pp

Melgar, D., Ganas, A., Geng, J., Liang, C., Fielding, E., Kassaras, I., Source characteristics of the 2015 Mw 6.5, Lefkada, Greece, strike-slip earthquake, Journal of Geophysical Research, 2017.

Papadimitriou, P., Kapetanidis, V., Karakonstantis, A., Voulgaris, N., Chousianitis, K., Agalos, A., Moshou, A., Kaviris, G., Kassaras I. and Makropoulos, K., 2012. Recent Significant Earthquakes in Western Greece. Book of Abstracts, 33rd ESC General Assembly, Moscow, Russia, p. 456.

Papadopoulos G, Karastathis V, Ganas A, Pavlides S, Fokaefs A, Orfanogiannaki K, 2003, The Lefkada, Ionian Sea(Greece), shock (Mw = 6.2) of 14 August 2003: evidence for the characteristic earthquake from seismicity and ground failures. Earth Planet Space 55:713–718

Papathanassiou G, Pavlides S and Ganas A, 2005, The 2003 Lefkas earthquake: Field observations and preliminary microzonation map based on liquefaction potential index for the town of Lefkas, Engineering Geology, 8

Papazachos B, Papazachou C, 2003, Earthquakes of Greece. Ziti Publications, Thessaloniki, 3rd edition, 286 pp

Power, M., Chiou, B. S.-J., Abrahamson, N. A., Bozorgnia, Y., Shantz, T., and Roblee, C., 2008. An overview of the NGA Project, Earthquake Spectra 24,3–21.*(16) (PDF) NGA-West2 Ground Motion Model for the Average Horizontal Components of PGA, PGV, and 5% Damped Linear Acceleration Response Spectra*.

Rontogiannis, P., 1995. Seismology of Lefkada (1469-1971), Year 8 Series, Lefkadian Studies Society.

SHARE INGV, (2009). *The European Database of Seismogenic Faults.*[online] Available at: http://diss.rm.ingv.it/share-edsf/SHARE_WP3.2_Database.html [Accessed 31 May 2012].

Spyropoulos, PI, 1997. Chronicle of the Earthquakes of Greece, Publications Dodona

Stucchi, M., Rovida, A., Gomez Capera, A.A., Alexandre, P., Camelbeeck, T., Demircioglu, M.B., Gasperini, P., Kouskouna, V., Musson, R.M.W., Radulian M., Sesetyan, K., Vilanova, S., Baumont, D., Bungum, H., Fäh, D., Lenhardt, W., Makropoulos, K., Martinez Solares, J.M., Scotti, O., Zivcic, M., Albini, P., Batllo, J., Papaioannou, C., Tatevossian, R., Locati, M., Meletti, C.,Viganò, D., Giardini, D., 2013. The SHARE European earthquake catalogue (SHEEC) 1000‑1899, Journal of Seismology, 17, 2:523-544